Organic carbon burial under greenhouse climate conditions: The regional expression of the
Late Cretaceous Oceanic Anoxic Event 3 within the Western Interior Seaway

by

Allyson Caroline Tessin

A dissertation submitted in partial fulfillment
of the requirements for the degree of
Doctor of Philosophy
(Geology)
in the University of Michigan
2016

Doctoral Committee:

      Associate Professor Ingrid L. Hendy, co-Chair
      Associate Professor Nathan D. Sheldon, co-Chair
      Professor G. Allen Burton
      Professor Emeritus Philip A. Meyers
      Associate Professor Christopher J. Poulsen

Acknowledgements

I've been lucky to meet many great people through this journey and would especially like to thank Meghan, Tiffany, Tom, Clay, Rich, Tara, Chris, Andy, and Miquela for all of the adventures, beers, and great conversations.

Last, but definitely not least, I'd like to thank Tim Gallagher, for being my partner in all things.

Table of Contents

List of Tables

List of Figures

List of Appendices

Abstract

The Cretaceous period (145−66 million years ago) was characterized by elevated atmospheric pCO$_2$ and an equable, warm climate. High Cretaceous sea levels flooded continental areas producing extensive shallow seaways, including the Western Interior Seaway (WIS) in North America. The resulting sedimentary record of the WIS includes episodic deposition of organic carbon-rich black shales, during a series of Oceanic Anoxic Events (OAEs). Multiple processes control marine black shale deposition, including changes in primary productivity, organic matter preservation, and sedimentary dilution. OAEs offer an opportunity to evaluate the relative roles of these forcing factors on marine carbon burial.

This dissertation centers on understanding the causes of enhanced organic carbon burial within the WIS during a particularly poorly studied OAE, the Coniacian-Santonian OAE 3 (~88−84 Ma). In Chapter 2, I use trace metal records from the USGS Portland core (drilled near Cañon City, Colorado) to reconstruct the degree of oxygenation before, during, and after OAE 3. These data are compared to bulk elemental and isotopic records of organic matter composition to demonstrate that oxygen depletion in pore and bottom waters provided a feedback to carbon burial, by triggering enhanced organic matter preservation within the WIS during OAE 3. In Chapter 3, I examine changes in organic carbon preservation in greater detail using biomarker and compound specific carbon isotope records. My results document distinct changes in the elemental composition of organic matter before, during, and after the OAE associated with varying degrees of bioturbation and therefore, oxygen exposure time. In Chapter 4, I explore the

feedbacks associated with changing iron chemistry in the WIS. Sequential iron extractions, phosphorus, and sulfur results indicate that low reactive iron availability promoted phosphorus remineralization from sediments, illustrating the importance of internal nutrient recycling during and after OAE 3. In Chapter 5, trends and timing of organic carbon accumulation are examined on a larger spatial scale. Trace metal and foraminiferal records from western Alberta are compared to time equivalent records from the central seaway. The reconstructed seaway-wide patterns indicate that anoxic conditions and the resulting sedimentary elevated organic carbon accumulation closely follow the sea-level transgression and expanding influence of nutrient-rich Tethyan (equatorially-sourced) water.

Chapter 1

Introduction

The Late Cretaceous is among the best examples of a greenhouse climate within the last 100 Ma of geologic history. Rocks deposited during this period provide an archive of environmental conditions, which can be used to assess how Earth's climate system operates under elevated temperatures and high atmospheric pCO$_2$. The warm climate, a lack of polar ice sheets, and high sea floor spreading rates during the Late Cretaceous resulted in average sea levels of 75–250 m above modern mean sea level (Haq, 2013), that flooded large areas of low lying continents. The sedimentary records of these continental seaways indicate widespread deposition of fine-grained, organic carbon (OC)-rich sedimentary rocks, known as black shales.

Black shales, which record enhanced marine sedimentary OC burial, continue to be the focus of significant research aimed at understanding ocean carbon cycle dynamics (e.g. Kuypers et al.; 1999, Damaste et al., 2010; Friedrich et al., 2012). The ocean is thought to be a major regulating force in the global carbon cycle throughout geologic history. Specifically, marine OC burial represents an important sink of CO$_2$ from the ocean-atmosphere carbon reservoirs. Determining how this CO$_2$ removal flux changes in response to warmer, higher CO$_2$ conditions is critical because humans are currently altering the global carbon cycle through CO$_2$ emissions.

Black shale deposition within shallow marine environments is of particular interest as OC burial in shallow marine environments plays a disproportionately significant role in the global

1

carbon cycle, with >40% of marine OC sequestration occurring on continental margins despite these regions comprising only 8% of the oceans area (Müller-Karger et al., 2005; Cai et al., 2015; Smith et al., 2015). Furthermore, fjords, which are both shallow and physically restricted marine inlets, make up 11% of marine OC burial while representing only one tenth of one percent of the ocean's surface area (Smith et al., 2015). As ice continues to melt in response to modern global warming, the total area of shallow marine environments will expand as sea levels rise. Therefore, a complete understanding of the mechanisms that enhance organic carbon burial within shallow marine regions is required to accurately predict how marine OC burial fluxes, and therefore CO_2 sequestration, will respond to anthropogenic climate change.

Research on the primary driver of enhanced OC burial has long focused on the dichotomy between elevated primary productivity and enhanced OC preservation under anoxic conditions (e.g. Pedersen and Calvert, 1990; Wignall, 1994; Mort et al., 2007). The recognition of widespread ocean anoxia coeval with extensive OC-rich 'black shale' deposition, specifically during Oceanic Anoxic Events (OAEs), highlights the important relationship between marine oxygen and carbon cycling. Subsurface water column oxygenation is controlled by a balance of (1) O_2 consumption through respiration of OC and (2) mixing with O_2-rich surface waters (ventilation). Both of these processes are intimately linked with sedimentary OC sequestration, as increased export *productivity* will deliver more OC to the sediments, while reduced water ventilation and increased O_2 consumption will increase OC *preservation* through decreased aerobic heterotrophy (Fig. 1.1). Furthermore, remineralization of nutrients under anoxic conditions may provide an additional feedback if these nutrients are able to return to the euphotic zone where primary productivity takes place. This dissertation focuses on reconstructing changes

in oxygenation and evaluating their relationship to enhanced OC accumulation within a restricted, shallow marine environment during a Late Cretaceous OC burial event.

Less Productivity ←→ More Productivity	Dominant Electron Acceptor	Redox State	Metal Proxy	Iron Proxy
Photic Zone — Aerobic respiration	O_2	Oxic	Mn	Fe/Al<0.5 $Fe_{HR}/Fe_T<0.38$
Nitrate reduction	NO_3^- Fe^{3+} Mn^{4+}	Suboxic	Re/Mo Re,U	$Fe_{HR}/Fe_T>0.38$ $Fe_{Py}/Fe_{HR}<0.8$
SWI — Sulfate reduction	SO_4^{2-}	Sulfidic/ Euxinic	Cd, Zn Mo	Fe/Al>0.5 $Fe_{HR}/Fe_T>0.38$ $Fe_{Py}/Fe_{HR}>0.8$
Fermentation	CH_2O			

O_2-rich Bottom Waters ←→ O_2-poor Bottom Waters

Figure 1.1

Schematic of sedimentary and water column oxygenation. Different colors represent the sequential steps in the remineralization of photosynthetically produced organic matter. Dominant electron acceptor, redox state and associated proxies for each step are listed. Conditions to the left are produced by low primary productivity and/or well-ventilated bottom waters, while conditions to the right are caused by elevated primary productivity and/or reduced ventilation of bottom waters.

1.1 Oceanic Anoxic Events

Mesozoic OAEs are associated with significant black shale deposition and are thought to represent significant perturbations to the carbon cycle (e.g. Jenkyns, 2010). The Cenomanian-Turonian boundary event, OAE 2, is the quintessential OAE, characterized by black shale deposition in many localities (Schlanger et al., 1987; Tsikos et al., 2002). OAE 2 is identified by a distinctive and relatively short-lived (~600 ka: Sageman et al., 2006) positive carbon isotope excursion that is expressed in almost every depositional environment that records the C-T

boundary (Arthur et al., 1987; Jenkyns, 2010). Enhanced nutrient delivery and subsequent increased primary productivity are thought to be the primary drivers of OAE 2 (e.g. Montiero et al., 2012). Potential sources of nutrients include pronounced volcanic activity associated with the emplacement of a large igneous province (LIP) and an accelerated hydrological cycle that intensifies continental weathering (Blättler et al., 2011; Pogge von Strandmann et al., 2013; Du Vivier et al., 2014; van Helmond et al., 2014). In addition to external nutrient inputs, enhanced phosphate regeneration (Mort et al., 2007; Kraal et al., 2010) and subsequent upwelling of nutrient-rich deep waters (Voigt et al., 2004; Jenkyns, 2010) would have fueled further primary productivity.

Unlike OAE 2, the Coniacian-Santonian OAE 3 was not expressed globally (Jenkyns, 2010; Locklair et al., 2011; Wagreich, 2012). Identified Coniacian-Santonian black shales are restricted to the equatorial Atlantic and adjacent continental shelves and seaways (e.g., Hofmann et al., 2003; Wagner et al., 2004; Beckmann et al., 2005; Marz et al., 2008; Locklair et al., 2011), including the North American Western Interior Seaway (WIS), whereas black shale deposition is notably absent in the Tethys and Pacific basins (Arthur and Sageman, 1994; Jenkyns, 2010; Wagreich, 2012). Identification of a single OAE 3 event is complicated because Coniacian-Santonian black shale deposition differs in age and duration (Locklair et al., 2011). Furthermore, while OAE 2 is easily identified in the rock record by a distinct >2‰ global carbon isotope excursion, OAE 3 is identified by a comparatively small (<1‰) isotope plateau (Pratt et al., 1993; Jarvis et al., 2006; Locklair et al., 2011). Despite the lack of a large isotope excursion, a notable characteristic of OAE 3 in the WIS is that organic carbon burial rates were roughly double that of OAE 2 and carbon burial persisted for a significantly longer duration (>3 Ma). Such significant shallow marine carbon burial during the Coniacian-Santonian represents a
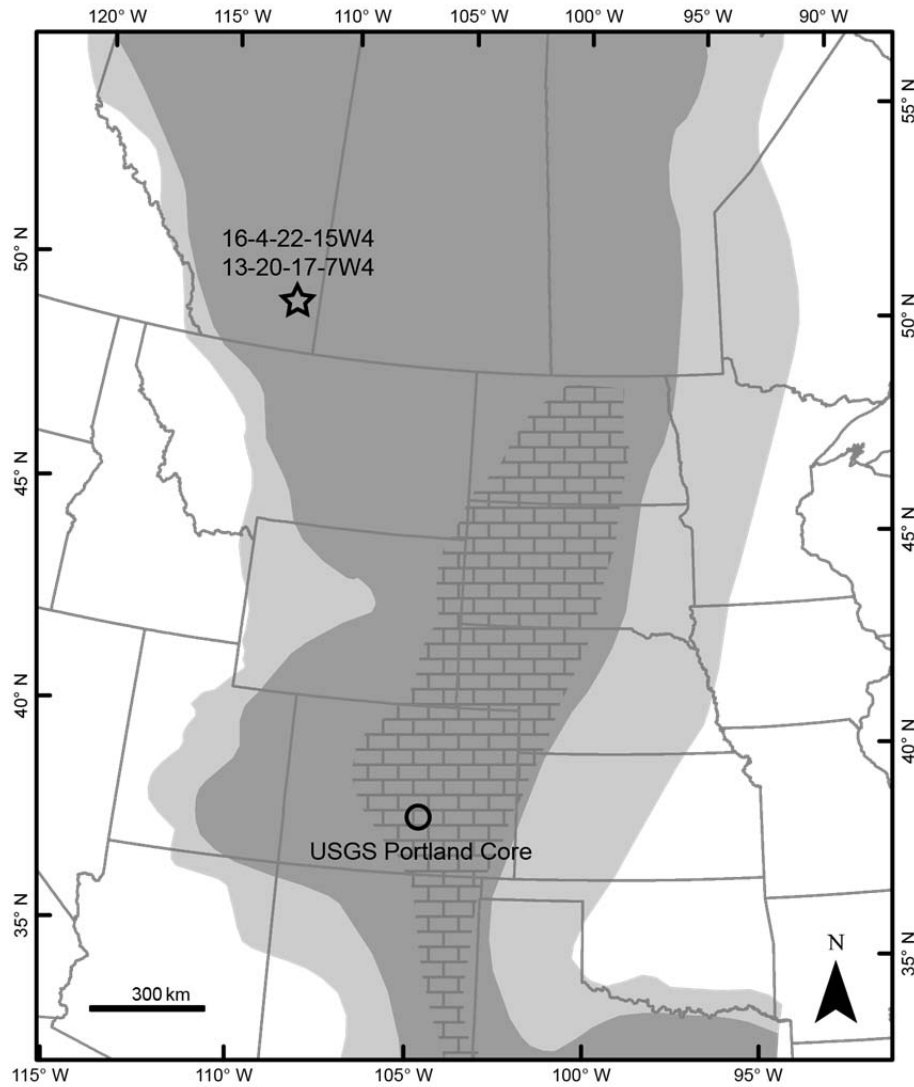
Figure 1.2

Map of the Coniacian extent of the Cretaceous Western Interior Seaway. The USGS Portland #1 core is the focus of Chapters 2—4 and the Sweetgrass Arch cores (starred) are the focus of Chapter 5.

significant carbon cycle perturbation, albeit with potentially different causal mechanisms than

OAE 2. It is important to reconstruct not only the driving mechanism of OAE 3, but also the

feedback mechanisms required to sustain elevated organic carbon burial throughout the

Coniacian-Santonian (Locklair et al., 2011; Wagreich 2012).

1.2 Western Interior Seaway

The shallow, silled North American Western Interior Seaway was a locus of significant organic carbon accumulation during the Late Cretaceous, making it an ideal location to study the causes of enhanced shallow marine black shale deposition. The WIS was a large, shallow epicontinental seaway that persisted from the Late Jurassic to the early Paleocene (Fig. 1.2). The Western Interior Basin was an asymmetrical foreland basin to the east of the Sevier mountain belt, such that the maximum subsidence and accumulation rates were to the west and the seaway shoaled to the east (McNeil and Caldwell, 1981; Shurr and Rice 1986). The seaway extended from the Gulf of Mexico to the Arctic Ocean and from central Utah to central Iowa during its maximum transgression. The WIS consisted of two primary water masses: warm, saline Tethyan water that entered the seaway in the south and cooler, more brackish polar water that entered the seaway from the north (e.g. Slingerland et al., 1996; Poulsen et al., 1999). Continental runoff from the uplifting Sevier mountain belt to the west provided an additional freshwater source (Floegel et al., 2005). Contrasting circulation patterns have been suggested for the WIS, including those suggesting dominantly Tethyan-sourced surface waters (Slingerland et al., 1996) or dominantly Arctic-sourced surface waters (Watkin, 1986; Poulsen et al., 1999; Coulson et al., 2011).

The Late Cretaceous sedimentary record of the WIS includes episodic black shale deposition, including those deposited during the two maximum sea level transgressions of the Greenhorn and Niobrara seas (Fig. 1.2; Kauffman, 1977). Peak transgression of the Greenhorn Sea is coeval with the Cenomanian-Turonian OAE 2, while the previously identified OAE 3 occurred during transgression of the Niobrara Sea. This dissertation focuses on the expression of OAE 3 within two regions of the WIS, central Colorado/western Kansas and southern Alberta. In

both regions, Coniacian-Santonian deposition and OAE 3 is recorded in the Niobrara Formation. Despite significant independent research on the Niobrara Formation within both Canadian and US sections, comparison of results between the two regions is rare.

In Kansas and central Colorado, the Niobrara Formation is divided into two formal units: the basal Fort Hays Limestone and the Smoky Hill Chalk (Scott and Cobban, 1964). Cyclic variations in lithology occur on timescales ranging from tens of thousands to millions of years and are the result of the interplay between eustatic sea level, local accommodation space, terrigenous input and marine productivity (e.g. Dean and Arthur, 1998). The Fort Hays Limestone was deposited in the Upper Turonian-Lower Coniacian and records the initial transgression of the Niobrara Sea (Sageman et al., 2015). It is characterized by ledge-forming limestones separated by thin organic carbon-rich shales (Scott and Cobban, 1964). The overlying Smoky Hill Chalk was deposited from the Lower Coniacian to the Lower Campanian (Sageman et al., 2015). The Smoky Hill Chalk consists of interbedded shales and chalks that Scott and Cobban (1964) divided into seven informal units (Fig. 1.3). Within this region, paleontological and sedimentary evidence indicate that the Fort Hays was initially deposited in water depths of 15–50 m and that the water column progressively deepened with the Niobrara transgression to water depths of 150–300 m during Smoky Hill deposition (Hattin, 1982). The Niobrara Formation includes several intervals of elevated organic carbon sedimentation and several possible "OAE 3 intervals" were identified based on carbon isotope stratigraphy (Pratt et al., 1993; Locklair et al., 2011). The main OAE 3 interval assigned by Locklair et al. (2011) and subsequently used by Joo and Sageman (2014) occurred during the Middle Coniacian *Scaphites depressus* biozone (Fig. 1.3).

Age (Ma)	Stage		Biozone		Pueblo reference section		Sweetgrass Arch	
83	CAMPANIAN	Lower	Scaphites hippocrepis III		Niobrara Foratmion	Smoky Hill Chalk	Niobrara Foratmion	First White Specks
			Scaphites hippocrepis II					
			Scaphites hippocrepis I					
84			Scaphites lee III					
	SANTONIAN		Desmoscaphites bassleri (Marsupites testudinarius)					Medicine Hat
85			Desmoscaphites erdmanni					
			Clioscaphites choteauensis					
86			Clioscaphites vemiformis					
		L	Clioscaphites saxitonianus					Verger
87	CONIACIAN	Upper	Scaphites depressus					
88								
		M	Scaphites ventricosus					
89		Lower	Scaphites preventricosus					
			Scaphites mariasensis			Fort Hays Limestone		
90	TURONIAN	Upper	Prinocyclus germari					Carlile Shale
			Scaphites nigricollensis Scaphites whitfieldi		Carlile Shale			
91		Middle	Inoceramus dimidius	S. ferronensis S. warreni P. macombi				
			Inoceramus howelli	Prionocyclus hyatti C. praecox				
92			Collignoniceras woollgari				Second White Specks	
					Greenhorn Formation			

Figure 1.3

Stratigraphy of the Pueblo reference section (equivalent to the USGS Portland #1 core) and the Sweetgrass Arch region.

In the Sweetgrass Arch region of S. Alberta, the Niobrara is divided into three formal members: the Verger Member, the Medicine Hat Member and the First White Specks Member (Fig. 1.3; Nielsen et al., 2003). The basal Verger Member is a non-calcareous shale with several minor sandstone beds (Nielsen et al., 2003). The Medicine Hat Member consists of fine-grained sandstones interbedded with shales and siltstones (Nielsen et al., 2003). These sandstones are thought to have been deposited as offshore sandbars on the uplifting Sweetgrass Arch (Nielsen et al., 2008). The First White Specks Member is a dark gray, calcareous shale with abundant

8

laminae of fecal pellets rich in nannofossils (Nielsen et al., 2003). During the Turonian-Campanian, water depths at the core sites are thought to vary from 10–30 m at sea level lowstand to 50–100 m during sea level highstand (Nielsen et al., 2008). While, no OAE 3 interval has been identified within the Sweetgrass Arch region, OAE 3 was identified in east central Alberta at Cold Lake (Schröder-Adams et al., 2012).

1.3 Structure of the dissertation

This dissertation includes four data chapters (Chapters 2–5) preceded by this introductory chapter and followed by a conclusions chapter (6), which summarizes the major results and discusses future directions. In Chapter 2 (Tessin et al., 2015), I investigate whether the development of anoxia plays a primary role in enhancing organic carbon preservation. To address this, I determined the amount and composition of organic matter preserved, as well as the geochemical conditions under which it accumulated before, during and after OAE 3 in central Colorado (USGS #1 Portland core). Redox conditions are reconstructed using a suite of redox-sensitive trace metals (Fig. 1.1; Mo, Mn, and Re). Comparison of trace metal and organic results allows for the relationship between evolving redox conditions and organic preservation before, during and after OAE 3. Chapter 3 (Tessin et al., in prep) further explores changes in organic matter source preservation based using hydrocarbon biomarkers and compound specific carbon isotope analyses.

Chapter 4 (Tessin et al., 2016) of this dissertation evaluates if changing Fe chemistry exerted a control on organic matter preservation and/or primary productivity during and after OAE 3 in the Portland core (Chapter 2–3). Changes in the delivery and availability of reactive Fe have been suggested as a significant feedback for organic carbon production and preservation

(e.g. Meyers, 2007). Iron limitation can reduce sedimentary sulfide buffering and phosphorus trapping in sediments (Meyers, 2007). This would subsequently cause elevated primary productivity due to phosphorus remineralization. Additionally organic matter preservation would be enhanced due to a reduction in bioturbation within the sediments. In Chapter 4, I present Fe speciation results to evaluate changes in Fe availability and reactivity. These Fe proxies have additionally been used to evaluate paleo-redox conditions (Fig. 1.1). Iron results are compared to P and S results to determine the effect of changing Fe chemistry on nutrient recycling and organic matter preservation.

While Chapters 2–4 comprise a detailed reconstruction of the organic matter preserved in the USGS Portland core and the geochemical conditions under which it accumulated, Chapter 5 (Tessin et al., in prep) investigates records from southern Canada to assess if a single driving mechanism can explain the onset of enhanced organic carbon throughout the WIS during the Coniacian-Santonian. New trace metal and Fe geochemical records are paired with foraminiferal results from two cores taken from the Sweetgrass Arch region in SE Alberta (13-20-17-7W4 and 16-4-22-15W4). Using ammonite and inoceramid biostratigraphy, records from Alberta are biostratigraphically correlated to results from Colorado (including the Portland core), allowing for the timing and intensity of anoxia and organic carbon burial to be compared between the northern and southern portions of the seaway before, during, and after OAE 3.

1.4 References

Arthur, M. A., and B. B. Sageman (1994), Marine black shales--depositional mechanisms and environments of ancient deposits, *Annual Review of Earth and Planetary Sciences*, *22*, 499–551.

Arthur, M. A., S.O. Schlanger, and H.C. Jenkyns (1987), The Cenomanian-Turonian Oceanic Anoxic Event, II, Paleoceanographic controls on organic matter production and preservation, in *Marine Petroleum Source Rocks, Geological Society of London Special Paper*, edited by J. a. A. F. Brooks, pp. 401–420.

Beckmann, B., T. Wagner, and P. Hofmann (2005), Linking Coniacian-Santonian (OAE 3) black shale deposition to African climate variability: a reference section from the eastern tropical Atlantic at orbital time scales (ODP 959, off Ivory Coast and Ghana), in *Deposition of Organic-Carbon-Rich Sediments: Models, Mechanisms, and Consequences*, edited by N. B. Harris, pp. 125–143.

Blatter, C., H. Jenkyns, L. Reynard, G. Henderson (2011), Significant increases in global weathering during Oceanic Anoxic Events 1a and 2 by calcium isotopes, *Earth and Planetary Science Letters 309,* 77–88.

Cai, W-J, G. Laruelle, X. Hu, and P. Regnier (2015), Ocean margins as an increasing sink for the atmospheric carbon dioxide, in *NASA Carbon Cycle & Ecosystems Joint Science Workshop.*

Coulson, A.B., M. J. Kohn, and R. E. Barrick (2011), Isotopic evaluation of ocean circulation in the Late Cretaceous North American seaway, *Nature Geoscience 4,* 852–855.

Du Vivier, A. D. C., D. Selby, B. B. Sageman, I. Jarvis, D. R. Groecke, and S. Voigt (2014), Marine Os-187/Os-188 isotope stratigraphy reveals the interaction of volcanism and ocean circulation during Oceanic Anoxic Event 2, *Earth and Planetary Science Letters*, *389*, 23–33.

Floegel, S., W. W. Hay, R. M. DeConto, and A. N. Balukhovsk (2005), Formation of sedimentary bedding couplets in the Western Interior Seaway of North America - implications from climate system modeling, *Palaeogeography Palaeoclimatology Palaeoecology*, *218*(1-2), 125–143.

Friedrich, O., R. Norris, and J. Erbacher (2012), Evolution of middle to Late Cretaceous oceans—A 55 m.y. record of Earth's temperature and carbon cycle, *Geology 40,* 107–110.

Haq, B.U. (2014), Cretaceous eustasy revisited, *Global and Planetary Change, 113*, 44–58. http://dx.doi.org/10.1016/j.gloplacha.2013.12.007 -.

Hattin, D.E., 1982. Stratigraphy and depositional environment of Smoky Hill Chalk Member, Niobrara Chalk (Upper Cretaceous) of the type area, Western Kansas. *Kansas Geological Society Bulletin* 225, 108 p.

Hofmann, P., T. Wagner, and B. Beckmann (2003), Millennial- to centennial-scale record of African climate variability and organic carbon accumulation in the Coniacian-Santonian eastern tropical Atlantic (Ocean Drilling Program Site 959, off Ivory Coast and Ghana), *Geology*, *31*(2), 135–138.

Jarvis, I., J. S. Lignum, D. R., Grocke, H. C. Jenkyns, and M. A. Pearce (2011) Black shale deposition, atmospheric CO_2 drawdown, and cooling during the Cenomanian-Turonian Oceanic Anoxic Event, *Paleoceanography, 26* (3).

Jenkyns, H. C. (2010), Geochemistry of oceanic anoxic events, *Geochemistry Geophysics Geosystems*, *11*.

Joo, Y. J., and B. B. Sageman (2014), Cenomanian to Campanian carbon isotope chemostratigraphy from the Western Interior Basin, USA, *Journal of Sedimentary Research*, *84*(7), 529–542.

Kauffman, E. G. (1977), Geological and biological overview: Western Interior Cretaceous Basin, in *Cretaceous Facies, Faunas and Paleoenvironments across the Western Interior Basin*, edited by E. G. Kauffman, pp. 75–99, Mountain Geologist.

Kraal, P., C. P. Slomp, A. Forster, M. M. M. Kuypers (2010), Phosphorus cycling from the margin to abyssal depths in the proto-Atlantic during oceanic anoxic event 2, *Palaeogeography Palaeoclimatology Palaeoecology 295* (1), 42–54.

Kuypers, M. M. M., R. D. Pancost, and J. S. S. Damste (1999), A large and abrupt fall in atmospheric CO2 concentration during Cretaceous times, *Nature 399*, 342–345.

Locklair, R., B. Sageman, and A. Lerman (2011), Marine carbon burial flux and the carbon isotope record of Late Cretaceous (Coniacian-Santonian) Oceanic Anoxic Event III, *Sedimentary Geology*, *235*(1-2), 38–49.

Marz, C., S. W. Poulton, B. Beckmann, K. Kuester, T. Wagner, and S. Kasten (2008), Redox sensitivity of P cycling during marine black shale formation: Dynamics of sulfidic and anoxic, non-sulfidic bottom waters, *Geochimica Et Cosmochimica Acta*, *72*(15), 3703–3717.

McNeil, D.H., Caldwell, W.G.E. (1981), Cretaceous rocks and their foraminifera in the Manitoba Escarpment, *Geological Association of Canada Special Paper*, vol. 21.

Monteiro, F., R. Pancost, A. Ridgwell, Y. Donnadieu (2012), Nutrients as the dominant control on the spread of anoxia and euxinia across the Cenomanian-Turonian oceanic anoxic event (OAE2): Model-data comparison, *Paleoceanography 27* (4).

Mort, H. P., T. Adatte, K. B. Follmi, G. Keller, P. Steinmann, V. Matera, Z. Berner, and D. Stuben (2007), Phosphorus and the roles of productivity and nutrient recycling during oceanic anoxic event 2, *Geology, 35,* 483–486.

Muller-Karger, F. E., R. Varela, R. Thunell, R. Luerssen, C. M. Hu, and J. J. Walsh (2005), The importance of continental margins in the global carbon cycle, *Geophysical Research Letters*, *32*(1).

Nielsen, K.S., Schröder-Adams, C.J., Leckie, D.A. (2003), A new stratigraphic framework for the Upper Colorado Group (Cretaceous) in southern Alberta and southwestern Saskatchewan, Canada, *Bulletin of Canadian Petroleum Geology 51* (3), 304–346.

Nielsen, K.S., Schröder-Adams, C.J., Leckie, D.A., Haggart, J.W., Elderbak, K (2008), Turonian to Santonian paleoenvironmental changes in the Cretaceous Western Interior Sea: The Carlile and Niobrara formations in southern Alberta and southwestern Saskatchewan, Canada, *Palaeogeography, Palaeoclimatology, Palaeoecology 270*, 64–91.

Pogge von Strandmann P.A.E., Jenkyns H.C., Woodfine R.G. (2013), Lithium isotope evidence for enhanced weathering during Oceanic Anoxic Event 2, *Nature Geoscience 6*, p. 668–672.

Poulsen, C. J., E. J. Barron, W. H. Peterson, P. A. Wilson (1999), A reinterpretation of mid-Cretaceous shallow marine temperatures through model-data comparison, *Paleoceanography 14* (6), 679–697.

Pedersen, T.F., and Calvert, S.E. (1990), Anoxia vs. Productivity: What Controls the Formation of Organic-Carbon-Rich Sediments and Sedimentary Rocks?, *American Association for Petroleum. Geologists Bulletin., 74,* p. 454–466.

Pratt, L. M., M. A. Arthur, W. E. Dean, P. A. Scholle (1993), Paleo-oceanographic Cycles and Events during the Late Cretaceous in the Western Interior Seaway of North America, in *Evolution of the Western Interior Basin*, edited by W. G. E. Caldwell and E. G. Kauffman, pp. 333-354, GAC Special Paper.

Sageman, B. B., S. R. Meyers, M. A. Arthur (2006), Orbital time scale and new C-isotope record for Cenomanian-Turonian boundary stratotype, *Geology 34* (2), 125–128.

Sageman, B. B. S., B. S.; Meyers, S. R.; Siewart, S. E.; Walaszczyk, I.; Condon, D. J.; Jicha, B. R.; Obradovich, J. D.; Sawyer, D. A. (2014), Integrating 40Ar/39Ar, U-Pb, and astronomical clocks in the Cretaceous Niobrara Formation, Western Interior Basin, USA, *Geological Society of America Bulletin*, *7-8*, 956–973.

Schlanger, S. O., and H. C. Jenkyns (1976), Cretaceous Oceanic Anoxic Events: Causes and consequences, *Geologie en Mijnbouw*, *55*(3-4), 179–184.

Schlanger, S. O., M. A. Arthur, H. C. Jenkyns, P. A. Scholle (1987), The Cenomanian-Turonian Oceanic Anoxic Event, I. Stratigraphy and distribution of organic carbon-rich beds and the marine δ^{13}C excursion, *Geological Society, London, Special Publications 26* (1), 371–399.

Schröder-Adams, C.J., Herrle, J.O., and Tu, Q. (2012), Albian to Santonian carbon isotope excursions and faunal extinctions in the Canadian Western Interior Sea: recognition of eustatic sea-level controls on a forebulge setting. *Sedimentary Geology 281*, 50–58.

Scott, G. R., and W. A. Cobban (1964), Stratigraphy of the Niobrara Formation at Pueblo, Colorado, *Professional Papers US Geological Survey*, *454-L*, L1-L30.

Shurr, G.W., Rice, D.D. (1986), Paleotectonic controls on deposition of the Niobrara Formation, Eagle Sandstone, and equivalent rocks (Upper Cretaceous), Montana and South Dakota. In: Peterson, J.A. (Ed.), *Paleotectonics and sedimentation in the Rocky Mountain region. Memoir*, vol. 41. American Association of Petroleum Geologists, pp. 193–211.

Sinninghe Damsté J.S., van Bentum E.C., Reichart G.-J., Pross J., Schouten S. (2010), A CO_2 decrease-driven cooling and increased latitudinal temperature gradient during the mid-Cretaceous Oceanic Anoxic Event 2, *Earth and Planetary Science Letters 293*, 97–103.

Slingerland, R., Kump, L.R., Arthur, M.A., Fawcett, P.J., Sageman, B.B., Barron, E.J. (1996), Estuarine circulation in the Turonian Western Interior Seaway of North America, *Geological Society of America Bulletin 108* (7), 941–952.

Smith, R., T. Bianchi, M. Allison, C. Savage, and V. Galy (2015), High rates of organic carbon burial in fjord sediments globally, *Nature Geoscience 8*, 450–453.

Tessin, A., I. Hendy, N.D. Sheldon, B. Sageman (2015), Redox-controlled preservation of organic matter during "OAE 3" within the Western Interior Seaway, *Paleoceanography 30* (6), 702–717.

Tessin, A., N.D. Sheldon, I. Hendy, and A. Chappaz (2016), Iron limitation in the Western Interior Seaway during the Late Cretaceous OAE 3 and its role in phosphorus recycling and enhancing organic matter preservation. *Earth and Planetary Science Letters 449*, 135–144.

Tessin, A., N.D. Sheldon, I. Hendy, K. Elderbak, and C. Schroder-Adams. Biological and geochemical evidence for the development of anoxia in Alberta during Oceanic Anoxic Event 3. To be submitted to *Palaeogeography, Palaeoclimatology, Palaeoecology*.

Tessin, A., T. Bianchi, I. Hendy, N.D. Sheldon, J. Hutchings, E. Arnold, and M. Shields. Organic geochemistry of the Western Interior Seaway during Oceanic Anoxic Event 3. To be submitted to *Palaeogeography, Palaeoclimatology, Palaeoecology*.

Tissot, B. (1979), Effects on prolific petroleum source rocks and major coal deposits caused by sea-level changes *Nature 277*, 463–465.

Tsikos, H., H.C. Jenkyns, B. Walsworth-Bell, M. R. Petrizzo, A. Forster, S. Kolonic, W. Erba, I. Premoli Silva, M. Baas, T. Wagner, J. Sinninghe Damste (2004) Carbon-isotope stratigraphy recorded by the Cenomanian-Turonian oceanic anoxic event: correlation and

implications based on three key-localities, *Journal of the Geological Society 161,* 711–720.

Van Helmond, N., A. Sluijs, G-J Reichart, J. Sinninghe Damste, C. Slomp, and H. Brinkhuis (2014), A perturbed hydrological cycle during Oceanic Anoxic Event 2, *Geology 42* (2), 123–126.

Voigt, S., Flogel, S. & Gale, A. S. (2004), Midlatitude shelf seas in the Cenomanian-Turonian greenhouse world: Temperature evolution and North Atlantic circulation. *Paleoceanography 19*, doi:10.1029/2004PA001015.

Wagner, T., J. S. S. Damste, P. Hofmann, and B. Beckmann (2004), Euxinia and primary production in Late Cretaceous eastern equatorial Atlantic surface waters fostered orbitally driven formation of marine black shales, *Paleoceanography*, *19*(3).

Wagreich, M. (2012), "OAE 3" --regional Atlantic organic carbon burial during the Coniacian-Santonian, *Climate of the Past*, *8*, 1447–1455.

Watkins, D. K. (1986), Calcareous nannofossil paleoceanography of the Cretaceous Greenhorn Sea, *Geological Society of America Bulletin 97*, 1239–1249.

Wignall, P.B. (1994), *Black Shales,* Claredon Press, 127 pp.

Williams, P., Lyle, D. (2011), Bring in the Rig, in Estes-Jackson, J.E., Anderson, D.S., ed., in *Revisiting and Revitalizing the Niobrara in the Central Rockies*: Denver, CO, Rocky Mountain Association of Geologists, p. 33–40.

Chapter 2

Redox controlled preservation of organic matter during "OAE 3" within the
Western Interior Seaway

2.0 Abstract

During the Cretaceous, widespread black shale deposition occurred during a series of
Oceanic Anoxic Events (OAEs). Multiple processes are known to control the deposition of
marine black shales, including changes in primary productivity, organic matter preservation and
dilution. OAEs offer an opportunity to evaluate the relative roles of these forcing factors. The
youngest of these events – the Coniacian to Santonian OAE 3 – resulted in a prolonged organic
carbon burial event in shallow and restricted marine environments including the Western Interior
Seaway (WIS). New high-resolution isotope, organic and trace metal records from the latest
Turonian to early Santonian Niobrara Formation are used to characterize the amount and
composition of organic matter preserved, as well as the geochemical conditions under which it
accumulated. Redox sensitive metals (Mo, Mn, Re) indicate a gradual drawdown of oxygen
leading into the abrupt onset of organic carbon rich (up to 8%) deposition. High Hydrogen
Indices (HI) and organic carbon to total nitrogen ratios (C:N) demonstrate that the elemental
composition of preserved marine organic matter is distinct under different redox conditions.
Local changes in $\delta^{13}C$ indicate that redox controlled early diagenesis can also significantly alter
$\delta^{13}C_{org}$ records. These results demonstrate that the development of anoxia is of primary

importance in triggering the prolonged carbon burial in the Niobrara Formation. Sea level reconstructions, $\delta^{18}O$ results, and Mo/TOC ratios suggest that stratification and enhanced bottom water restriction caused the drawdown of bottom water oxygen. Increased nutrients from benthic regeneration and/or continental runoff may have sustained primary productivity.

2.1 Introduction

Over the many years of research on black shale deposition, a primary goal has been identification of the key mechanism(s) responsible for organic matter burial rates sufficient to produce these important facies. As with so many other issues, the tendency to dichotomize has been attractive, and thus, following the seminal work of Demaison and Moore (1980) and Pedersen and Calvert (1990) on organic-rich sedimentation, "production vs. preservation" dominated the discussion for many years. More recent efforts to develop a comprehensive model have argued that at least three major factors play key roles in the development of organic carbon-rich black shales: rate of export production, rate of organic matter decomposition during early burial (in particular, oxygen exposure time: Hartnett et al., 1997), and rate of organic matter dilution by other sedimentary materials (e.g., Sageman and Lyons, 2003; Bohacs et al., 2005; Sageman et al., 2014). Together these factors likely account for most organic matter burial in marine and lacustrine deposits, although there may be variations in the relative contribution of each, and in some cases additional influences, such as mineral surface area, may play a contributing role (e.g., Kennedy et al., 2002; Kennedy and Wagner, 2011). Nonetheless, reduced benthic oxygen levels, whether a consequence of hydrographic factors such as water column stratification, or enhanced consumption due to extreme export production, appear to be a consistent feature.

17

Mesozoic ocean anoxic events, the canonical examples of oxygen depletion and massive

organic matter accumulation, were first defined almost forty years ago, when black shales were

discovered in stratigraphic intervals of deep-sea cores suggesting widespread anoxic deposition

in the marine realm (Schlanger and Jenkyns, 1976). Although only two of the designated

Mesozoic OAEs have proven to be consistently expressed globally (OAE 1a and OAE 2), the

term has been applied to as many as nine intervals during the late Jurassic to early Cenozoic

(Jenkyns, 2010). Because the individual events differ in duration, expression, and geographic

extent, most likely because they are triggered by different environmental conditions and

depositional mechanisms, they offer an opportunity to deconvolve the relative roles of these

forcing factors more effectively.

Coniacian-Santonian-age black shales represent one of the non-global OAEs, termed OAE 3

(e.g., Locklair et al., 2011; Wagreich, 2012). It is unlike the quintessential Cenomanian-Turonian

boundary event (C-T OAE 2), which is clearly defined by black shales in many localities

(Schlanger et al., 1987; Tsikos et al., 2002), and has a distinctive and relatively short-lived (~600

ka: Sageman et al., 2006) positive carbon isotope excursion that is expressed almost everywhere

in the world that C-T deposits are preserved (Arthur et al., 1987; Jenkyns, 2010). In contrast,

organic carbon-rich sedimentation during OAE 3 was restricted to the equatorial Atlantic and

adjacent continental shelves and seaways (e.g., Hofmann et al., 2003; Wagner et al., 2004;

Beckmann et al., 2005; Marz et al., 2008; Locklair et al., 2011), including the North American

Western Interior Seaway (WIS), with an absence of significant black shale deposition in the

Tethys and Pacific basins (Arthur and Sageman, 1994; Jenkyns, 2010; Wagreich, 2012). In

localities where Coniacian-Santonian organic-rich strata have been found, the age and duration

of carbon burial varies considerably, further complicating the identification of the event

(Locklair et al., 2011). In some regions, including the WIS, organic carbon burial rates were roughly double that of OAE 2 and carbon burial persisted for a significantly longer duration (>3 Myrs), indicating that despite the lack of global organic carbon burial, OAE 3 represents a significant carbon cycle perturbation (Locklair et al., 2011; Wagreich 2012). While the triggering mechanisms and feedbacks of short-lived, near-global OAEs, such as OAE 2, have become increasingly well understood (e.g., Turgeon and Creaser, 2008; Duvivier et al., 2014), the prolonged period of carbon burial within the WIS during the Coniacian-Santonian requires different depositional mechanisms. Under modern climatic conditions, organic carbon burial in similar shallow marine environments plays an important role in the global carbon cycle with >40% of marine organic carbon sequestration occurring on continental margins (Muller-Karger et al., 2005). Therefore, while Coniacian-Santonian carbon burial may not manifest in the rock record as an OAE *sensu stricto*, a better understanding of such regional shallow marine carbon burial events has important implications for predicting how carbon burial in shallow marine settings may change in response to anthropogenically driven expansion of low-oxygen marine environments in response to future warming and marine eutrophication.

A better understanding of the extended period of Coniacian-Santonian black shale deposition and the role that oxygenation played requires regional records of carbon burial and redox history. Here we present high-resolution isotope, organic and trace metal records from the latest Turonian to early Santonian Niobrara Formation of the WIS to help characterize the amount and composition of organic matter preserved in the region, as well as the geochemical conditions under which it accumulated. These results allow for the evaluation of redox-controlled preservation as a potential mechanism for regional organic carbon-rich deposition in the WIS and a possible mechanism for black shales deposited in other regions and at other times.

2.2 Background

2.2.1 Geologic Setting

During Cretaceous peak highstand intervals, the WIS flooded the North American continental interior, linking the northern Boreal Sea with the Tethys Ocean to the south (Figure 2.1). The WIS formed due to glacio- and tectono-eustatic forces, as well as accommodation space created by the subsidence of a retroarc foreland related to crustal loading of the Sevier Orogenic Belt to the west (Kauffman and Caldwell, 1993). The record of the WIS includes episodic deposition of organic carbon-rich shales and chalks, including those recorded during the two maximum transgressions of the Greenhorn and Niobrara cyclothems (Kauffman, 1977). The seaway had two main sources of water: warm, saltier Tethyan waters from the south and cooler, lower salinity Boreal waters from the north (e.g., Hay et al., 1993, Fisher et al., 1994). Continental runoff from the Sevier Highlands delivered freshwater and nutrients to the seaway (e.g. Floegel et al., 2005).

The Niobrara Formation was deposited in an asymmetrical foreland basin from the Late Turonian to the Early Campanian (Scott and Cobban, 1964; Locklair and Sageman, 2008) and is formally divided into two members: the basal Fort Hays Limestone and the overlying Smoky Hill Chalk (Figure 2.2). The late Turonian-early Coniacian Fort Hays Limestone consists of ledge-forming limestone beds separated by thin organic carbon-rich shales (Scott and Cobban, 1964). The Smoky Hill Chalk consists of interbedded shales and chalks that Scott and Cobban (1964) divided into seven informal units (Figure 2.2).

Previous research on the Niobrara Formation illustrates the difficulty in identifying a single distinct carbon burial event during the Coniacian-Santonian associated with OAE 3, as there are

20
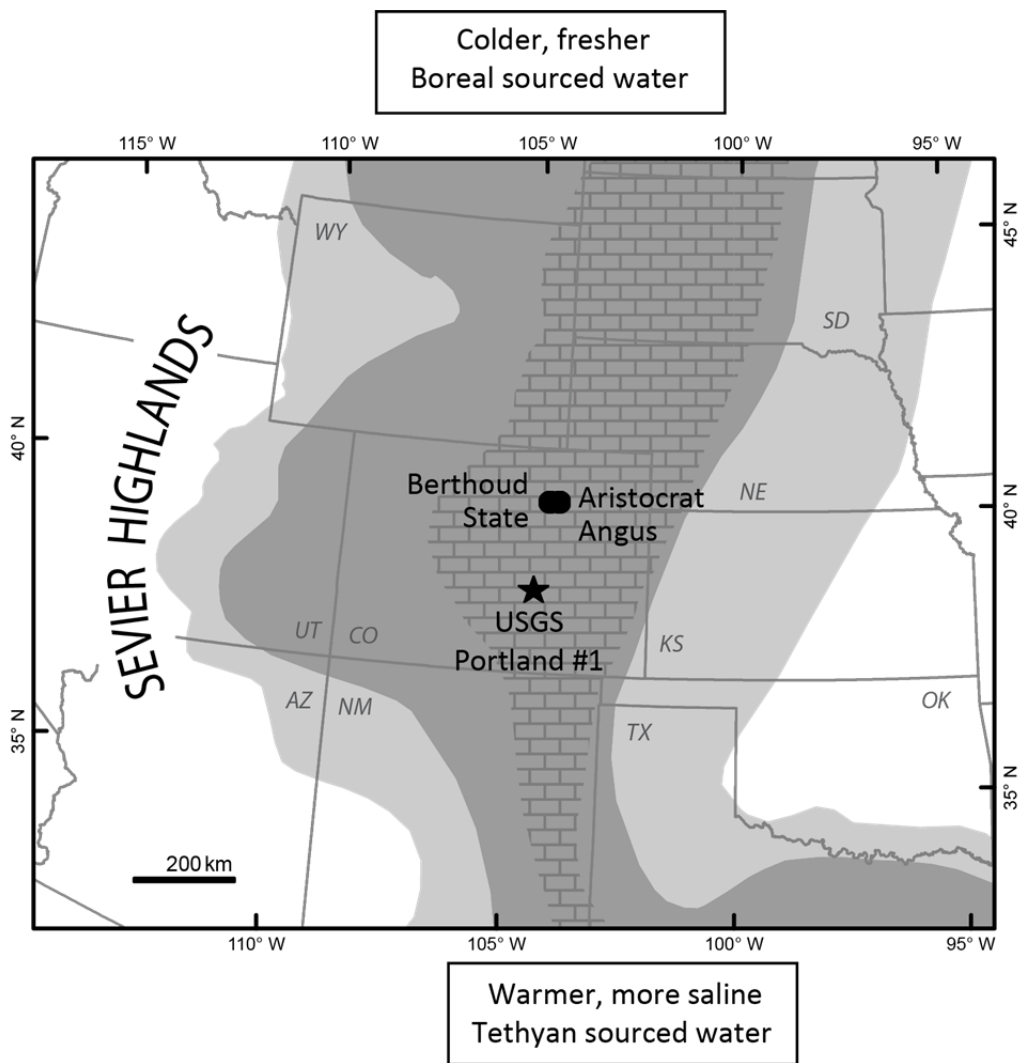
Figure 2.1
Map of the Cretaceous Western Interior Seaway (WIS) with Coniacian-Santonian paleogeography (adapted from Roberts and Kirschbaum, 1995). Dark gray represents marine shales and limestones, light gray represents the coastal plain, and white represents the alluvial plain. The USGS #1 Portland core location is marked with a star. The Berthoud State #3 and Aristocrat Angus cores are marked with circles. The Sevier Highlands are labeled to the west and the major water sources are indicated to the north and south of the WIS.

several periods of elevated organic carbon burial (Pratt et al., 1993; Locklair et al., 2011).

Locklair et al. (2011) define three possible "OAE 3 intervals" during the middle Coniacian, the

early Santonian, and at the Santonian-Campanian boundary. They assign the main OAE 3

interval to the middle Coniacian section and this designation has been used in subsequent work

(Locklair et al., 2011; Joo and Sageman, 2014). OAEs are traditionally defined by significant

21

positive global carbon isotope excursions (>2‰; Jenkyns, 2010), however, records defined as the main OAE 3 interval from the WIS and elsewhere correspond to a comparatively small (<1‰) isotope excursion (Pratt et al., 1993; Jarvis et al., 2006; Locklair et al., 2011). For these reasons, the OAE 3 designation has been debated in the literature.

2.2.2 Trace metal geochemistry

Trace metal geochemistry has been used to study the mechanisms and characteristics of organic carbon burial in modern and paleo- environments (e.g., Calvert and Pedersen, 1993; Brumsack, 2006). Molybdenum, Re, and Mn accumulate in sediments under variable redox conditions and can be used to identify differences in benthic oxygenation throughout the WIS records. Molybdenum accumulates in reducing sediments in the presence of free H_2S above a threshold concentration (Helz et al., 1996). Molybdenum concentrations enriched over background concentrations, but less than 25 ppm indicate the presence of pore water sulfide, while concentrations of greater than 100 ppm are interpreted as evidence for abundant water column sulfide. Concentrations between 25 and 100 likely indicate intermittent to persistent euxinia (Scott and Lyons, 2012). Rhenium also accumulates in reducing sediments but unlike Mo, sedimentary enrichment does not require the presence of H_2S (Crusius et al., 1996; Morford et al., 2001). As opposed to the other metals discussed here, Mn is soluble in reducing waters as Mn^{2+}, which results in sedimentary Mn depletion in reducing environments, with the exception of settings in which Mn carbonates are formed (Hild and Brumsack, 1998). Rhenium and Mo are enriched in reducing sediments and should be precipitated in sediments at different reduction potentials (Crusius et al., 1996). In oxic settings, the Re/Mo ratio will be low due to the low crustal ratio of Re/Mo. In suboxic settings, the Re/Mo ratio will be very high, due to large Re

enrichments and little to no Mo enrichment. In more reducing settings, the Re/Mo ratio will be the seawater ratio, as both Re and Mo are removed from seawater (Crusius et al., 1996). Ratios of >9 mmol mol^{-1} indicate suboxic conditions, while ratios of <9 mmol mol^{-1} indicate anoxic conditions (Crusius et al., 1996). Thus, taken together, the suite of Mo, Re, U, and Mn can be used to differentiate between oxidizing and reducing and sulfidic and non-sulfidic conditions.

2.3 Methods and materials

The Niobrara Formation within the USGS #1 Portland core was sampled at 0.5 m resolution at the USGS Core Research Center in Denver, CO (Figure 2.1). The Portland core was drilled and continuously cored in the Cañon City Basin, CO where Cretaceous strata, including half of the Niobrara Formation were collected (Dean and Arthur, 1998).

Bulk carbonate stable isotopes analyses were run on a ThermoFinnigan MAT 253 triple-collector gas source mass spectrometer coupled to a Finnegan Kiel automated carbonate device at the University of Michigan's Stable Isotope Laboratory. Isotope values were corrected to Vienna Pee Dee Belemnite using National Bureau of Standards (NBS) 19 (n= 32, $\delta^{18}O$ = -2.18 $\pm$ 0.07‰, $\delta^{13}C$ = 1.98 $\pm$ 0.07‰). Samples reproduced with average standard deviations of 0.11‰ and 0.07‰ respectively. Organic carbon isotope analyses were run on a Delta V Plus mass spectrometer at the University of Michigan's Stable Isotope Laboratory. IAEA 600 caffeine (n=9, $\delta^{13}C$ = -27.77$\pm$ 0.04‰) and IAEA-CH-6 Sucrose (n=9, $\delta^{13}C$ = -10.45$\pm$ 0.05‰) standards were used to verify isotopic values. $\Delta^{13}C$ values were calculated as:

$$\Delta^{13}C = \delta^{13}C_{carb} - \delta^{13}C_{org} \qquad (1)$$

Carbon and nitrogen concentrations were measured on a Costech ECS4010 elemental analyzer. Total organic and inorganic carbon were determined using paired acidified (organic) and unacidified (total) carbon measurements. In preparation for analysis of total organic carbon, samples were acidified in 7% HCl until all carbonate was removed. Dried samples were homogenized and loaded in tin capsules. Acetanilide standards were used to verify concentrations (n= 48, %C= 10.21 ± 0.05, %N= 71.37 ± 0.15) and 20% of sample concentrations were replicated. Replicates reproduced with average standard deviations of 0.13% and 0.05%.

RockEval pyrolysis analyses were performed at a commercial laboratory (Espitalie et al, 1977; Locklair, 2007). Hydrogen index (HI) is calculated as $(S_2*100)/TOC$ where S_2 equals the amount of hydrocarbons produced through thermal cracking of nonvolatile organic matter in mg hydrocarbons/g of rock. Oxygen index (OI) is calculated as S_3/TOC where S_3 is the amount of CO_2 produced during pyrolysis of kerogen in mg CO_2/g of rock.

Samples for major and trace element geochemistry were ground to <75 μm and homogenized in an alumina shatterbox to minimize trace element contamination. Elemental analysis was completed on samples from the Portland core at ALS Laboratories in Vancouver, BC. Whole rock samples were digested with perchloric, hydrofluoric, nitric, and hydrochloric acids. Concentrations were determined by inductively coupled plasma-atomic emission spectroscopy (ICP-AES) and inductively coupled plasma-mass spectroscopy (ICP-MS). GRM908, OREAS 90 and MRGeo08 standards were used to verify elemental concentrations. Sample replicates reproduced with average standard deviations as follows: Al = 0.09%, Mn =11 ppm, Mo = 0.21 ppm, and Re = 0.007 ppm.

Trace metal records are presented as excess concentrations, which are calculated as follows:

$$TM_{xs} = TM_{sample} - Al_{sample}(\frac{TM}{Al})_{crustal} \qquad (2)$$

where *TM* is the trace metal in question and *Al* is aluminum content. Excess concentrations are used to determine the non-lithogenic concentration of elements of interest and to compare between intervals of the core with distinctly different aluminum concentrations. This normalization is used rather than a simple ratio or enrichment factor because many of the elements studied herein have low crustal concentrations and large changes in aluminum could lead to overestimates of the change in metal enrichment (Taylor and McLennan, 1985; McLennan, 2001).

2.4 Results

2.4.1 Stratigraphy

Portland core stratigraphy is plotted in Figure 2.2. The Portland core includes the basal Fort Hays Limestone Member (FHL) and the lower shale and limestone (lsl), lower shale (ls), lower limestone (ll), and middle shale (ms) units of the Smoky Hill Chalk Member (Scott and Cobban, 1964). Turonian, Coniacian, and Santonian boundaries are assigned based on comparison to the recent integrated astrochronological and radioisotopic age model of Sageman et al. (2014). The Portland core is correlated to the Niobrara chronology using analogous lithostratigraphic units. Several possible diastems, including one at the top of the lower shale and limestone unit (LSL, Fig. 2), have been identified in the Niobrara outcrops in Pueblo, Colorado based on biostratigraphic data (Walaszczyk and Cobban, 2000, 2006, 2007). Recent astrochronological work (Locklair and Sageman, 2008) did not indicate evidence of hiatuses, but some were later identified by biostratigraphy (Walaszczyk et al., 2014), reflecting the fact that it is possible for

25

hiatuses with certain characteristics to remain undetected by spectral methods (Meyers and Sageman, 2004). Based on comparison of radioisotopically and astrochronologically derived durations spanning the proposed hiatuses of the lower Niobrara Formation, Sageman et al. (2014) concluded that their duration did not exceed 0.5 million years. If short-term hiatuses were present, the geochemical record of transitions between units would likely be sharper than the transitions actually were, but this should not alter the overall conclusions presented in this paper.

For the following discussion, three intervals are assigned based on geochemical results. In the Portland core, Interval 1 includes the FHL and the lsl member of the Smoky Hill (Figure 2.2). This unit is defined as the period before the OAE 3 positive carbon isotope plateau. Based on correlation to radioisotopically-dated sections, this interval spans the Latest Turonian to the Middle Coniacian. Interval 2 is defined as the OAE 3 positive isotope plateau and corresponds to an OAE 3 interval defined by Locklair et al. (2011). In the Portland core, this corresponds to the ls and ll units of the Smoky Hill. This interval was deposited during the Middle to Late Coniacian. While not the focus of this paper, Interval 3 is defined by the lower δ^{13}C values recorded after the OAE 3 isotope plateau and was deposited during the Santonian. In the Portland core, Interval 3 includes the ms unit of the Smoky Hill (Figure 2.2).

2.4.2 Bulk carbonate and organic δ^{13}C

Bulk carbonate and organic δ^{13}C results on the Portland core are plotted in Figure 2.2. Bulk δ^{13}C$_{carb}$ values increase by ~2‰ from the base of the Niobrara Formation during Interval 1. This isotope excursion occurs in two steps with δ^{13}C$_{carb}$ increasing throughout the Fort Hays Limestone and again leading into Interval 2. δ^{13}C$_{carb}$ values then decrease through the Coniacian-Santonian boundary with 0.5 to 1‰ positive excursions occurring at 45 and 35 m.
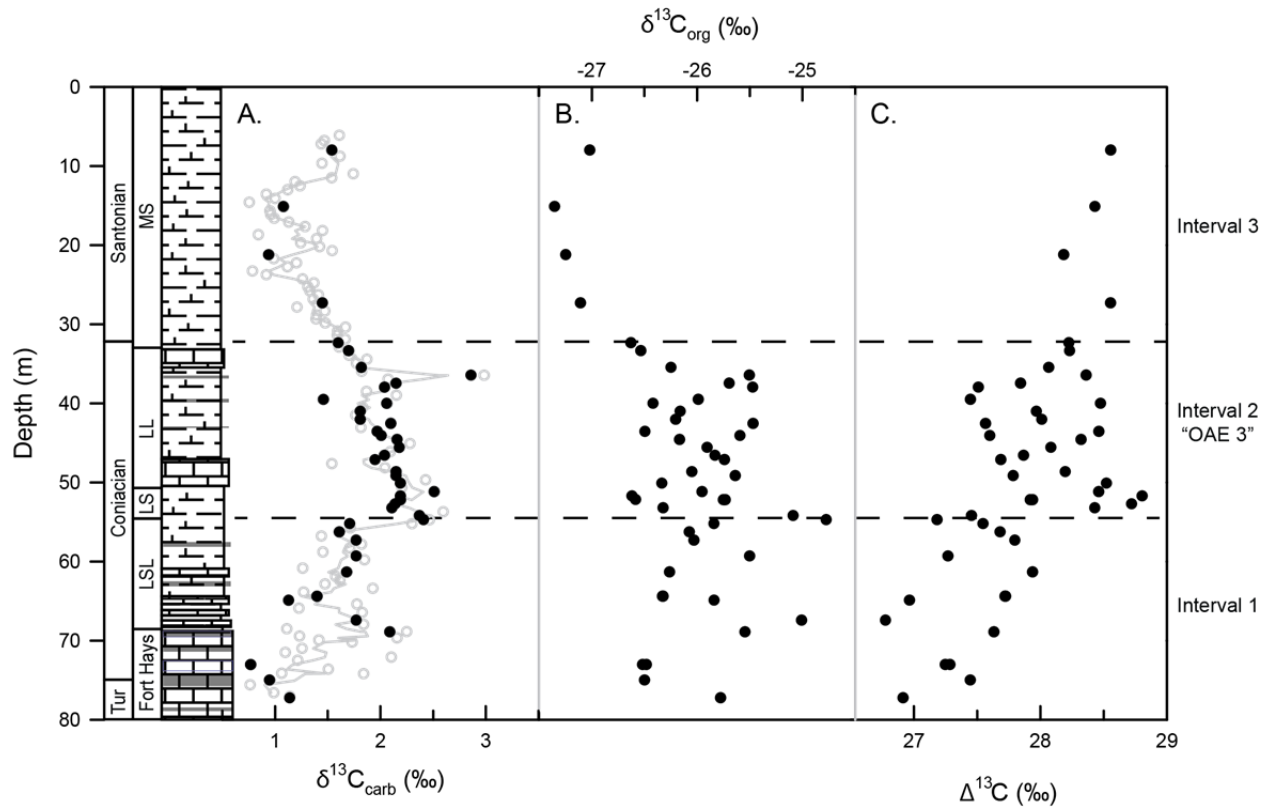
Figure 2.2
Stratigraphy and carbon isotope results from the USGS #1 Portland core. Lithostratigraphy was adapted from Dean and Arthur (1998). $\delta^{13}C_{carb}$, $\delta^{13}C_{org,}$ and $\Delta^{13}C$ records are plotted. $\delta^{13}C_{carb}$ are plotted as gray circles with a three point running average plotted as a gray line. The black symbols correspond to samples with $\delta^{13}C_{org,}$ and $\Delta^{13}C$ measurements. Dashed lines designate the three intervals studied. Interval 2 corresponds to Ocean Anoxic Event (OAE) 3 as defined by Locklair and Sageman (2011).

Bulk $\delta^{13}C_{org}$ values range between -26.6 and -27.8‰ during Intervals 1 and 2. Short-term positive excursions at 67 and 55 m, similar to those recorded in the carbonate record, are found in the $\delta^{13}C_{org}$. During Interval 3, $\delta^{13}C_{org}$ values decrease to an average of -27.1‰ (Figure 2.2). During Interval 1, $\Delta^{13}C$ values range between 26.8 and 27.9‰ with a generally increasing trend from the base to the onset of Interval 2. Above 50 m, $\Delta^{13}C$ values are consistently greater than 27.5‰ with values as high as 28.8‰.

2.4.3 TOC, CaCO$_3$, Al, and δ^{18}O

Total organic carbon (TOC), carbonate (CaCO$_3$), aluminum (Al) and δ^{18}O records for the Portland core are plotted in Figure 2.3. The new TOC results are generally consistent with previously published high-resolution data from Locklair et al. (2011). Interval 1 corresponds to relatively low TOC concentrations, generally less than 0.5%, with higher values representing thin shale interbeds (Figure 2.3). TOC increases dramatically in both cores during Interval 2. TOC concentrations during Interval 2 are characterized by two periods of TOC values >5% from 55 to 50 m and 42 to 34 m with lower concentrations in between.

In general, Al and CaCO$_3$ concentrations inversely covary (Figure 2.3). Al concentrations increase during the second half of Interval 1 and remain relatively constant throughout Interval 2 before increasing dramatically at the base of Interval 3. Intervals 1 and 2 are associated with an average CaCO$_3$ concentration of 71%. A distinct drop in the CaCO$_3$ concentration occurs at the base of Interval 3, with CaCO$_3$ concentrations averaging 39%. The greatest variability in Al and CaCO$_3$ concentrations occur during Interval 1 and is a product of the highly variable lithology found in the FHL. The characteristic rhythmic bedding within the FHL that produces variable limestone and organic-rich clay interbeds has been interpreted as either changes in dilution by riverine input or changes in carbonate productivity (i.e., Dean and Arthur, 1998; Locklair and Sageman, 2008). Values of δ^{18}O in the Portland core range from -4 to -8.5‰. Significant variability exists within the first half of Interval 1, which records the cyclic deposition of the Fort Hays. Generally, the highest values are recorded in the middle of Interval 1 with generally lower values throughout Interval 2. The average δ^{18}O values recorded during Interval 1 and Intervals 2 and 3 are -6.39‰ and 7.48‰, respectively.
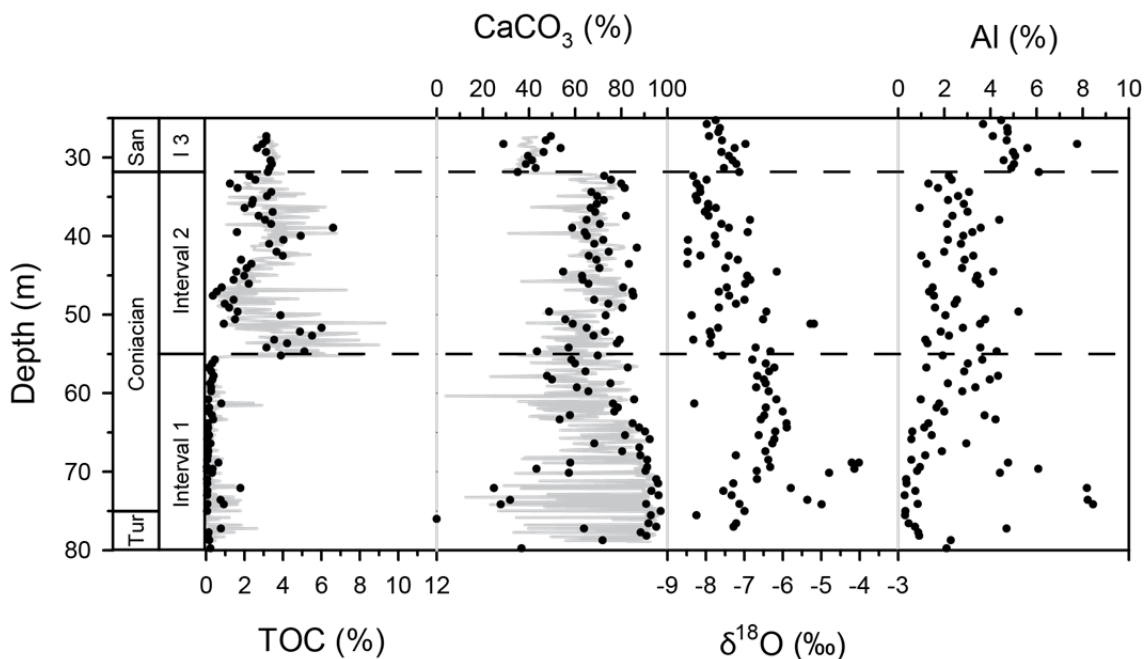
Figure 2.3
Total organic carbon, carbonate, $\delta^{18}O$ and aluminum for the Portland core are plotted. High-resolution organic carbon and carbonate data from Locklair and Sageman (2011) for the Portland core are plotted in gray and new results are plotted in black. Dashed lines indicate the correlated intervals.

2.4.4 Trace metals

Records of Mo and Re excess concentrations exhibit patterns that generally covary with the TOC record (Figure 2.4). During Interval 1, Mo and Re excess concentrations are relatively low (less than 0.5 ppm and 5 ppb, respectively). Excess concentrations of both Mo and Re increase dramatically at the base of Interval 2, with maximum excess concentrations of ~100 ppm and ~450 ppb respectively. Mo and Re excess concentrations track TOC during Interval 2, during which low TOC concentrations between 51 and 45 m correspond to excess concentrations similar to those found in Interval 1. At the base of Interval 3, Mo and Re excess concentrations decrease to intermediate values of ~20 ppm and ~120 ppb.

Re/Mo values and Mn excess concentrations trend opposite to those of Mo and Re excess
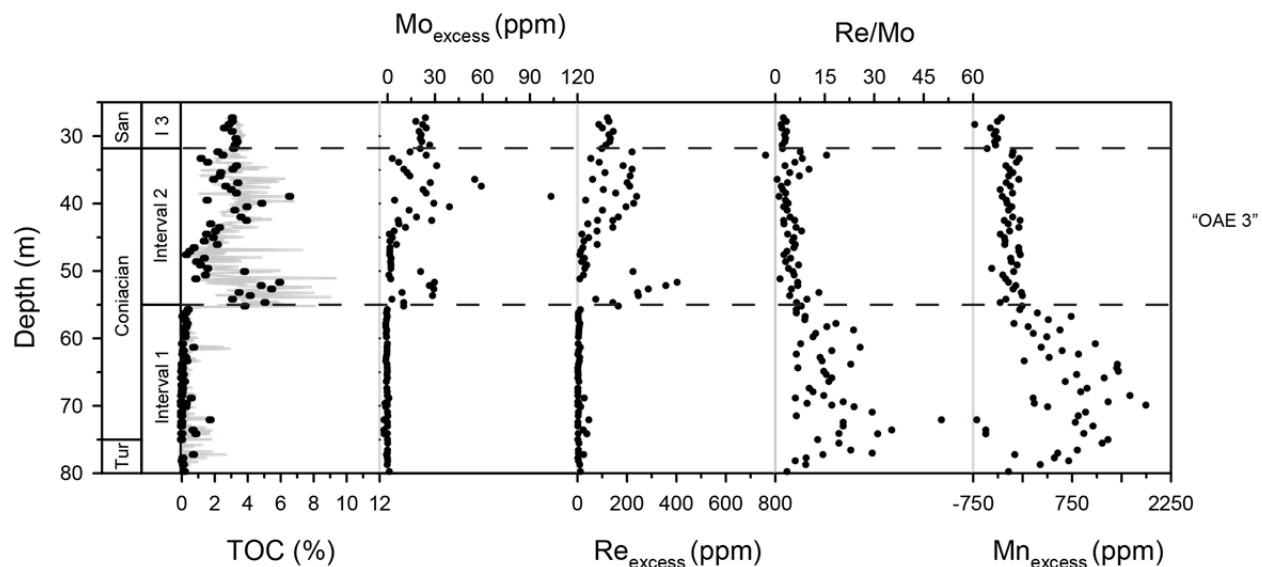
Figure 2.4
Excess concentrations of redox sensitive trace metals (Re, Mo, Re/Mo, and Mn) plotted with total organic carbon from the Portland core. High-resolution organic carbon data from Locklair and Sageman (2011) for the Portland core are plotted as gray lines and new results that are paired with trace metal concentrations are plotted as black dots. Dashed lines indicate the correlated intervals.

concentrations (Figure 2.4). During Interval 1, Re/Mo values are generally >9 mmol mol^{-1}.

Values increase from the base of Interval 1 to 72 m before decreasing to the base of Interval 2.

Throughout the rest of the records, Re/Mo values are consistently <9 mmol mol^{-1}. Manganese

excess concentrations increase from the base of Interval 1 to 70 m reaching maximum values of

~1900 ppm. Manganese excess concentrations then decrease throughout the rest of Interval 1 and

remain <0 ppm throughout the rest of the record (Figure 2.4).

2.4.5 C:N and RockEval

C:N ratios are plotted in Figure 2.5; Redfield ratio values are included as dashed lines for

comparison. The C:N record generally covaries with TOC, with high ratios corresponding to

elevated organic carbon samples. C:N values from Interval 1 average 8.4, which is within the

range expected for marine phytoplankton derived organic matter (Emerson and Hedges, 1988). However, the first half of Interval 1 records larger C:N values (mean = 10.3), as compared to the second half of Interval 1 (mean = 6.5). During Interval 2 and 3, C:N ratios average 26.6, significantly above Redfield ratio values. RockEval results from Locklair (2007) are also plotted in Figure 2.5. The H index record exhibits trends similar to the C:N record, while the O index record behaves opposite to the other organic proxies discussed here.
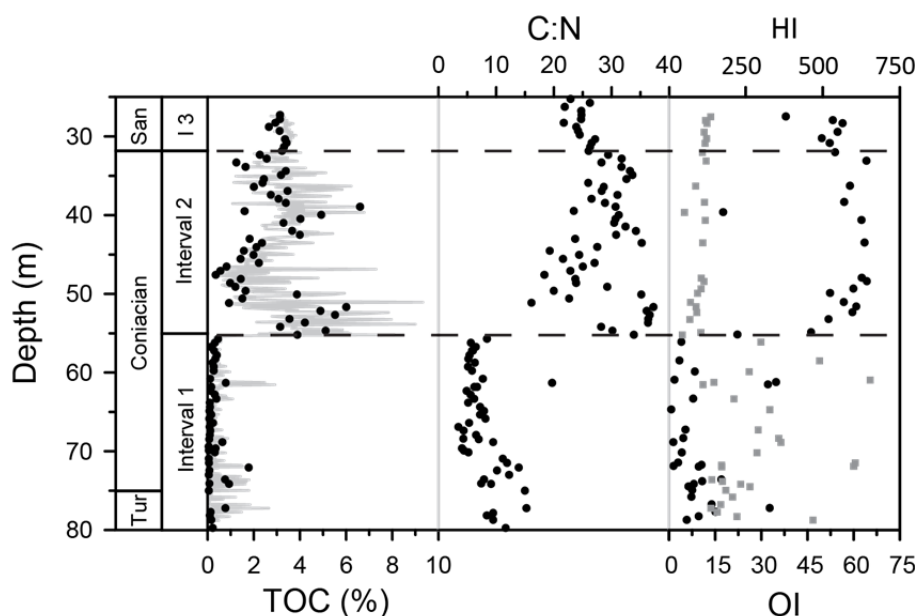
Figure 2.5
Total organic carbon (TOC), organic carbon to nitrogen (C:N) ratios, and RockEval (H-Index and O-Index) results from the Portland core. Dashed lines indicate correlated intervals.

2.5 Discussion

2.5.1 Carbon isotope stratigraphy in the Late Cretaceous

Despite the lack of global organic carbon burial, a correlative broad positive $\delta^{13}C_{carb}$ excursion associated with OAE 3 has been identified in many localities, including those that do not exhibit black shale deposition (Jenkyns et al., 1994; De Romero et al., 2003). A previously published record from the Berthoud State core demonstrates that WIS $\delta^{13}C_{carb}$ trends can be

generally correlated to records globally (Pratt et al., 1993; Wendler, 2013). The Berthoud record, however, is highly variable and must be smoothed before attempting correlation (Pratt et al., 1993; Locklair et al., 2011; Wendler, 2013). A new record presented herein from the USGS Portland core illustrates similar broad-scale trends to the Berthoud record, but provides a much less variable record for correlation, requiring less data manipulation to produce correlatable trends. The Portland record exhibits a clear two-step $\delta^{13}C_{carb}$ excursion from the base of the Fort Hays into the high organic carbon burial interval. The first step is a positive 1‰ shift, which corresponds to the onset of the Niobrara transgression (Figure 2.2). After an isotopic plateau, the $\delta^{13}C_{carb}$ record indicates a second positive 1‰ isotopic shift in the early Coniacian (Figure 2.2). This isotopic shift is coeval with the onset of regional enhanced burial of ^{13}C-depleted organic carbon and corresponds to the identified OAE 3 plateau in global and regional records Figure A.1).

High-resolution $\delta^{13}C_{org}$ isotope records from the Niobrara interval of the Portland core lack a positive isotope excursion or plateau associated with the "OAE 3" interval (Joo and Sageman, 2014). To address the inconsistency in the two reconstructions, paired $\delta^{13}C_{org}$ and $\delta^{13}C_{carb}$ data measured on the same samples are presented here (Figure 2.2). Our new $\delta^{13}C_{org}$ results similarly do not exhibit the "OAE 3" isotope plateau and instead show generally more positive values as compared to other records from the WIS (Joo and Sageman, 2014). The $\delta^{13}C_{org}$ results from the Portland core thus do not track $\delta^{13}C_{carb}$ records from the same core, or from other localities in the seaway, implying that secular changes in the marine carbon reservoir are overprinted by a local signal in the Portland $\delta^{13}C_{org}$ record. This is not the case for all $\delta^{13}C_{org}$ records within the WIS, as the record from the Aristocrat Angus Core exhibits a clearly identifiable OAE 3 excursion (Joo and Sageman, 2014). The discrepancy in the Portland $\delta^{13}C_{org}$ record is discussed further below.

2.5.2 Redox history

The Portland geochemical records indicate that Fort Hays sediments were deposited under the most oxic conditions (Figure 2.4). Low Re and Mo enrichments, high Mn concentrations, and high Re/Mo ratios indicate that the bottom waters in the WIS were well-oxygenated and that the sediments were suboxic. Isolated clay-rich interbeds within the Fort Hays contain higher concentrations of organic carbon and trace metals than the more carbonate-rich facies, consistent with brief instances of increased carbon burial and oxygen limitation. However, significant bioturbation of the limestone beds suggests moderately to well-oxygenated substrates predominated during Interval 1 (Savrda, 1998).

During the second half of Interval 1, excess Mn concentrations and Re/Mo ratios increase, indicative of expanding suboxic conditions. However, the second half of Interval 1 remained largely bioturbated, but with burrow types and sizes indicating lower levels of oxygenation than within the Fort Hays (Savrda, 1998). Notably, this gradual change in evidence for oxygen limitation is not paralleled by an increase in organic carbon or trace metal concentrations. It is not until a threshold or 'tipping-point' is reached that TOC and trace metal concentrations increase abruptly, at the onset of Interval 2 (OAE 3). The possibility of small hiatuses in the record near the transition from Interval 1 to 2 exists that may have produced the apparent abrupt "tipping point" or threshold. However, even if the transition into suboxic conditions was more gradual the overall observation does not change that a threshold oxygen concentration was reached causing a distinct increase in TOC and trace metal accumulations.

High excess trace metal concentrations (Mo and Re), low Re/Mo ratios, and Mn concentrations below background levels indicate that reducing conditions prevailed in the WIS

during both organic carbon burial peaks within Interval 2 (Figure 2.4). Mo concentrations (30–105 ppm) indicate that periods of intermittent to persistent euxinia likely occurred during the peak carbon burial (Scott and Lyons, 2012). The absence of trace fossils and the presence of laminated strata during this period indicate that low bottom water oxygen concentrations prevented macrofauna from bioturbating sediments (Savrda, 1998).

Variations in trace metal accumulation and TOC during Interval 2 suggest that there were brief periods of increased oxygenation and reduced organic carbon burial during Interval 2 (Figure 2.5). The significantly reduced trace metal accumulation, paired with indistinct laminations, which are suggestive of some bioturbation, support the conclusion that the middle of Interval 2 was associated with occasional oxygenation events of the bottom waters (Savrda, 1998). However, even within this period, TOC concentrations remain significantly above those recorded during Interval 1 (<2%), suggesting that conditions did not return to those experienced prior to OAE 3. At the onset of Interval 3, trace metals and TOC shift to values between those found in Intervals 1 and 2. Although a change in bottom water oxygenation and/or marine productivity may have occurred from Interval 2 to 3, marine environmental conditions did not return to those of Interval 1.

2.5.3 Redox controlled degradation of organic matter

The effect of oxygen availability on organic matter (OM) preservation has been a longstanding focus of black shale studies (eg. Hunt, 1996; Demaison and Moore, 1980; Pedersen and Calvert, 1994), however, the exact relationship between water column anoxia and OM preservation remains a subject of active study (eg. Heinrichs and Reeburgh, 1987; Arndt, 2013). Complications include reactivity of OM, macrofaunal processes, oxygen exposure time, and

redox oscillations (eg. Aller, 1994; Canfield, 1994, Arndt, 2013). Organic matter preservation of TOC-rich sediments deposited in the WIS during OAE 2 has been studied by focusing on the relationship between RockEval and bioturbation (Pratt, 1984), the role of sulfide formation and highly reactive iron availability (Meyers et al., 2005), and the characteristics of individual organic molecules (Hayes et al., 1989, 1990; Pancost et al., 1998). New results herein allow for the characterization of relationships between redox conditions, bioturbation, and the amount and composition of OM preserved during the prolonged organic carbon burial event recorded in the Niobrara Formation.

Observed variations in OM elemental composition (H- and O-Indices and C:N ratios) in the Portland core, most likely record variations in the mode of OM remineralization under different redox conditions (Figure 2.6a and b).Variations in the elemental composition of OM can also indicate changes in OM source (i.e. dominantly terrestrial vs. marine material; Meyers, 1994; Purdue and Koprivnjak, 2007). However, comparison of RockEval and C:N ratios within the Portland core are difficult to interpret in terms of variable influences of terrestrial OM (Figure 2.6a). For example, the high C:N ratios (up to 40) measured during Interval 2 deviate from typical marine OM and could be consistent with the signature of C3 plant OM (Meyers et al., 2006), but H and O Index values indicate a predominantly marine origin.

C:N values in the Portland core covary with redox conditions reconstructed from trace metal records (Figure 2.6). Under the well-oxygenated conditions characteristic of deposition during Interval 1, C:N values are consistent with typical marine OM, which has C:N values of 5–8 (Emerson and Hedges, 1988; Meyers, 2006). Elevated C:N values recorded during the first half of Interval 1 are associated with slightly elevated TOC and H index values and may be indicative of brief periods of minor oxygen limitation in the shale interbeds of the FHL. Upon development
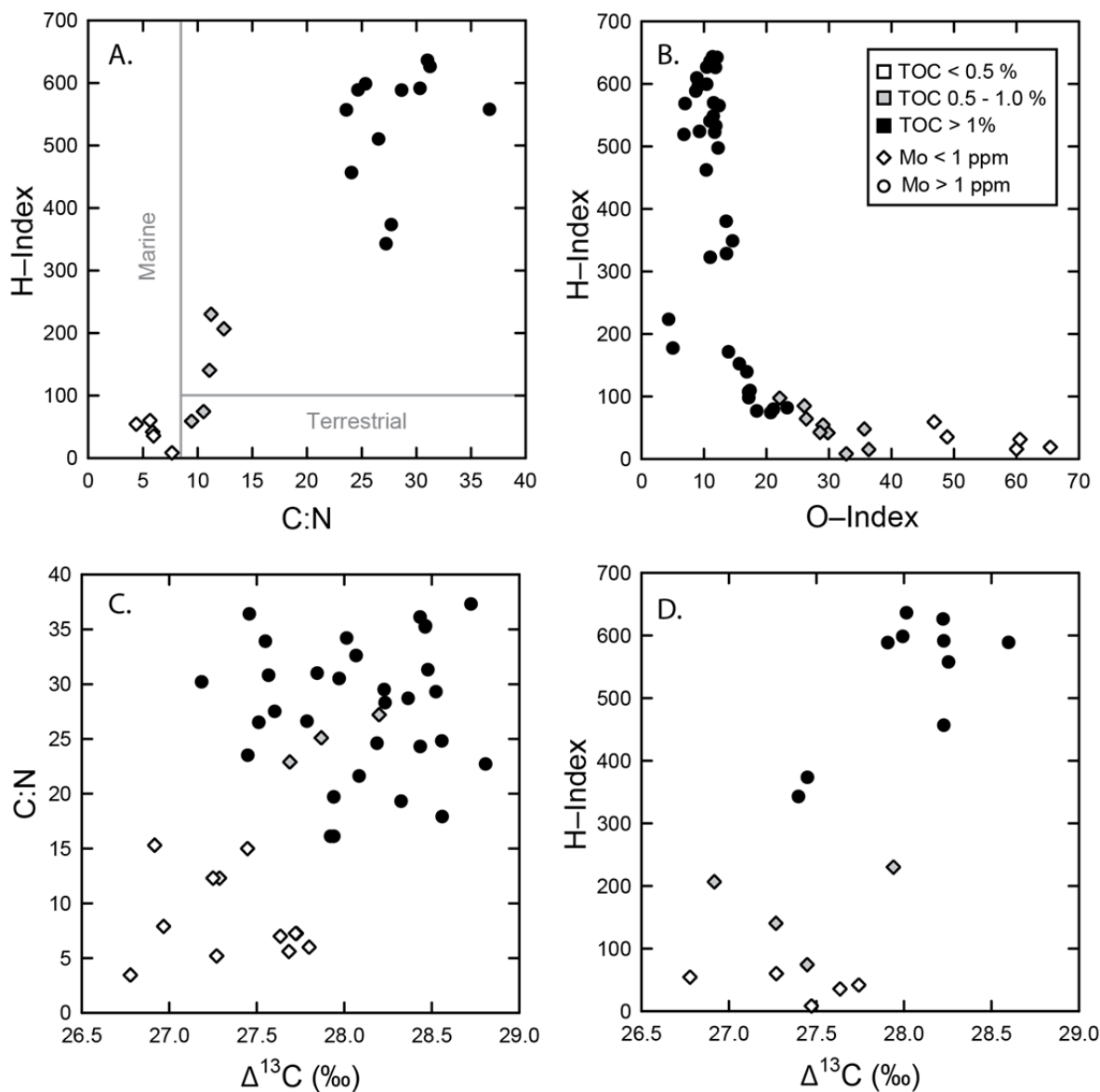
Figure 2.6
a. C:N and H-Index crossplot with typical terrestrial and marine organic matter labeled, b. H-Index and O-Index crossplot, c. C:N and Δ¹³C crossplot, and d. H-Index and Δ¹³C crossplot. Mo concentrations are plotted as diamonds (<1 ppm) or circles (>1 ppm). TOC concentrations are plotted as white (<0.5%), gray (0.5-1.0%), or black (>1.0%).

of water column anoxia, C:N ratios increase sharply to between 15 and 40, similar to elevated

C:N ratios of marine OM found in sapropels, Cretaceous black shales, and recent sediments

deposited under upwelling regions (Meyers, 2006; Junium and Arthur, 2007). Incubation

experiments and modern observations suggest that a suboxic water column affects the

composition of residual organic material as well as the rate of OM degradation, supporting

preferential degradation of N-rich proteins and preservation of N-poor lipids (Harvey et al.,

1995; Van Mooy et al., 2002). Proteins and carbohydrates are more susceptible to degradation

because they contain N and O functional groups, while lipids contain more hydrocarbon-like

carbon chains that make them less degradable (Meyers, 2014). Furthermore,, anaerobic bacteria

are less able to depolymerize certain large complex molecules including saturated hydrocarbons

and lignin than aerobic bacteria (Benner, 1984; Schink, 1988; Kristensen, 2000). Model results

indicate that complete removal of N-rich amino acids and nucleic acids can increase the C:N

ratio, but that the accumulation of marine OM with C:N ratios of >20 during the Late Cretaceous

requires an additional mechanism, such as ammonium loss under euxinic conditions (Junium and

Arthur, 2007).

RockEval results support a shift towards preferential preservation of lipids as O-poor, H-rich

organic matter characterizes Intervals 2 and 3. Similar to results from the Greenhorn Formation

(Pratt, 1984), our data from the Niobrara Formation indicate that changes in H- and O-Indices

are closely linked to changes in bioturbation. Bioturbation influences the composition of the pore

water and solid constituents in sediments when infaunal animals ventilate the substrate with

oxygen-rich waters, stimulating microbial activity (Aller, 1978; Kristensen, 2000; Zonneveld et

al., 2010). When oxygen limitation reduces macrofaunal activity, the loss of these processes

provides a positive feedback to the development of anoxia. In moderately to highly bioturbated

sections, burrowing organisms and the associated oxidative processes result in near complete

OM loss from the sediments, while poorly oxygenated conditions preserve significant hydrogen-

rich OM in laminated or microbioturbated sediments.

Comparison of C:N and RockEval results with the TOC record supports a direct effect of changing redox conditions on the amount of TOC preserved within sediments (Figure 2.6). Interval 1 is characterized by dominantly aerobic degradation of OM facilitated by significant bioturbation that removes almost all OM from the sediments. A shift occurs at the beginning of Interval 2 to anaerobic degradation of OM that coincides with the distinct increase in the amount of TOC preserved within sediments. This suggests that a shift in the mode of OM recycling acts as the trigger of black shale (>1% TOC) deposition within the Portland core, whereby OM preservation increased once a threshold redox condition was met.

2.5.4 Variations in $\Delta^{13}C$

In addition to variations in the elemental composition of organic matter, $\Delta^{13}C$ values highlight that changes in OM degradation can alter primary $\delta^{13}C_{org}$ signals (Figure 2.2). Calculation of $\Delta^{13}C$ is one approach for evaluating changes in the relationship between the isotopic records of carbonate, representing the DIC pool, and OM, representing the photosynthate pool. Several factors can influence the carbon isotope fractionation factor itself (ϵ_p), such as changes in pCO_2 or the growth rate of photosynthesizers (controlled by nutrient availability), and the preserved isotopic records may be subject to post-depositional alteration, including carbonate diagenesis affecting the $\delta^{13}C_{carb}$ record, or OM degradation, influencing the $\delta^{13}C_{org}$ record; in addition, variations in the contributions of OM from different sources can also influence the $\delta^{13}C_{org}$ signal (Popp et al.,1989; Freeman and Hayes, 1992; Hayes et al., 1999; Kump and Arthur, 1999; Kienast et al., 2001; Royer et al., 2001; Pagani et al. 2002). As such, attempts to employ $\Delta^{13}C$ as a proxy for changes in pCO_2 (e.g., Jarvis et al. 2011) require that all other potential influences be ruled out.

Although the $\delta^{13}C_{carb}$ values used in our calculation are bulk data rather than pristine shell carbonate, they are derived from chalky lithologies that are dominated by nannofossil shell material. In addition, the lack of diagenetic covariation between $\delta^{13}C_{carb}$ vs. $\delta^{18}O_{carb}$ and the presence of the OAE 3 $\delta^{13}C_{carb}$ plateau that is found in global and regional $\delta^{13}C$ records suggests that diagenesis has not significantly altered our $\delta^{13}C_{carb}$ record (Figures A.1 and A.2). There are several indications, however, that the OM record does not preserve the isotopic signature of primary photosynthate.

For example, coeval shifts in C:N ratios, H-indices, and $\Delta^{13}C$ values in the Portland core suggest that changes in redox-controlled OM degradation affected both the isotopic and elemental composition of the preserved sedimentary OM (Figure 2.6). On one hand, the oxidative degradation of OM in Interval 1 may have led to preferential preservation of material with a more positive $\delta^{13}C_{org}$ signature. On the other, preservation of H-rich OM in laminated black shale facies can produce anomalous $\delta^{13}C_{org}$ values that would influence the $\Delta^{13}C$ calculation (Joachimski, 1997). For example, marine lipids are depleted in $\delta^{13}C_{org}$ by 8–10 ‰ relative to marine carbohydrates and proteins (Degens et al., 1968) and the effect of selective diagenesis can alter $\delta^{13}C_{org}$ by 2–3 ‰ (Dean et al., 1986; Meyers 2014). Thus, the preferential preservation of H-rich OM in Interval 2 may have led to $\delta^{13}C_{org}$ values that are depleted relative to primary values. These results indicate that redox-controlled isotope effects should be considered before $\delta^{13}C_{org}$ records are used for stratigraphy or pCO_2 reconstructions.

2.5.5 Mechanisms for the development of anoxia

New results indicate that changes in redox conditions were of primary importance in the amount of OM preserved and its elemental and isotopic composition. Sediment pore water and

bottom water oxygenation distinctly changed between the three intervals highlighted in the Portland core, but multiple causes for the development of low oxygen conditions are possible. Previous work within the WIS has highlighted the importance of reduced ventilation of bottom waters (Pratt, 1984; Barron et al., 1985; Kauffman, 1988; Hay, 1993), increased oxidant demand associated with elevated export productivity (Watkins, 1989), or a combination of the two with highly productive surface waters overlying seasonally or intermittently stratified bottom waters (Tyson and Pearson, 1991; Sageman and Bina, 1997; Arthur and Sageman; 2005; Meyers et al., 2005; White and Arthur, 2006).

2.5.5.1 Stratification

Stable or seasonal stratification has been invoked as a mechanism for the development of anoxia within the WIS by many authors (e.g. Pratt, 1984; Sageman, 1989; Arthur and Sageman, 2005). Variations in sea level within the shallow WIS may have aided in the development of stratification as a deeper water column would reduce the influence of wind-driven and tidal mixing. The role of sea level on the development of stable salinity stratification has been discussed for the WIS in association with the deposition of organic carbon-rich sediments of the Greenhorn Formation. This interpretation is based on the relationship between changes in current-induced sedimentary structures, extent of bioturbation, and organic carbon accumulation (Pratt, 1984). The Niobrara Formation was deposited during the Niobrara second order marine cycle (Kauffman, 1977), which is comparable to the Greenhorn marine cycle in terms of interpreted sea level rise and flooding extent (Kauffman and Caldwell, 1993). Paleontological and sedimentary evidence indicate that the Fort Hays was initially deposited in water depths of

15–50 m and that the water column progressively deepened to water depths of 150–300 m during Smoky Hill deposition (Hattin, 1982).

Prolonged stratification within the WIS would require a significant density contrast between surface and bottom waters. New $\delta^{18}O$ results suggest that despite significant variability within the Fort Hays shale-limestone couplets, deposition during Interval 1 was generally characterized by more normal marine salinity, and deposition during Intervals 2 and 3 was characterized by comparatively reduced salinity perhaps consistent with development of a low salinity surface layer (Figure 2.3). Although new $\delta^{18}O$ results were measured on bulk carbonates, which can be susceptible to diagenetic alteration, $\delta^{18}O$ values and patterns are similar to inoceramid $\delta^{18}O$ results from nearby Lyons, CO, which indicate a shift from normal marine to more brackish conditions within the lower Smoky Hill (Pratt and Barlow, 1985). A significant freshwater contribution to water masses is supported by fossil- and biophosphate-derived oxygen isotope evidence from throughout the WIS, as well as low diversity of surface dwelling organisms (Tourtelot and Rye, 1964; Hattin, 1982; Wright, 1987; Fisher and Arthur, 2002; Coulson et al., 2011). Continental paleoprecipitation estimates suggest that the increased freshwater influence may be derived from elevated runoff from the Sevier Highlands (Retallack, 2009), while shifts to more Boreal faunal communities support dominance of fresher, northern sourced surface water (Da Gama et al., 2014). Although the freshwater influence would aid in development of stratification, previous studies from the WIS suggest that ventilation events occurred even within TOC-rich units (Sageman, 1989; Sageman and Bina, 1997), which is consistent with variability in TOC and redox indicators in the Niobrara, specifically from 45-51 m in the Portland core. However, these variations might also be caused by reduced export productivity or changes in bottom water source area and/or ventilation.

Mo/TOC ratios within the Portland core further support the development of significant bottom water restriction, as would be expected with a water column subject to frequent and/or prolonged stratification. Mo/TOC ratios have been used as a proxy for the degree of restriction in ancient silled basins based on measurements from modern silled basins including the Black Sea, Cariaco Basin, Framvaren Fjord, and Saanich Inlet (Algeo and Lyons, 2006). The average Mo/TOC ($\times 10^{-4}$) for Intervals 2 and 3 within the Portland core is 5.6 (with a range of 1.2 to 17.4). These values are most similar to those of the Framvaren Fjord (4.5 ± 1) and the Black Sea (9 ± 2), the most restricted of the modern anoxic basins studied, suggesting that the WIS experienced significant bottom water restriction throughout the period of enhanced carbon burial.

Taken together, the observations cited above suggest that stratification played an important role in Western Interior carbon burial during the Coniacian-Santonian. The Fort Hays Limestone was deposited in a shallow well-mixed and well-oxygenated water column, and under these conditions, OM was nearly completely oxidized. As the water column progressively deepened and the freshwater influence increased, significant water column stratification developed, leading to a prolonged dominance of oxygen deficiency within bottom waters. When conditions became sufficiently oxygen limited, changes in OM remineralization fueled elevated TOC accumulation within sediments.

2.5.5.2 Nutrient Input and Recycling

Studies of the Cenomanian-Turonian have argued that elevated productivity is of primary importance for the development of OAEs. Enhanced organic carbon burial in the late Cenomanian was likely initiated due to increased nutrient input from both volcanogenic and continental sources (Adams et al., 2012; Du Vivier et al., 2013). Extreme trace metal enrichment

(Brumsack, 2005; Snow et al., 2005), interpreted to reflect significant increases in volcanogenically sourced nutrients during OAE2, does not exist for the Coniacian-Santonian. However, continental runoff may have influenced nutrient availability within the seaway, as nannofossil and palynology studies from the Niobrara Formation show a relationship between increased freshwater runoff and surface water fertility, (Burns and Bralower, 2000; Da Gama et al., 2014).

Lithogenic element concentrations, such as Al, might be expected to increase with an increased flux of detrital material and nutrients to the seaway. However, interpreting Al concentrations is difficult because they are controlled by both the amount of detrital input and carbonate dilution. The relationship between Al and TOC concentrations is unclear as Al concentrations fluctuate throughout the record with no distinct change associated with the onset of organic carbon burial (Figure 2.3). Therefore, better constraints on sediment provenance, terrestrial weathering, and hydrology are required to confirm a relationship between carbon burial and terrestrially derived nutrient input into the WIS.

Changes in benthic regeneration of nutrients could also play a significant role in sustaining primary productivity. Cretaceous ocean modeling studies suggest that enhanced P regeneration from anoxic sediments facilitated black shale deposition during OAE 2 (Handoh and Lenton, 2003, Nederbragt et al., 2004, Bjerrum et al., 2006; Tsandev and Slomp, 2009), while evidence of enhanced P recycling during OAE 2 has been found from the Tethys, WIS and proto-Atlantic Ocean (Mort et al., 2007; Tsandev and Slomp, 2009; Kraal et al., 2010). Better constraints are required to assess changes in nutrient recycling within the seaway, but enhanced productivity and an increased oxidant demand could have exacerbated the oxygen limitation and the accumulation of TOC within the WIS.

2.6 Conclusions

The $\delta^{13}C_{carb}$ record from the Portland core illustrates that the bulk carbonate carbon isotope record is correlatable between regional and global records in the seaway during the Late Cretaceous. The trends within the Portland core indicate a two-step positive $\delta^{13}C_{carb}$ excursion during the Late Turonian and early Coniacian that corresponds to (1) the Niobrara sea level transgression and (2) regional carbon burial that has been previously identified as OAE 3. Calculated $\Delta^{13}C$ values indicate a decoupling between $\delta^{13}C_{carb}$ and $\delta^{13}C_{org}$ during this time.

Significant quantities of organic carbon accumulated in the Niobrara Formation, demonstrating that the WIS sustained extended periods of organic carbon burial during the Coniacian-Santonian. Records of redox sensitive metals indicate deposition within a well-oxygenated, shallow seaway during initial transgression that became increasingly oxygen limited as the water column deepened, with the onset of significant oxygen depletion preceding the onset of organic carbon burial. The abrupt shift in TOC accumulation was associated with a redox-controlled shift in OM alteration. Coupled C:N, H-Index, O-Index, and Mo results indicate a shift from dominantly aerobic degradation of OM during Interval 1 to more anaerobic degradation during Interval 2 and 3. $\Delta^{13}C$ values covary with changes in the elemental composition of OM suggesting a redox control on the decoupling of $\delta^{13}C_{carb}$ and $\delta^{13}C_{org}$ during this time, suggesting that variable redox conditions can complicate the use of $\delta^{13}C_{org}$ for stratigraphy of pCO_2 reconstructions. The correspondence between TOC, redox sensitive metals and organic proxies indicate that the redox shift caused an increase in the amount of TOC preserved in the sediments. Sea level reconstructions, $\delta^{18}O$ results, and Mo/TOC ratios suggest that stratification and bottom water restriction caused the drawdown of bottom water oxygen.

Increased nutrients from benthic regeneration, open ocean import, and/or runoff from the Sevier highlands may have helped sustain primary productivity, providing a significant oxidant demand throughout the prolonged period of organic carbon burial.

2.7 Acknowledgements

2.8 References

Adams, D. D., M. T. Hurtgen, and B. B. Sageman (2010), Volcanic triggering of a biogeochemical cascade during Oceanic Anoxic Event 2, *Nature Geoscience*, *3*(3), 201-204.

Algeo, T. J. and T. W. Lyons (2006), Mo–total organic carbon covariation in modern anoxic marine environments: Implications for analysis of paleoredox and paleohydrographic conditions, *Paleoceanography, 21(1).*

Aller RC (1978) Experimental studies of changes produced by deposit feeders on pore water, sediment and overlying water chemistry. *American Journal of Science,* 278: 1185–1234.

Aller RC (1994) Bioturbation and remineralization of sedimentary organic matter: effects of redox oscillation. *Chemical Geology,* (3–4), 331–345.

Arndt, S., B. B. Jørgensen, D. E. LaRowe, J. J. Middelburg, R. D. Pancost, P. Regnier (2013), Quantifying the degradation of organic matter in marine sediments: A review and synthesis, *Earth-science reviews 123*, 53-86.

Arthur, M. A., and B. B. Sageman (1994), Marine black shales--depositional mechanisms and environments of ancient deposits, *Annual Review of Earth and Planetary Sciences*, *22*, 499-551.

Arthur, M. A., and B. B. Sageman (2005), Sea level control on source rock development: perspectives from the Holocene Black Sea, the mid-Cretaceous Western Interior Basin of North America, and the Late Devonian Appalachian Basin, in *Deposition of Organic-Carbon-Rich Sediments: Models, Mechanisms, and Consequences*, edited by N. B. Harris, pp. 35-59.

Arthur, M. A., S.O. Schlanger, and H.C. Jenkyns (1987), The Cenomanian-Turonian Oceanic Anoxic Event, II, Paleoceanographic controls on organic matter production and preservation, in *Marine Petroleum Source Rocks, Geological Society of London Special Paper*, edited by J. a. A. F. Brooks, pp. 401-420.

Barron, E. J., M. A. Arthur, E. G. Kauffman (1985), Cretaceous rhythmic bedding sequences: a plausible link between orbital variations and climate, *Earth and Planetary Science Letters 72* (4), 327-340.

Beckmann, B., T. Wagner, and P. Hofmann (2005), Linking Coniacian-Santonian (OAE 3) black shale deposition to African climate variability: a reference section from the eastern tropical Atlantic at orbital time scales (ODP 959, off Ivory Coast and Ghana), in *Deposition of Organic-Carbon-Rich Sediments: Models, Mechanisms, and Consequences*, edited by N. B. Harris, pp. 125-143.

Benner R., Maccubbin A. E., and Hodson R. E. (1984) Anaerobic biodegradation of the lignin and polysaccharide components of lignocellulose and synthetic lignin by sediment

microflora. *Applied and Environmental Microbiology, 47*, 998 – 1004.

Bjerrum, C. J., J. Bendtsem, J. J. F. Legarth (2006), Modeling organic carbon burial during sea level rise with reference to the Cretaceous, *Geochemistry, Geophysics, Geosystems, 7*(5).

Bohacs, K.M., Grabowski, G.J., Jr., Carroll, A.R., Mankiewicz, P.J., Miskell-Gerhardt, K.J., Schwalbach, J.R., Wegner, M.B. And Simo, J.A. (2005), Production, Destruction, and Dilution— The Many Paths To Source-Rock Development, in Harris, N., ed., *The Deposition of Organic-Carbon-Rich Sediments: Models, Mechanisms, and Consequences,* SEPM Special Publication No. 82, p. 61-101.

Brumsack, H. J. (2006), The trace metal content of recent organic carbon-rich sediments: Implications for Cretaceous black shale formation, *Palaeogeography Palaeoclimatology Palaeoecology*, *232*(2-4), 344-361.

Burns, C. E., T. J. Bralower (1998), Upper Cretaceous nannofossil assemblages across the Western Interior Seaway: implications for the origins of lithologic cycles in the Greenhorn and Niobrara Formations, in *Stratigraphy and Paleoenvironments of the Cretaceous Western Interior Seaway*, edited by W. E. Dean and M. A. Arthur, pp. 227-255, SEPM Concepts in Sedimentology and Paleontology.

Calvert, S. E., and T. F. Pedersen (1993), Geochemistry of recent oxic and anoxic marine sediments--implications for the geologic record, *Marine Geology*, *113*(1-2), 67-88.

Canfield, D. E. (1994), Factors influencing organic carbon preservation in marine sediments, *Chemical Geology, 114*, 315–329.

Coulson, A. B., M. J. Kohn, and R. E. Barrick (2011), Isotopic evaluation of ocean circulation in the Late Cretaceous North American seaway, *Nature Geoscience*, *4*(12), 852-855.

Crusius, J., S. Calvert, T. Pedersen, and D. Sage (1996), Rhenium and molybdenum enrichments in sediments as indicators of oxic, suboxic and sulfidic conditions of deposition, *Earth and Planetary Science Letters*, *145*(1-4), 65-78.

Da Gama, R. O. B. P., B. Lutz, P. Desjardins, M. Thompson, I. Prince, I. Espejo (2014), Integrated paleoenvironmental analysis of the Niobrara Formation: Cretaceous Western Interior Seaway, northern Colorado, *Palaeogeography Palaeoclimatology Palaeoecology*, 413, 66-80.

De Romero, L. M., I. M. Truskowski, T. J. Bralower, J. A. Bergen, O. Odreman, J. C. Zachos, and F. A. Galea-Alvarez (2003), An integrated calcareous microfossil biostratigraphic and carbon-isotope stratigraphic framework for the La Luna Formation, western Venezuela, *Palaios*, *18*(4-5), 349-366.

Dean, W. E., M. A. Arthur, G. E. Claypool (1986), Depletion of 13 C in Cretaceous marine organic matter: Source, diagenetic, or environmental signal?, *Marine Geology, 70*(1), 119-157.

Dean, W. E. a. M. A. A. (1998), Geochemical expressions of cyclicity in Cretaceous pelagic limestone sequences: Niobrara Formation, Western Interior Seaway, in *Stratigraphy and Paleoenvironments of the Cretaceous Western Interior Seaway*, edited by W. E. Dean and M. A. Arthur, pp. 227-255, SEPM Concepts in Sedimentology and Paleontology.

Degens, E. T., M. Behrendt, B. V. Gotthardt, and E. Reppmann (1968), Metabolic fractionation of carbon isotopes in marine plankton, Deep Sea Research and Oceanographic Abstracts, 15, 11–20.

Demaison, G. J. and Moore, G. T. (1980), Anoxic Environments and Oil Source Bed Genesis, *American Association of Petroleum Geologists Bulletin, 64*, p. 1179-1209.

Du Vivier, A. D. C., D. Selby, B. B. Sageman, I. Jarvis, D. R. Groecke, and S. Voigt (2014), Marine Os-187/Os-188 isotope stratigraphy reveals the interaction of volcanism and ocean circulation during Oceanic Anoxic Event 2, *Earth and Planetary Science Letters, 389*, 23-33.

Emerson S. and Hedges J. I. (1988) Processes controlling the organic carbon content of open ocean sediments. *Paleoceanography 3*, 621–634.

Espitalie, J., J.L. Laporte, M. Madec, F. Marquis, P. Leplat, J. Paulet, and A. Boutefeu, 1977, Rapid method for source rock characterization, and for determination of their petroleum potential and degree of evolution, *Revue de l'Institut Francais du Petrole et Annales des Combustibles Liquides, v. 32*(1), p. 23-42.

Fisher, C. G., W. W. Hay, D. L. Eicher (1994), Oceanic front in the Greenhorn Sea (Late Middle through Late Cenomanian), *Paleoceanography, 9*(6), 879-892.

Fisher, C. G., and M. A. Arthur (2002), Water mass characteristics in the Cenomanian US Western Interior seaway as indicated by stable isotopes of calcareous organisms, *Palaeogeography Palaeoclimatology Palaeoecology, 188*(3-4), 189-213.

Floegel, S., W. W. Hay, R. M. DeConto, and A. N. Balukhovsk (2005), Formation of sedimentary bedding couplets in the Western Interior Seaway of North America - implications from climate system modeling, *Palaeogeography Palaeoclimatology Palaeoecology, 218*(1-2), 125-143.

Freeman, K. H., J. M. Hayes, (1992), Fractionation of carbon isotopes by phytoplankton and estimates of ancient CO_2 levels, *Global Biogeochemical Cycles, 6*(2), 185-198.

Handoh, I. C., T. M. Lenton (2003), Periodic mid-Cretaceous oceanic anoxic events linked by oscillations of the phosphorus and oxygen biogeochemical cycles. *Global Biogeochemical Cycles, 17*(1092).

Hartnett, H.E., Keil, R.G., Hedges, J.I., and Devol, A.H. (1998), Influence of oxygen exposure time on organic carbon preservation in continental margin sediments, *Nature, 391*, 572-575. doi:10.1038/35351.

Harvey H. R., Tuttl J. H., and Bell J. T. (1995) Kinetics of phytoplankton decay during simulated sedimentation: changes in biochemical composition and microbial activity under oxic and anoxic conditions. *Geochimica Et Cosmochimica Acta 59*, 3367–3377.

Hattin, D.E., 1982. Stratigraphy and depositional environment of Smoky Hill Chalk Member, Niobrara Chalk (Upper Cretaceous) of the type area, Western Kansas. *Kansas Geological Society Bulletin* 225, 108 p.

Hay, W. W., Eicher, D.L, Diner, R. (1993), Physical oceanography and water masses in the Cretaceous Western Interior Seaway, in *Stratigraphy and Paleoenvironments of the Cretaceous Western Interior Seaway*, edited by W. E. Dean and M. A. Arthur, pp. 297-318, SEPM Concepts in Sedimentology and Paleontology.

Hayes, J. M., B. N. Popp, R. Takigiku, and M. W. Johnson (1989), An isotopic study of biogeochemical relationships between carbonates and organic matter in the Greenhorn Formation, *Geochimica Et Cosmochimica Acta, 53*, 2961–2972.

Hayes, J. M., K. H. Freeman, B. N. Popp, C. H. Hoham (1990), Compound-specific isotopic analyses: a novel tool for reconstruction of ancient biogeochemical processes, *Organic Geochemistry 16* (4), 1115-1128.

Helz, G. R., C. V. Miller, J. M. Charnock, J. F. W. Mosselmans, R. A. D. Pattrick, C. D. Garner, and D. J. Vaughan (1996), Mechanism of molybdenum removal from the sea and its concentration in black shales: EXAFS evidence, *Geochimica Et Cosmochimica Acta, 60*(19), 3631-3642.

Henrichs, S. M., and W. S. Reeburgh (1987), Anaerobic mineralization of marine sediment organic matter: Rates and the role of anaerobic processes in the oceanic carbon economy, *Journal of Geomicrobiology, 5*, 191–237.

Hild, E., and H. J. Brumsack (1998), Major and minor element geochemistry of Lower Aptian sediments from the NW German Basin (core Hoheneggelsen KB 40), *Cretaceous Research, 19*(5), 615-633.

Hofmann, P., T. Wagner, and B. Beckmann (2003), Millennial- to centennial-scale record of African climate variability and organic carbon accumulation in the Coniacian-Santonian eastern tropical Atlantic (Ocean Drilling Program Site 959, off Ivory Coast and Ghana), *Geology, 31*(2), 135-138.

Hunt, J. M. (1996), Petroleum Geochemistry and Geology: New York, Freeman Press.

Jarvis, I., A. S. Gale, H. C. Jenkyns, and M. A. Pearce (2006), Secular variation in Late Cretaceous carbon isotopes: a new delta C-13 carbonate reference curve for the Cenomanian-Campanian (99.6-70.6 Ma), *Geological Magazine, 143*(5), 561-608.

Jarvis, I., J. S. Lignum, D. R., Grocke, H. C. Jenkyns, and M. A. Pearce (2011) Black shale deposition, atmospheric CO_2 drawdown, and cooling during the Cenomanian-Turonian Oceanic Anoxic Event, *Paleoceanography, 26* (3).

Jenkyns, H. C. (2010), Geochemistry of oceanic anoxic events, *Geochemistry Geophysics Geosystems, 11*.

Jenkyns, H. C., A. S. Gale, and R. M. Corfield (1994), Carbon-isotope and oxygen isotope stratigraphy of the English Chalk and Italian Scaglia and its paleoclimatic significance, *Geological Magazine, 131*(1), 1-34.

Joachimski, M. M. (1997), Comparison of organic and inorganic carbon isotope patterns across the Frasnian–Famennian boundary, *Palaeogeography, Palaeoclimatology, Palaeoecology, 132* (1), 133-145.

Joo, Y. J., and B. B. Sageman (2014), Cenomanian to Campanian carbon isotope chemostratigraphy from the Western Interior Basin, USA, *Journal of Sedimentary Research, 84*(7), 529-542.

Junium, C. K., M. A. Arthur (2007), Nitrogen cycling during the Cretaceous, Cenomanian Turonian oceanic anoxic event II, *Geochemistry, Geophysics, Geosystems, 8*(3).

Kauffman, E. G. (1977), Geological and biological overview: Western Interior Cretaceous Basin, in *Cretaceous Facies, Faunas and Paleoenvironments across the Western Interior Basin*, edited by E. G. Kauffman, pp. 75-99, Mountain Geologist.

Kauffman, E.G. (1988), Concepts and methods of high-resolution event stratigraphy, *Annual Review of Earth and Planetary Sciences, 16,* p. 605–654.

Kauffman, E. G., and W. G. E. Caldwell (1993), The Western Interior basin in space and time, in *Evolution of the Western Interior Basin*, edited by W. G. E. Caldwell and E. G. Kauffman, pp. 1 – 30, Geological Association of Canada, Toronto, Ontario.

Kennedy, MJ & Wagner, T (2011) Clay mineral continental amplifier for marine carbon sequestration in a greenhouse ocean. *Proceedings Of The National Academy Of Sciences 108*, 9776–9781.

Kennedy, MJ, Pevear, D, & Hill, R (2002) Mineral surface control of organic carbon in black shale. *Science 295*, 657–660.

Kienast, M., S. E. Calvert, C. Pelejero, J. O. Grimalt (2001), A critical review of marine sedimentary δ^{13}Corg pCO2 estimates: New palaeorecords from the South China Sea and a revisit of other low   latitude δ^{13}Corg pCO2 records, *Global Biogeochemical Cycles,*

15 (1), 113-127.

Kraal, P., C. P. Slomp, A. Forster, M. M. M. Kuypers (2010), Phosphorus cycling from the margin to abyssal depths in the proto-Atlantic during oceanic anoxic event 2, *Palaeogeography Palaeoclimatology Palaeoecology 295* (1), 42-54.

Kristensen, E. (2000), Organic matter diagenesis at the oxic/anoxic interface in coastal marine sediments, with emphasis on the role of burrowing animals, *Hydrobiologia*, 426, 1-24.

Kump, L. R., M. A. Arthur (1999), Interpreting carbon-isotope excursions: carbonates and organic matter, *Chemical Geology, 161*(1), p. 181-198.

Locklair, R.E., 2007, Causes and Consequences of Marine Carbon Burial: Examples from the Cretaceous Niobrara Formation and the Permian Brushy Canyon Formation, unpublished Ph.D. thesis, Northwestern University, 515 p.

Locklair, R., B. Sageman, and A. Lerman (2011), Marine carbon burial flux and the carbon isotope record of Late Cretaceous (Coniacian-Santonian) Oceanic Anoxic Event III, *Sedimentary Geology*, *235*(1-2), 38-49.

Locklair, R. E., and B. B. Sageman (2008), Cyclostratigraphy of the Upper Cretaceous Niobrara Formation, Western Interior, USA: A Coniacian-Santonian orbital timescale, *Earth and Planetary Science Letters*, *269*(3-4), 539-552.

Marz, C., S. W. Poulton, B. Beckmann, K. Kuester, T. Wagner, and S. Kasten (2008), Redox sensitivity of P cycling during marine black shale formation: Dynamics of sulfidic and anoxic, non-sulfidic bottom waters, *Geochimica Et Cosmochimica Acta*, *72*(15), 3703-3717.

McLennan, S. M. (2001), Relationships between the trace element composition of sedimentary rocks and upper continental crust, *Geochemistry Geophysics Geosystems*, *2*, art. no.-2000GC000109.

Meyers, P. A. (1994), Preservation of elemental and isotopic source identification of sedimentary organic matter, *Chemical Geology, 114* (3), 289-302.

Meyers, P. A. (2006), Paleoceanographic and paleoclimatic similarities between Mediterranean sapropels and Cretaceous black shales, *Palaeogeography Palaeoclimatology Palaeoecology*, *235*(1-3), 305-320.

Meyers, P. A. (2014), Why are the $\delta^{13}C_{org}$ values in Phanerozoic black shales more negative than in modern marine organic matter?, *Geochemistry Geophysics Geosystems 15* (7), 3085-3106.

Meyers, S. R., B. B.Sageman (2004), Detection, quantification, and significance of hiatuses in pelagic and hemipelagic strata: *Earth and Planetary Science Letters*, v. 224, p. 55-72.

Meyers, S. R., B. B. Sageman, T. W. Lyons (2005), Organic carbon burial rate and the molybdenum proxy: Theoretical framework and application to Cenomanian-Turonian oceanic anoxic event 2, *Paleoceanography, 20*(2).

Morford, J. L., A. D. Russell, and S. Emerson (2001), Trace metal evidence for changes in the redox environment associated with the transition from terrigenous clay to diatomaceous sediment, Saanich Inlet, BC, *Marine Geology*, *174*(1-4), 355-369.

Mort, H. P., T. Adatte, K. B. Follmi, G. Keller, P. Steinmann, V. Matera, Z. Berner, and D. Stuben (2007), Phosphorus and the roles of productivity and nutrient recycling during oceanic anoxic event 2, *Geology, 35,* 483–486.

Muller-Karger, F. E., R. Varela, R. Thunell, R. Luerssen, C. M. Hu, and J. J. Walsh (2005), The importance of continental margins in the global carbon cycle, *Geophysical Research Letters*, *32*(1).

Nederbragt, A. J., Thurow, J. W., Vonhof, H., Brumsack, H. -. J. (2004). Modelling oceanic carbon and phosphorus fluxes: Implications for the cause of the late Cenomanian Oceanic Anoxic Event (OAE2). *Journal of Geological Society* 161(4), 721-728.

Pagani, M., Freeman, K.H., Ohkouchi, K., and Caldeira, K. (2002) Comparison of water column $[CO_{2aq}]$ with sedimentary alkenone-based estimates: a test of the alkenone-CO_2 proxy, *Paleoceanography, 17*, 1069.

Pancost, R. D., K. A. Freeman, M. A. (1998), Arthur Organic geochemistry of the Cretaceous Western Interior Seaway: A trans-basinal evaluation, in *Stratigraphy and Paleoenvironments of the Cretaceous Western Interior Seaway*, edited by W. E. Dean and M. A. Arthur, pp. 227-255, SEPM Concepts in Sedimentology and Paleontology.

Pedersen, T.F., and Calvert, S.E. (1990), Anoxia vs. Productivity: What Controls the Formation of Organic-Carbon-Rich Sediments and Sedimentary Rocks?, *American Association for Petroleum. Geologists Bulletin., 74,* p. 454-466.

Popp, B. N., R. Takigiku, J. Hayes, J. W. Louda, E. W. Baker (1989), The post-Paleozoic chronology and mechanism of ^{13}C depletion in primary marine organic matter, *American Journal of Science 289*, 436-454.

Pratt, L. M. (1984), Influence of paleoenvironmental factors on the preservation of organic matter in middle Cretaceous Greenhorn Formation near Pueblo, Colorado, *American Association for Petroleum. Geologists Bulletin, 68*, 1146–1159.

Pratt, L, M., L. K. Barlow (1985), Isotopic and sedimentalogical study of the lower Niobrara Formation, Lyons, Colorado, in *Fine-grained deposits and biofacies of the Cretaceous Western Interior Seaway: Evidence of Cyclic Sedimentary Processes. Society of Economic Paleontology. and Mineralogy Field Trip Guideboo*k 4, 288 pp.

Pratt, L. M., M. A. Arthur, W. E. Dean, P. A. Scholle (1993), Paleo-oceanographic Cycles and Events during the Late Cretaceous in the Western Interior Seaway of North America, in *Evolution of the Western Interior Basin*, edited by W. G. E. Caldwell and E. G. Kauffman, pp. 333-354, GAC Special Paper.

Purdue, E.M., Koprivnjak, J.F., 2007. Using the C/N ratio to estimate terrigenous inputs of organic matter to aquatic environments. *Estuarine, Coastal, and Shelf Science* 73, 65–72.

Retallack, G. J. (2009), Greenhouse crises of the past 300 million years, *Geological Society of America Bulletin*, *121*(9-10), 1441-1455.

Roberts, L. N. K., Mark A. (1995), Paleogeography and the Late Cretaceous of the Western Interior of middle North America; coal distribution and sediment accumulation, edited by United States Geological Society.

Royer D. L., R. A. Berner, D. J. Beerling (2001), Phanerozoic atmospheric CO 2 change: evaluating geochemical and paleobiological approaches, *Earth-Science Reviews, 54* (4), 349-392.

Sageman, B. B. (1989), The benthic boundary biofacies model: Hartland Shale Member, Greenhorn Formation (Cenomanian), Western Interior, North America, *Palaeogeography Palaeoclimatology Palaeoecology, 74*, 87-110.

Sageman, B. B., C. Bina (1997), Diversity and species abundance patterns in Late Cenomanian black shale biofacies, Western Interior, U.S., *Palaios, 12*, 449-466.

Sageman, B. B., and Lyons, T. W. (2003), Geochemistry of fine-grained sediments and sedimentary rocks, in *Treatise on Geochemistry*, edited by F. MacKenzie, pp. 115-158, Elsevier, Oxford.

Sageman, B. B., S. R. Meyers, M. A. Arthur (2006), Orbital time scale and new C-isotope record for Cenomanian-Turonian boundary stratotype, *Geology 34* (2), 125-128.

Sageman, B. B. S., B. S.; Meyers, S. R.; Siewart, S. E.; Walaszczyk, I.; Condon, D. J.; Jicha, B. R.; Obradovich, J. D.; Sawyer, D. A. (2014), Integrating 40Ar/39Ar, U-Pb, and astronomical clocks in the Cretaceous Niobrara Formation, Western Interior Basin, USA, *Geological Society of America Bulletin, 7-8*, 956-973.

Savdra, C. E. (1998), Ichnocoenoses of the Niobrara Formation: Implications for benthic oxygenation histories, in *Stratigraphy and Paleoenvironments of the Cretaceous Western Interior Seaway*, edited by W. E. Dean and M. A. Arthur, pp. 227-255, SEPM Concepts in Sedimentology and Paleontology.

Schink B (1988) Principles and limits of anaerobic degradation: environmental and technological aspects. In: Zehnder AJB (ed) *Biology of anaerobic microorganisms*, John Wiley & Sons, New York, p 771–846.

Schlanger, S. O., and H. C. Jenkyns (1976), Cretaceous Oceanic Anoxic Events: Causes and consequences, *Geologie en Mijnbouw*, *55*(3-4), 179-184.

Schlanger, S. O., M. A. Arthur, H. C. Jenkyns, P. A. Scholle (1987), The Cenomanian-Turonian Oceanic Anoxic Event, I. Stratigraphy and distribution of organic carbon-rich beds and the marine $\delta^{13}C$ excursion, *Geological Society, London, Special Publications 26* (1), 371-399.

Scott, C., and T. W. Lyons (2012), Contrasting molybdenum cycling and isotopic properties in euxinic versus non-euxinic sediments and sedimentary rocks: Refining the paleoproxies, *Chemical Geology*, *324*, 19-27.

Scott, G. R., and W. A. Cobban (1964), Stratigraphy of the Niobrara Formation at Pueblo, Colorado, *Professional Papers US Geological Survey*, *454-L*, L1-L30.

Snow, L. J., R. A. Duncan, and T. J. Bralower (2005), Trace element abundances in the Rock Canyon Anticline, Pueblo, Colorado, marine sedimentary section and their relationship to Caribbean plateau construction and oxygen an- oxic event 2, *Paleoceanography, 20*, PA3005.

Stramma, L., G. C. Johnson, J. Sprintall, V. Mohrholz (2008), Expanding Oxygen-Minimum Zones in the Tropical Oceans, *Science, 320*(5876), pp. 655-658.

Taylor S. R., M. S. M. (1985), *The continental crust: its composition and evolution*, 312 pp., Blackwell Scientific Publication, Carlton.

Tourtelot, H. A., and R. O. Rye (1969), Distribution of oxygen and carbon isotopes in fossils of Late Cretaceous age western interior region of North America, *Geological Society of America Bulletin*, *80*(10), 1903-1922.

Tsandev, I., C. P. Slomp (2009), Modeling phosphorus cycling and carbon burial during Cretaceous Oceanic Anoxic Events, *Earth and Planetary Science Letters 286* (1), 71-79.

Tsikos, H., H.C. Jenkyns, B. Walsworth-Bell, M. R. Petrizzo, A. Forster, S. Kolonic, W. Erba, I. Premoli Silva, M. Baas, T. Wagner, J. Sinninghe Damste (2004) Carbon-isotope stratigraphy recorded by the Cenomanian-Turonian oceanic anoxic event: correlation and implications based on three key-localities, *Journal of the Geological Society, 161,* 711-720.

Turgeon, S.C., Creaser, R.A. (2008), Cretaceous Anoxic Event 2 triggered by a massive magmatic episode, *Nature, 454*, 323–326.

Tyson, R. V., and T. H. Pearson (1991), Modern and ancient continental shelf anoxia: An overview, in *Modern and Ancient Continental Shelf Anoxia*, edited by R. V. Tyson and T. H. Pearson, pp. 1 –24, Geological Society, London.

Van Mooy, B.A.S., Keil, R.G. and Devol, A.H. (2002) Impact of suboxia on sinking particulate organic carbon: Enhanced carbon flux and preferential degradation of amino acids via denitrification. *Geochimica et Cosmochimica Acta* 66: 457-465.

Wagner, T., J. S. S. Damste, P. Hofmann, and B. Beckmann (2004), Euxinia and primary production in Late Cretaceous eastern equatorial Atlantic surface waters fostered orbitally driven formation of marine black shales, *Paleoceanography*, *19*(3).

Wagreich, M. (2012), "OAE 3" --regional Atlantic organic carbon burial during the Coniacian-Santonian, *Climate of the Past*, *8*, 1447-1455.

Walaszczyk, I., and W. A. Cobban (2000), Inoceramid faunas and biostratigraphy of the Upper Turonian-Lower Coniacian of the Western Interior of the United States, *Special Papers in Palaeontology*, *64*, 1-118.

Walaszczyk, I., and W. A. Cobban (2006), Palaeontology and biostratigraphy of the Middle-Upper Coniacian and Santonian inoceramids of the US Western Interior, *Acta Geologica Polonica*, *56*(3), 241-348.

Walaszczyk, I., and W. A. Cobban (2007), Inoceramid fauna and biostratigraphy of the upper Middle Coniacian-lower Middle Santonian of the Pueblo Section (SE Colorado, US Western Interior), *Cretaceous Research*, *28*(1), 132-142.

Walaszczyk, I., J. A. Shank, A. G. Plint, W. A. Cobban (2014), Interregional correlation of disconformities in Upper Cretaceous strata, Western Interior Seaway: Biostratigraphic and sequence-stratigraphic evidence for eustatic change, *Geological Society of America Bulletin, 126*(3-4), p. 307-316.

Watkins, D. K. (1989), Nannoplankton productiv- ity fluctuations and rhythmically-bedded pelagic carbonates of the Greenhorn Limestone (Upper Cretaceous), *Palaeogeography Palaeoclimatology Palaeoecology, 74*, 75 – 86.

Wendler, I. (2013), A critical evaluation of carbon isotope stratigraphy and biostratigraphic implications for Late Cretaceous global correlation, *Earth-Science Reviews, 126*, 116-146.

White, T., M. A. Arthur (2006), Organic carbon production and preservation in response to sea-level changes in the Turonian Carlile Formation, US Western Interior Basin, *Palaeogeography Palaeoclimatology Palaeoecology 235* (1), 223-244.

Wright, E. K. (1987), Stratification and paleocirculation of the late Cretaceous Western Interior Seaway of North America, *Geological Society of America Bulletin*, *99*(4), 480-490.

Zonneveld, K. A. F., et al. (2010), Selective preservation of organic matter in marine environments; processes and impact on the sedimentary record, *Biogeosciences*, **7**, 483–511.

Chapter 3

Characterization of organic matter sources within the Western Interior Seaway
during Oceanic Anoxic Event 3

3.0 Abstract

Determining the causes of enhanced organic carbon burial has important implications for
both petroleum research and our understanding of marine carbon cycling. The Late Cretaceous
sedimentary record is characterized by cyclic deposition of organic carbon-rich sediments,
including an interval of enhanced organic carbon accumulation during the Coniacian-Santonian
that is captured within the USGS Portland #1 core. In this study, we present lipid biomarker and
compound specific carbon isotope records from the Portland core to constrain the thermal
maturity of the organic matter and the contributions of various organic matter sources. Sterane
and hopane indices of thermal maturity indicate that the samples have not undergone significant
thermal alteration. Based on the distribution of n-alkanes, steranes, and hopanes, there is a
significant increase in the contribution of algal organic matter during and after OAE 3, coeval
with increased organic carbon accumulation. Of particular note is the consistent influence of
even-over-odd predominantly mid-chain length (C_{21} to C_{25}) organic matter. Furthermore, a
consistent terrestrial contribution is observed, however, it is only a minor source of organic
matter at the Portland core location. Pristane (Pr) and phytane (Ph) abundances are inconsistent
with a redox control on Pr/Ph ratios and suggest an increase in the delivery and/or preservation

of phototrophic organic matter as the source for pristane and phytane in the Portland core. Trends in compound specific carbon isotopes are consistent with the bulk organic $\delta^{13}C$ record but highlight that mid-chain length n-alkanes are isotopically distinct from coeval short chain length n-alkanes. Biomarker results indicate that increased organic carbon burial during and after OAE 3 are associated with a change in organic matter source.

3.1 Introduction

Within the North America Western Interior Seaway (WIS), Late Cretaceous deposition is characterized by cyclic deposition of organic carbon-rich sediments (e.g. Pratt et al., 1993; Dean and Arthur, 1998; Meyers et al., 2005), including during Oceanic Anoxic Events 2 and 3 (Meyers et al., 2005; Locklair et al., 2011). The latter event is of particular interest within the WIS because it represents a prolonged period (~3 Myrs) of elevated sedimentary organic carbon accumulation (Locklair et al., 2011; Tessin et al., 2015). Understanding the factors driving these organic carbon burial events has been the focus of significant research based on both their potential as petroleum reserves and as recorders of marine carbon cycling (e.g. Schlanger and Jenkyns, 1976; Tissot, 1979; Williams, 2011). Recent work has highlighted that redox-controlled changes in organic matter preservation played a dominant role in enhanced organic carbon burial during OAE 3 in the WIS based on observed changes in bulk organic matter elemental and isotopic composition (Tessin et al., 2015). However, petrographic and bulk geochemical analyses are insufficient to rule out a shift from significant terrestrial organic matter to dominantly marine organic matter entirely.

Lipid biomarkers and compound specific carbon isotopes have been used within the WIS to constrain paleoenvironmental conditions during the Cenomanian-Turonian OAE 2, but not during the Coniacian-Santonian OAE 3 (Pratt et al., 1984; Hayes et al., 1989; Pancost et al.,

1998). When evaluating changes in organic matter contributions and paleoenvironmental condition, it is necessary to constrain the degree of thermal maturity, as increasing maturity can significantly alter biomarker distributions. Organic thermal maturity indices have been developed based on sterane and hopane stereochemistry that allow the degree of thermal maturity with respect to oil generation to be evaluations (Mackenzie et al., 1980; Seifert and Moldowan, 1986). With samples that have not undergone significant thermal alteration, the distribution of n-alkanes provides information on the relative contributions of different organic matter sources (e.g. marine algal vs. terrestrial marine; Eglinton and Hamilton, 1967; Collister et al., 1992; Meyers, 1997). The distribution of steranes C_{27}-C_{30} and sterane/hopane ratios can further be used to distinguish between organic matter sources including marine phytoplankton and zooplankton, higher plants, algae, and bacteria (e.g. Moldowan et al., 1985; Peters et al., 2005).

In this study, we present lipid biomarker and compound specific carbon isotope records from the USGS Portland core (Fig. 3.1). Thermal maturity of the samples will be evaluated using sterane and hopane indices. Contributions from different organic matter sources before, during, and after OAE 3 will be constrained based on the distribution of n-alkanes, acyclic isoprenoids (pristane and phytane), steranes, and hopanes.

3.2 Methods and materials

The USGS #1 Portland core was drilled and continuously cored near Cañon City, CO (Dean and Arthur, 1998). The 75-m thick Late Cretaceous Niobrara Formation section of the Portland core was sampled at 0.5 m resolution at the USGS Core Research Center in Denver, CO (Fig. 3.1). Chemostratigraphy for the core is based on carbon isotope and total organic carbon
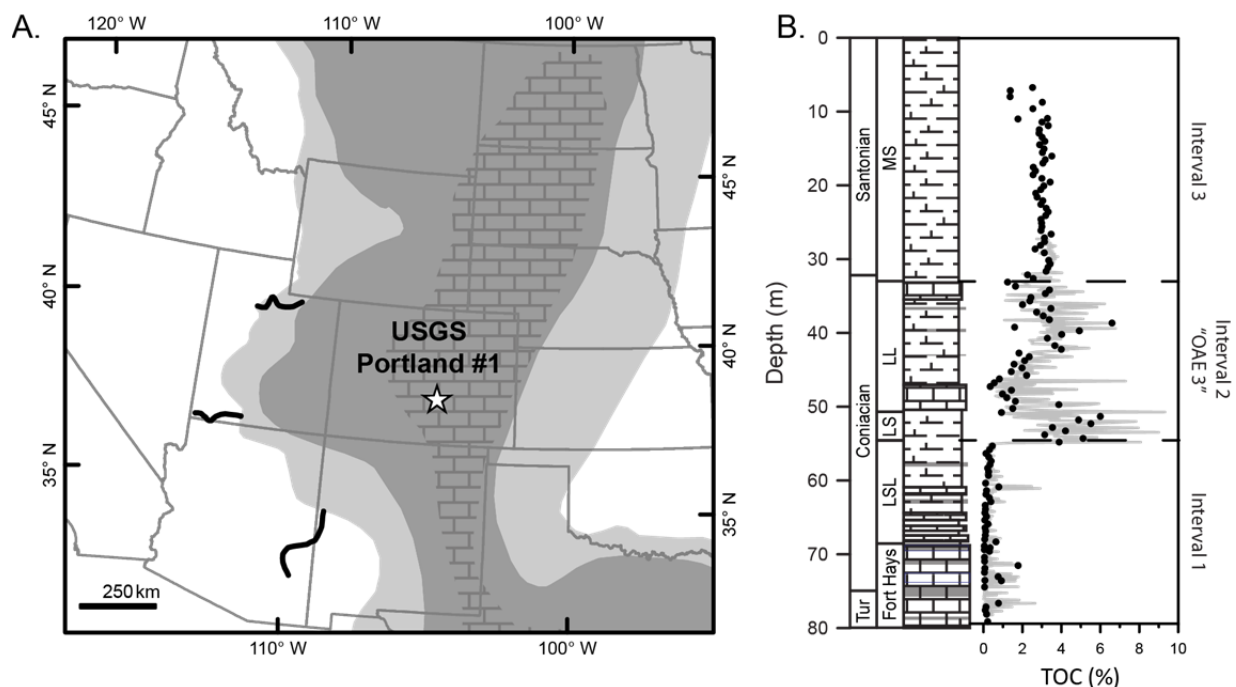
Figure 3.1

(a) Map of the Coniacian lithology of the Western Interior Seaway (adapted from Roberts and Kirshbaum (1996) and (b) stratigraphy and total organic carbon (TOC) from the USGS Portland #1 core (adapted from Tessin et al., 2015). Intervals 1, 2, and 3 are designated with dashed lines.

(TOC) records presented in Tessin et al. (2015), which was used to identify pre-OAE, OAE, and post-OAE intervals. Deposition during Interval 1, the pre-OAE interval, was characterized by oxic conditions and low total organic carbon (Tessin et al., 2015). During Intervals 2 and 3, the identified OAE 3 and post-OAE intervals, conditions become more reducing and organic matter preservation is enhanced (Tessin et al., 2015).

Samples analyzed for organic geochemsitry were ground to <75 μm and homogenized in an alumina shatterbox. Between 5 and 20 g of sample was then extracted on a Dionex Automated Solvent Extractor (ASE) 300 with a 9:1 DCM:MeOH mixture at 100°C and 1200 psi. Each extract was concentrated and separated into three fractions using silica open column chromatography. Successive elution with 3 ml hexane and 4 ml hexane/DCM (3:1 v/v) resulted in apolar and aromatic fractions, respectively. The apolar hydrocarbon and aromatic fractions

were then dried under a gentle N_2 flow and dissolved in hexane.

Apolar and aromatic compounds were identified via gas chromatography-mass spectrometry (ThermoScientific Q8000 Triple Quadropole MS paired to a Trace 1310 Gas Chromatograph; with a mass range of m/z 50–550 and a cycle time of 1.53s) and comparison with retention times of reference compounds. The GC was equipped with a HP-5MS column (30 m x 0.25 mm) and samples were injected from an auto sampler at an inlet temperature of 320°C. Helium was used as the carrier gas and initial oven temperature was 40°C held for 1.5 minutes; this was increased at 20°C min^{-1} to 130°C, and then to 320°C where it was held for 10 minutes until the end of the run. Compound specific $\delta^{13}C$ were run on a GC/Combustion III device coupled to a Finnigan-MAT DeltaPlus isotope ratio mass spectrometer.

Mass spectrometer data was analyzed using OpenChrom. The total abundance of steranes and hopanes were determined based on the total mass of m/z 217 and 191, respectively. Odd/even preferences of n-alkanes are determined using carbon preference index (CPI) and odd-even predominance centered at n-C_{31} (OEP$_{31}$), which are calculated as follows:

$$CPI = \frac{2(n-C_{23}+n-C_{25}+n-C_{27}+n-C_{23})}{n-C_{22}+2(n-C_{24}+n-C_{26}+n-C_{28})+n-C_{30}} \quad \text{(Bray and Evans, 1961)} \quad (1)$$

$$OEP_{31} = \frac{n-C_{29}+6(n-C_{31})+n-C_{33}}{4(n-C_{30}+n-C_{32})} \quad \text{(Scanlon and Smith, 1970)} \quad (2)$$

The terrigenous/aquatic ratio (TAR) is used to evaluate the relative abundance of long-chain (C_{27}–C_{31}) to short-chain (C_{15}–C_{19}) n-alkanes as follows:

$$TAR = \frac{n-C_{27}+n-C_{29}+n-C_{31}}{n-C_{15}+n-C_{17}+n-C_{19}} \quad \text{(Bourbonniere and Meyers, 1995)} \quad (3)$$

3.3 Results

3.3.1 Steranes and hopanes

The 20S/(20S+20R) ratios for the C_{27} C_{29} steranes range from 0.13−0.34 and 0.21−0.31,

respectively. The C_{31} hopane 22S/(22S+22R) ratio varies between 0.54−0.59, while the C_{30}

hopane to moretane ratio ranges from 0.11−0.21 (Fig.3.2). Ratios of steranes (m/z 217) to

hopanes (m/z 191) are plotted in Figure 3.3. Sterane/hopane ratios average 0.04 in samples

between 59.8 to 74.2 m before beginning to increase at 55.2 m. Sterane/hopane reaches a

maximum value of 0.48 at 34.9 m, before subsequently decreasing upcore to a value of 0.22 at

9.7 m. Of steranes C_{27}, C_{28}, and C_{29}, C_{27} is the most abundant in the record, with the only

exception being samples collected at 40.0 and 45.1 m. Between 59.8 and 74.2 m, ratios of

C_{28}/C_{27} gradually increase, with an abrupt increase at 55.2 m and relatively stable values

throughout the remainder of the core. Ratios of C_{28}/C_{29} exhibit an increasing trend upcore (Fig.

3.3).
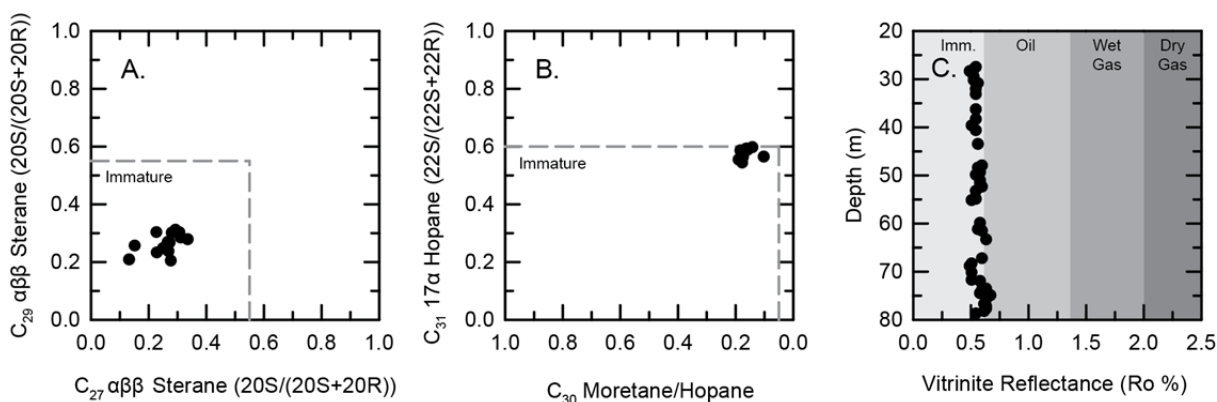
Figure 3.2

Thermal maturity indicators from the USGS Portland #1 core, (a) C_{27} and C_{29} 5α,14α,17α(H)-sterane 20S/(20S+20R), (b) C_{30} Moretane/Hopane ratios and C_{31} 17α-hopane 22S/(22S+22R), and (c) vitrinite reflectance from Locklair, 2007 with expected maturity values. Dashed lines indicate equilibrium values for thermal maturity indices (Seifert and Moldowan, 1986).

3.3.2 Distribution of n-alkanes and isoprenoids

Characteristic m/z 57 chromatograms from the lower (62.8 m) and upper (30.4) portions

of the core are presented in Figure 3.4. In general, all samples are dominated by mid-chain length
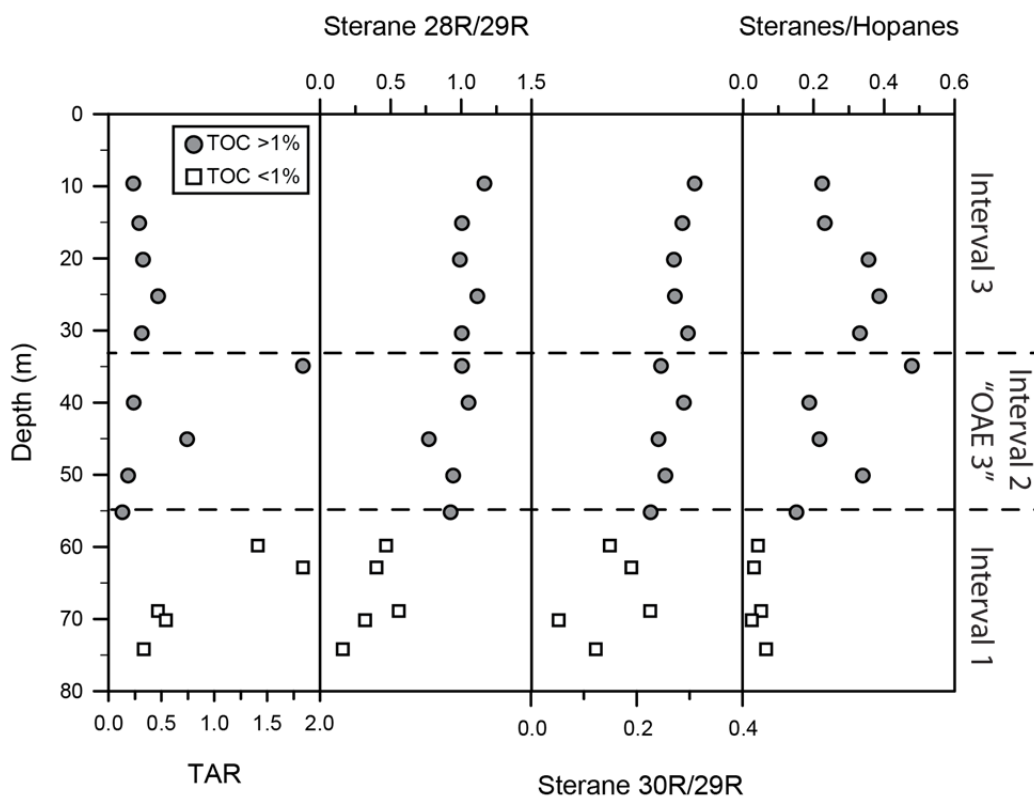
Figure 3.3

(a) Terrestrial-aquatic ratios, (b) sterane C_{28}/C_{29} ratios, (c) sterane C_{30}/C_{29} ratios, and (d) sterane/hopane ratios from the USGS Portland #1 core. Gray symbols indicate samples with >1% TOC and white symbols indicate samples with <1% TOC. Dashed lines indicate Intervals 1, 2, and 3 as designated by Tessin et al., 2015.

alkanes (C_{20}–C_{25}), whereas long-chain n-alkanes ($>C_{25}$) comprise a small portion of all samples.

In samples between 74 and 59 m, short chain length n-alkane ($<C_{20}$) abundance is relatively low

as compared to mid-chain length n-alkanes. These samples are also characterized by significant

amounts of branched and cyclic alkanes. Beginning at 56 m, both short chain length n-alkanes

and isoprenoids (norpristane, pristane, and phytane) increase in abundance (Fig. 3.5). This shift

in organic matter composition at 55 m is illustrated by a change in the most abundant compound

(MAC; Table D.2). In samples below 56 m, *n*-C21 or *n*-C22 is the MAC, while pristane is the

most abundant compound in samples above 56 m with the exception of samples 40.01 and 45.09,

pristane is consistently the most abundant compound (Table D.2). Throughout the record, carbon
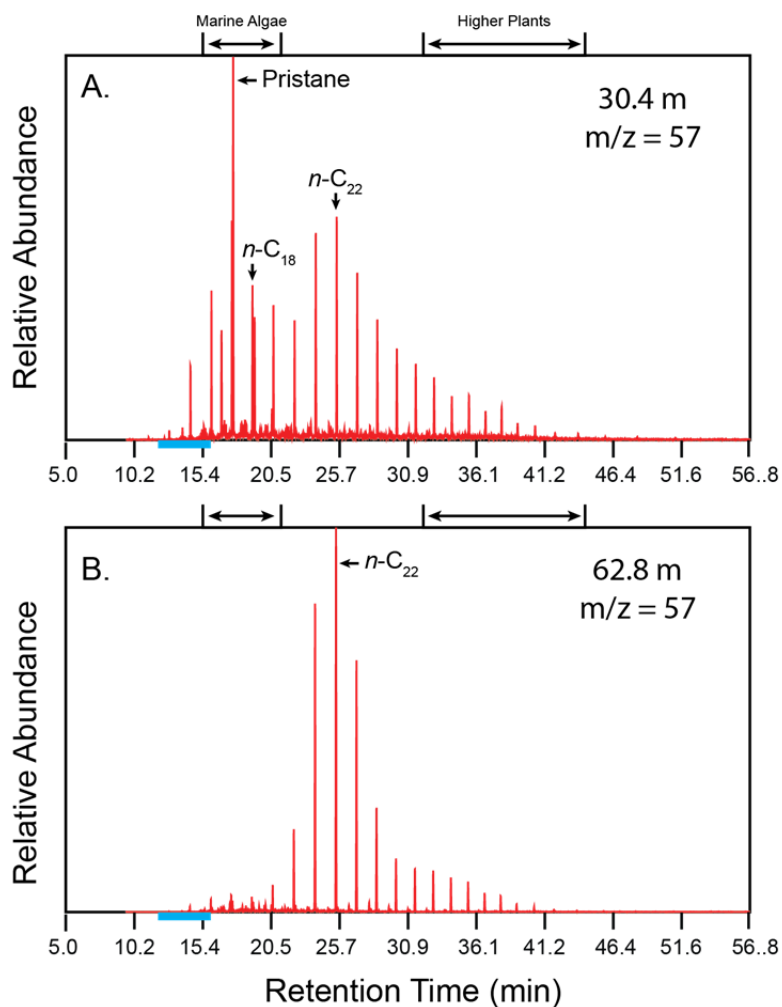
Figure 3.4

Characteristic m/z 57 chromatograms from (a) the lower (62.8 m) and (b) upper (30.4) portions of the core. The most abundant *n*-alkanes and isoprenoids are labeled. Blue lines indicate the portion of the chromatogram plotted in Figure 5.

preference index (CPI) values range from 0.94 to 1.12 (Table D.3). Odd-even-preference

(OEP$_{31}$) values vary between 1.22 and 1.75, with the lowest values recorded between

34.93−45.01 m and 59.79−68.86 m (Table D.3). Terrestrial-Aquatic Ratio (TAR) range between

0.23−1.84 with all values indicating a dominantly aquatic organic matter source with the

exception of samples from 34.93, 59.79, and 62.84 m (Fig. 3.3).

Pristane to phytane ratios (Pr/Ph) range from 0.98−3.41 (Fig. 3.6). Between 74.2 and 62.8
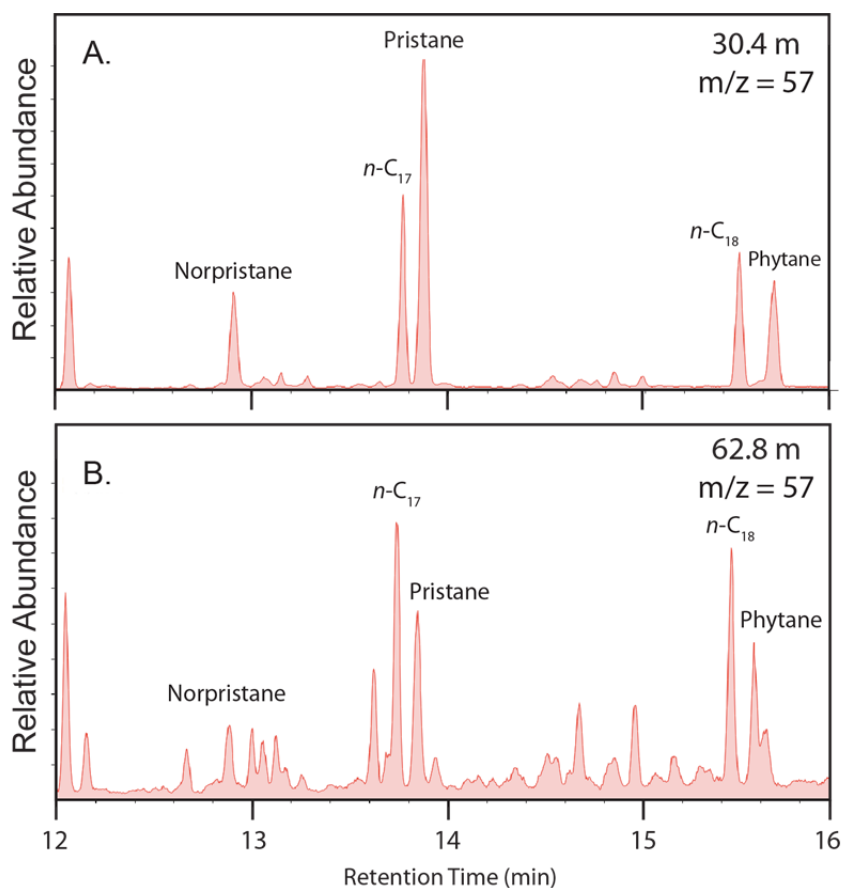
Figure 3.5

Characteristic m/z 57 chromatograms from 12-16 minutes of retention time ($n\text{-}C_{16}$–$n\text{-}C_{18}$) from (a) the lower (62.84 m) and (b) upper (30.38) portions of the core. Pristane, phytane and *n*-alkanes are labeled.

m, Pr/Ph values average 1.20 (with the exception of an elevated value of 3.40 at 68.9 m) before beginning to increase at 59.8 m. Pr/Ph values then increase to 3.01 at 50.1 m, before falling to 1.25 at 34.9 m. Above 34 m, Pr/Ph abruptly rise and stabilize at an average value of 2.74. Ratios of pristane and phytane to their corresponding n-alkane (Pr/*n*-C17 and Ph/*n*-C18) range between 0.52−2.04 and 0.29−0.94, respectively. Both ratios generally increase upcore, with the exception of elevated Ph/*n*-C18 rations between 74.1 and 70.2 m.

3.3.3 Compound specific carbon isotopes

Compound specific carbon isotope records from C_{19} to C_{24} n-alkanes are, on average,

64
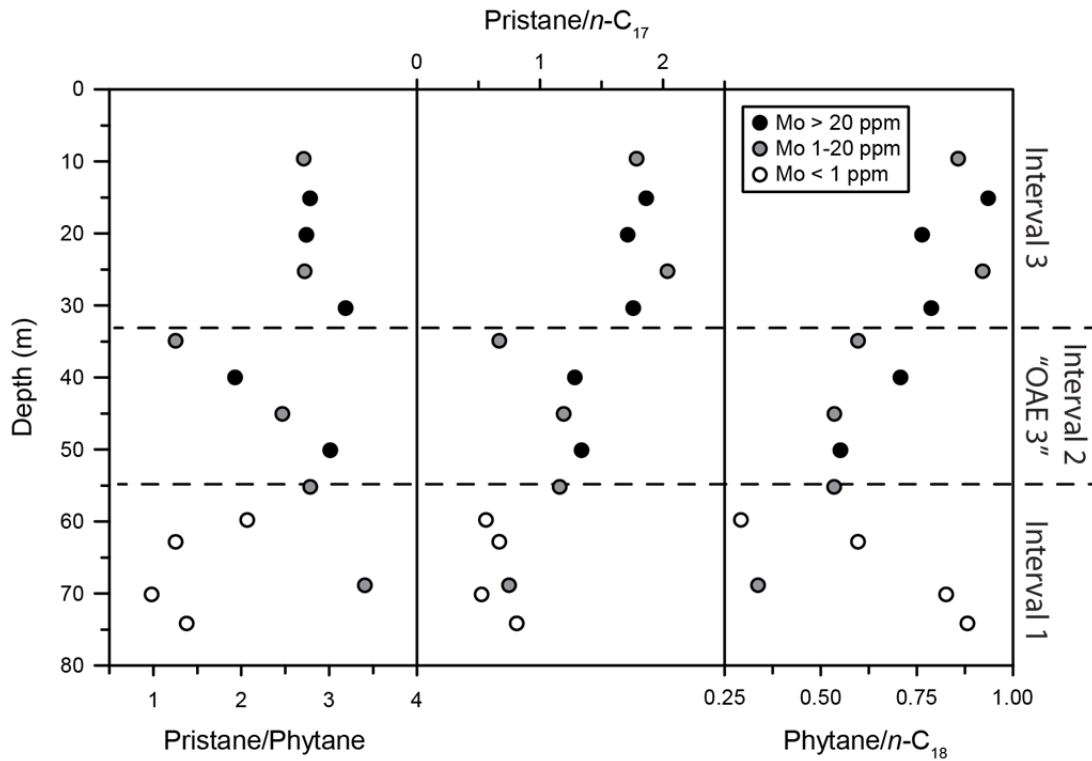
Figure 3.6

Pristane/phytane, pristane/ *n*-C$_{17}$, and phytane/ *n*-C$_{18}$ from the USGS Portland #1 core. White, gray, and black symbols indicate samples with Mo concentrations of <1 ppm, 1-20 ppm, and >20 ppm, respectively. Dashed lines indicate Intervals 1, 2, and 3 as designated by Tessin et al., 2015.

2.5−3.5‰ more negative than bulk organic δ^{13}C values (Fig. 3.7). Compound specific δ^{13}C values range between -27.9−32.0‰. The average δ^{13}C values of *n*-C$_{19}$ and *n*-C$_{20}$ are more negative than average δ^{13}C values of *n*-C$_{21}$ to *n*-C$_{24}$. The most negative values in each n-alkane record are found in the upper 30 m of the core, with an observed difference of 0.3−2.2‰ when comparing average values between 74.2−35.0 m and 9.7−25.3 m (Fig. 3.7).

3.4 Discussion

3.4.1 Thermal maturity

Thermal maturity describes the extent of alteration of organic matter by heat-driven reactions – an important process in the conversion of sedimentary organic matter into petroleum.
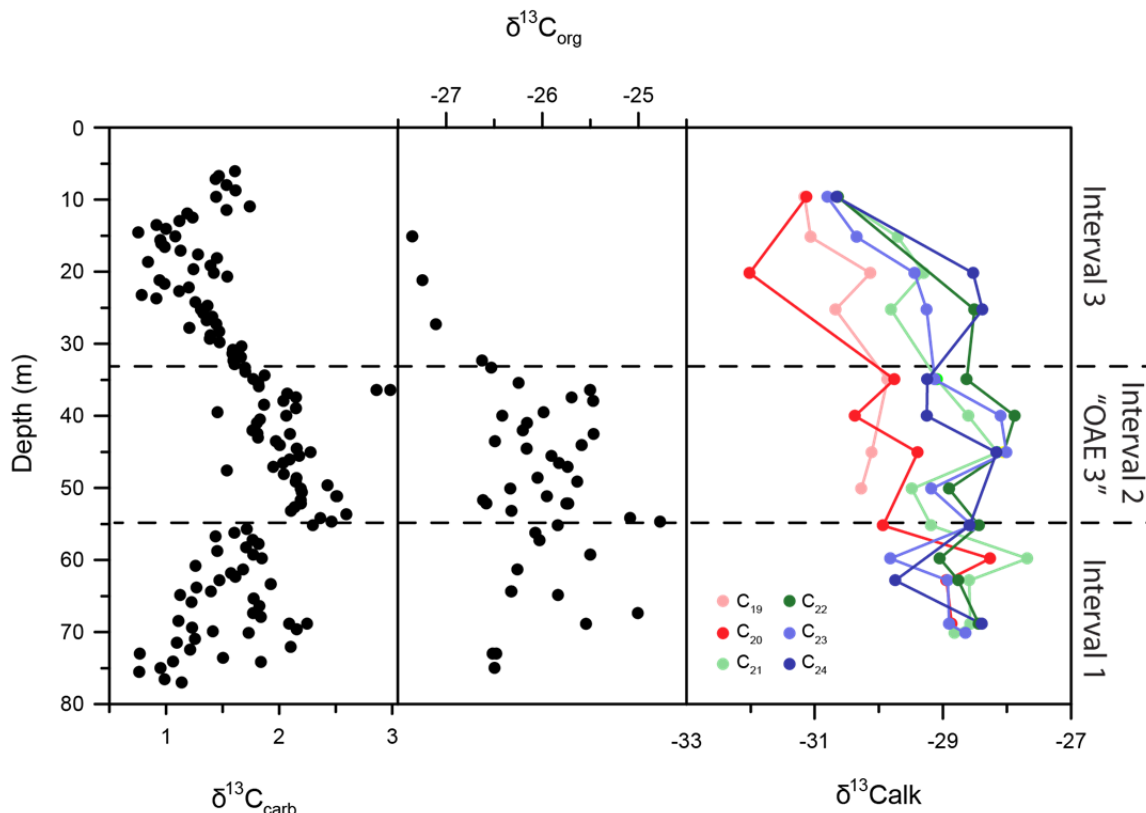
Figure 3.7

Carbon isotopes from the USGS Portland #1 core, (a) bulk carbonate $\delta^{13}C$ (b) bulk organic $\delta^{13}C$, and (c) n-alkane $\delta^{13}C$. Dashed lines indicate Intervals 1, 2, and 3 as designated by Tessin et al., 2015.

A series of biomarker indices to evaluate the degree of thermal maturity (Fig. 3.2) have been developed based on the predictable transformation of the stereochemical configuration of terpanes and steranes associated with increasing thermal maturity (see Peters et al. (2005) for discussion of biomarker stereochemistry). For example, as thermal maturity increases, the isomerization of C-20 in the C_{27} and C_{29} $5\alpha,14\alpha,17\alpha(H)$-steranes has been shown to increase the 20S/(20S+20R) from 0 to an equilibrium value of 0.55 (Seifert and Moldowan, 1986). Similarly, the isomerization of 17α-hopanes at C-22 from S to R is predictable, with values of 22S/(22S+22R) increasing from 0 to 0.6 with maturation (Seifert and Moldowan, 1986). Moretane/hopane ratios provide an additional constraint of thermal maturity, because the $\beta\alpha$ configuration (moretanes) are less thermally stable than the $\alpha\beta$ configuration (hopanes).

66

Abundances of C_{30} moretanes will decrease relative to C_{30} hopanes with increasing thermal

maturity from ~0.8 to 0.05, with most oils from pre-Tertiary source rocks showing

moretane/hopane ratios of <0.1 (Mackenzie et al., 1980; Seifert and Moldowan, 1986; Peters et

al., 2005).

Based on the sterane 20S/(20S+20R) results from the Portland core, the samples analyzed

are thermally immature (Fig. 3.2a). Conversely the C_{31} hopane 22S/(22S+22R) and C_{30}

moretane/hopane ratios are closer to the equilibrium values (Seifert and Moldowan, 1986; Peters

et al., 2005), which indicate maturity close to early oil production (Fig. 3.2b). These results

demonstrate that the Portland core samples are immature but nearing early oil formation, which

is supported by previous thermal maturity estimates derived from vitrinite reflectance (Locklair,

2007; Fig. 3.2c).

3.4.2 Organic Matter Source

Determining the source of organic matter within the Portland core is necessary to

determine if changes in organic carbon burial are associated with changing organic matter

sources. The distribution of *n*-alkanes can be used to assess the relative contribution of algal and

terrigenous organic matter, because short chain *n*-alkanes (*n*-C_{15} to *n*-C_{19}) are predominantly

derived from marine algae (Collister et al., 1992) and long chain *n*-alkanes (>*n*-C_{25}) are derived

from higher plant waxes (Peters et al., 2005). The *n*-alkane distribution in the Portland core

samples is dominated by *n*-alkanes that are intermediate to the algal and terrestrial end members

(Fig. 3.4). Organic matter with a biomarker composition characterized by dominantly odd

molecular weight, mid-chain length *n*-alkanes has previously been attributed to macrophytes

(Viso et al., 1993; Ficken et al., 2000). However, within the C_{21} to C_{25} n-alkanes, an even-over-

odd predominance is observed at all depths except 9.65 and 59.79 m indicating that macrophytes are not a likely source of mid-chain length n-alkanes. In many Portland core samples, n-C_{22} is the most abundant compound (MAC). Organic matter characterized by the dominance of n-C_{22} alkanes has been observed in many pre-Miocene source rocks; however, the primary source of the n-C_{22} dominated organic matter remains enigmatic (Schenck, 1968).

Even-over-odd predominance within C_{12} to C_{22} has been observed in a number of recent sedimentary systems and was linked to contributions from algae, bacteria, fungi, and yeast (Nishimura and Baker, 1986; Grimalt and Albaiges, 1987). Even-over-odd predominance in C_{22} to C_{30} has also been observed (Welte and Waples 1973; Tissot et al. 1977; Ogihara and Ishiwatari 1998), but was attributed to hypersaline or hydrothermal environments. More recently, an even-over-odd predominance was reconstructed within OAE 1 deposits in the Basque-Cantabrian Basin, which was neither hypersaline nor hydrothermal (Chaler et al., 2005). In this case, the even-over-odd predominance was attributed to highly reducing conditions and the presence of methogenic bacteria (Chaler et al., 2005). However, within the Portland core, the even-over-odd predominance is associated with both oxidizing and reducing sedimentary conditions and an absence of biomarkers for methanogenic bacteria, suggesting that redox conditions are not driving the enigmatic n-alkane distribution (Table D3).

A significant shift occurs in the *n*-alkane record at the onset of Interval 2. As compared to underlying samples, the contribution of short-chain length (algal) *n*-alkanes becomes more pronounced and remains significant throughout Intervals 2 and 3 (Fig. 3.4). The marked increase in algal organic matter at the onset of Interval 2 could represent an increase in planktonic primary productivity and/or increased preservation of labile organic matter that includes short-chain length *n*-alkanes.

In addition to short and mid-chain length n-alkanes, all Portland core samples contain a small contribution of long-chain n-alkanes, indicating a minor contribution of terrestrial-derived organic matter. The presence of terrestrial plant-derived organic matter can be verified based on predominantly odd molecular weight n-alkanes between C_{25} and C_{35}, which are thought to be related to the input of wax lipids derived from higher plants (Eglinton and Hamilton, 1967; Hedberg, 1968; Peters et al., 2005). However, determination of odd-or-even predominance in our samples is complicated by low abundances of n-alkanes $>C_{33}$. Furthermore, in some samples mid-chain length n-alkanes exhibit an even-over-odd predominance while longer chain n-alkanes in the same sample exhibit an odd-over-even predominance. With these factors in mind, we favor the OEP_{31} index (Scanlon and Smith, 1970), which is based only on n-alkanes between n-C_{29} and n-C_{33}. The OEP_{31} results indicate a consistent odd-over-even preference in the long-chain alkanes, supporting a terrestrial source for the long-chain n-alkanes (Table D3). Conversely, the Carbon Preference Index (CPI; Bray and Evans, 1961), which integrates results from n-C_{22} to n-C_{30}, does not show a significant odd-over-even predominance, likely due to the high abundance of n-C_{22} and n-C_{24} in some samples. OEP_{31} values of >1 further support the interpretation that the Portland samples underwent relatively low thermal alteration, as elevated thermal maturity is known to overprint the odd-over-ever predominance (Table D3; Scalan and Smith, 1970).

The terrigenous/aquatic ratio (TAR; Fig. 3.3) offers an additional way to assess the relative contributions of terrigneous and aquatic organic matter by comparing the abundances of short and long- chain length n-alkanes (Meyers, 1997). Therefore, an increase in TAR could represent either enhanced delivery of terrigneous organic matter or preferential degradation of more labile, algal organic matter. TAR values from the Portland core support the significant predominance algal organic matter, with the exception of three samples: 34.9, 59.8, and 62.8 m
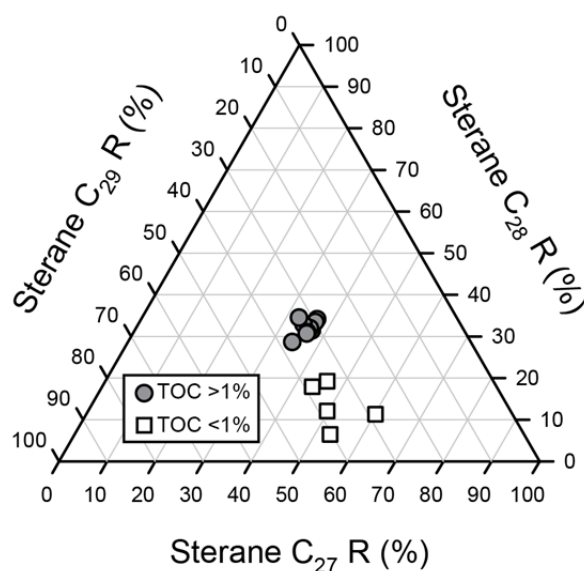
Figure 3.8

Ternary diagram of steranes C_{27} R, C_{28} R, and C_{29} R from the USGS Portland #1 core. Gray symbols indicate samples with >1% TOC and white symbols indicate samples with <1% TOC.

(Fig. 3.3). It must be noted, however, that TAR values can potentially overestimate terrigneous influence because of preferential preservation of more refractory, terrestrially derived organic matter (Volkman et al., 1987).

The distribution of C_{27}-C_{29} steranes can be used to further differentiate sources of organic matter because C_{27} steranes are attributed to red algae and zooplankton, C_{28} steranes dominate in phytoplankton organic matter (green algae and diatoms) and are present in yeast, fungi, and bacterial plankton, and C_{29} steranes are sourced predominantly from land plants (Huang and Meinschein, 1979; Volkman et al., 2003; Peters et al., 2005). Therefore C_{28}/ C_{29} ratios can evaluate relative algal contributions (Peters et al., 2005). Ratios of steranes C_{28}/ C_{29} increase markedly at the onset of Interval 2 and remain elevated throughout the rest of the record (Fig. 3.3), indicating that the contribution of phytoplankton was greater during Intervals 2 and 3. Fig. 3.8 highlights that, when separated by TOC, two distinct pools of organic matter exist. All samples have a relatively constant contribution of sterane C_{29}, however, low TOC (<1%) samples

are characterized by more C_{27}, while high TOC (>1%) samples are characterized by more C_{28}. As both C_{27} and C_{28} are predominantly sourced from marine organic matter, this suggests a change in marine source material or preservation. A significant marine algal contribution is further supported by the presence in the analyzed samples of C_{30} steranes, which are diagnostic of marine chrysophytes algae that are found in Cretaceous calcareous and siliceous sediments (Moldowan et al., 1985; Moldowan et al., 1990; Peters et al., 2005). The ratio of C_{30}/ C_{29} increases upcore (Fig. 3.3), indicating that the algal influence increases throughout the record.

The ratio of steranes/hopanes reflects the relative contribution of eukaryotic (algae and higher plants) vs. prokaryotic (bacteria) organic matter (Moldowan et al., 1985). Within the Portland core, the sterane/hopane ratio correlates relatively well with TOC (Fig. 3.8). Lower sterane/hopane ratios are recorded in TOC-poor Interval 1 as compared to Intervals 2 and 3, suggesting that the relative contribution of eukaryotic organic matter increases coeval with TOC (Fig. 3.8). The overall distribution of alkanes, steranes, and hopanes indicates that at the onset of Interval 2, the contribution of marine algal organic matter to the sediments increases abruptly and remains elevated throughout. These results suggest that a change in marine algal organic matter controlled enhanced organic carbon burial in the Portland core during the Coniacian-Santonian.

It is evident that the increase in algal organic matter, as shown by changing alkane and sterane distributions, is tightly coupled to increasing TOC values (Fig. 3.9). Therefore, it is likely that all samples contain a relatively minor baseline amount of terrestrial, refractory organic matter and that increased organic carbon accumulation is primarily associated with enhanced abundance of algal organic matter. It remains difficult to discern whether the increase in algal organic matter at the onset of Interval 2 was driven by enhanced preservation or increased

71
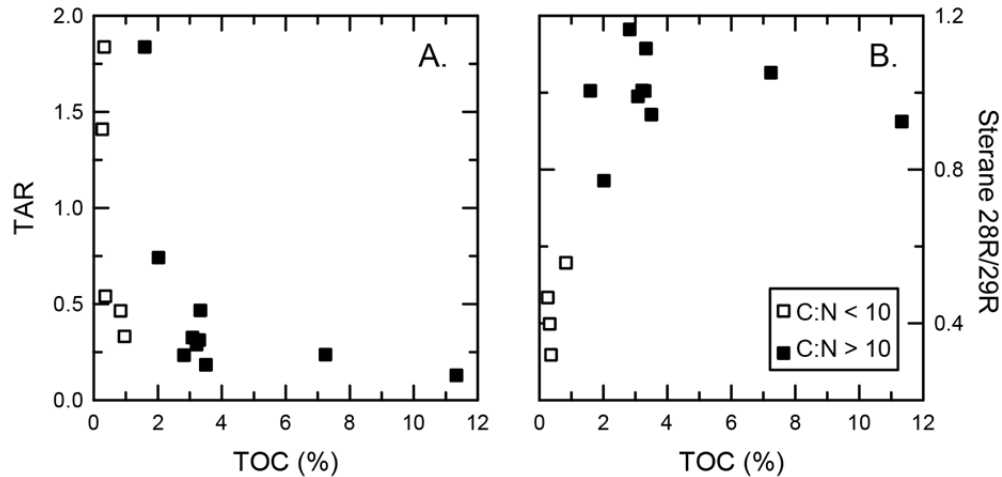
Figure 3.9

Crossplots of (a) total organic carbon (TOC) and terrestrial-aquatic ratio (TAR) and (b) TOC and sterane C_{28}/C_{29}. White symbols indicate total organic carbon/total nitrogen (C:N) ratios of <10 and black symbols indicate C:N ratios of >10.

productivity. The onset of Interval 2 is characterized by a sea level highstand and trace-metal evidence of low O_2 conditions (Tessin et al., 2015). Therefore, the increased algal contribution could be a result of higher marine planktonic productivity fueled by the influx of nutrient-rich Tethyan water and/or reduced organic matter degradation driven low O_2 availability under enhanced density stratification.

3.4.3 Pristane and Phytane

Most sedimentary pristane and phytane is assumed to derive from the phytyl side chain of chlorophyll *a* within phototrophic organisms (e.g. Brooks et al., 1969; Powell and McKirdy, 1973). Sedimentary redox conditions may affect the relative production of the two alkanes during biodegradation of these phototrophic organisms. Low pristane/phytane ratios (<1) have been interpreted as accompanying anoxic conditions, as preferential phytane production during reduction of phytol is expected under reducing conditions (Didyk et al., 1978). However , compared to other redox indicators from the Portland core, such as Mo concentrations, which

increase under reducing conditions (Fig. 3.6; e.g. Erickson and Helz, 2000; Chappaz et al., 2014). However, no relationship exists between redox and Pr/Ph ratios. Furthermore, the only samples exhibiting Pr/Ph ratios of <1 also have low Mo concentrations, which instead suggests preferential phytane production under relatively oxic sedimentary conditions (Fig. 3.6). Because the Mo concentrations are consistent with other redox sensitive trace metal and biological indicators of well-oxygenated conditions during Interval 1 (Tessin et al., 2015), it appears that the Pr/Ph ratios were not primarily controlled by oxygenation at the site of the Portland core. This assessment is consistent with other research, which documented that Pr/Ph can be affected by other environmental factors and that care should be taken when applying Pr/Ph ratios as a redox proxy (e.g. Ten Haven et al., 1987; Peters et al., 2005).

Low ratios of acyclic isoprenoids to n-alkane (Pr/n-C_{17} and Ph/n-C_{18}) are used to indicate degree of biodegradation of organic matter (Winters and Williams, 1969; Miget et al., 1969) due to preferential degradation of the isoprenoid over the n-alkane (Pirnik et al., 1974). Similar to the Pr/Ph record, these ratios conflict with previous assessments of organic matter preservation in the Portland core. The Pr/n-C_{17} and Ph/n-C_{18} results (Fig. 3.6) indicate that the highest levels of biodegradation occurred during Intervals 2 and 3, despite documented enhanced organic matter preservation during these intervals (e.g. Tessin et al., 2015). However, the relationship between Pr/n-C_{17} and Ph/n-C_{18} and biodegradation is based on aerobic bacteria experiments (Pirnik et al., 1974). Tessin et al. (2015) highlighted that the shift between aerobic and anaerobic organic matter degradation at the onset of Interval 2 in the Portland core significantly enhanced lipid preservation. Modern experiments are required to understand how these reducing conditions affect the preferential degradation of isoprenoids vs. n-alkanes.

In general, it is difficult to reconcile Pr/Ph, Pr/n-C_{17}, and Ph/n-C_{18} results from the

73

Portland core with previous reconstructions of redox conditions and biodegradation. Other sources of pristane and phytane in sediments have been suggested, including dihydrophytol, - a building block of kerogen and a component of archael cell membranes (Chappe et al., 1982). Tocopherols, a constituent of plant and algal lipid membranes, have also been proposed as a major source of pristane (Goosens et al., 1984). As a coeval increase of Pr/Ph, Pr/n-C$_{17}$, and Ph/n-C$_{18}$ occurs alongside indicators of elevated algal organic matter, despite the onset of more reducing conditions, we propose enhanced abundances of pristane and phytane are caused by increased delivery and/or preservation of phototrophic organic matter.

3.4.4 Compound specific carbon isotopes

Carbon isotope analyses are commonly used to identify organic matter source (e.g. Freeman et al., 1990; 1994), however, these interpretations are complicated during the Cretaceous because marine and terrestrial organic matter had overlapping carbon isotope compositions (-26‰ to -28‰ for marine organic matter and -24‰ to -30‰ for mixed terrestrial and marine; Dean et al., 1986; Meyers, 2014). However, despite these complications, δ^{13}C values in the shorter chain n-alkanes (C$_{19}$ and C$_{20}$) are distinct from those in the mid-chain n-alkanes (C$_{21}$ to C$_{24}$). A difference of 0.5‰ to 1.9‰ (Fig. 3.7) is recorded between the average short chain and mid-chain length n-alkanes, with mid-chain length n-alkanes an average of 1.3‰ more positive than short chain length n-alkanes. This difference suggests that the even-over-odd predominant mid-chain length n-alkanes that are consistently present within the Portland core represent a distinct organic matter source, possibly associated with a shift in the community of primary producers as indicated by n-alkane and sterane distributions. This source apparently does not change throughout the onset of OAE 3 and increase in carbon burial. While the *n*-alkane

$\delta^{13}C$ records are highly variable, each record displays a similar range of values during Intervals 1 and 2. The most negative values in each record do not occur until Interval 3. The trend towards more negative $\delta^{13}C$ at the end of the identified OAE 3 Interval is consistent with decreasing values in both the bulk carbonate and bulk organic $\delta^{13}C$ records.

3.5 Conclusions

Thermal maturity indices from the USGS Portland #1 core indicate that samples have not undergone significant thermal alteration. Sterane 20S/(20S+20R) results significantly below the equilibrium value of 0.55 support thermal immaturity. However, C_{30} hopane/moretane ratios and C_{31} hopane 22S/(22S+22R) ratios are closer to equilibrium values. These results broadly agree with thermal maturity estimates from vitrinite reflectance, which suggest that the samples were nearing early oil formation.

Organic matter in the Portland core is dominated by marine algal and bacterial sources. The distribution of *n*-alkanes in the Portland record is characterized by a large abundance of mid-chain length *n*-alkanes, especially *n*-C_{22}, likely representing contributions from bacteria, fungi, and/or yeast. This observation represents an expansion of the sedimentary systems in which even-over-odd predominance has been observed in mid-chain length n-alkanes. Further, new compound specific isotope results highlight that these mid-chain length n-alkanes are isotopically distinct, with an average of 1.3‰ more positive $\delta^{13}C$ values than coeval short chain length n-alkanes. The presence of long-chain *n*-alkanes ($>C_{25}$) with a clear odd-over-even predominance supports a small, but consistent, contribution of terrigneous organic matter. The onset of Interval 2 is characterized by a significant increase in the abundance of short-chain *n*-alkanes, suggesting an elevated contribution from algal organic matter. A significant increase in

the contribution of algal organic matter during and after OAE 3 (Intervals 2 and 3) is supported by elevated sterane C_{28}/C_{29} and C_{28}/C_{29} ratios. This observed increase in algal organic matter is coupled with the onset of enhanced organic carbon burial, as evidenced by the relationship between biomarker proxies and TOC.

Based on previous observations about redox and organic matter preservation, the pristane and phytane abundances do not appear to be controlled by either factor and likely represent changing contributions of different algal sources. However, the effects of oxic vs. reducing conditions on the preferential degradation of isoprenoids or *n*-alkanes require further investigation.

3.6 References

Bray, E.E. and E. D. Evans (1961), Distribution of *n*-paraffins as a chlue to recognition of source beds, *Geochimica et Cosmochimica Acta 22,* 2-15.

Brooks, J. D., K., Gould, and J. W. Smith (1969), Isoprenoid hydrocarbons in coal and petroleum, *Nature 222,* 257-259.

Chappaz, A., T. Lyons, D. Gregory, C. Reinhard, B. Gill, C. Li, R. Large (2014), Does pyrite act as an important host for molybdenum in modern and ancient sediments?, *Geochimica et Comsmochimica Acta, 126*, 112-122.

Chappe, B., P. Albrecht, and W. Michaelis (1982), Polar lipids of archaebacteria in sediments and petroleums, *Science 217*, 65-66.

Collister, J., R. E. Summons, E. Lichtfouse, and J. M. Hayes (1992), An isotopic biogeochemical study of the Green River oil shale, *Organic Geochemistry 19,* 265-276.

Dean, W. E., M. A. Arthur, G. E. Claypool (1986), Depletion of 13 C in Cretaceous marine organic matter: Source, diagenetic, or environmental signal?, *Marine Geology, 70*(1), 119-157.

Dean, W. E. a. M. A. A. (1998), Geochemical expressions of cyclicity in Cretaceous pelagic limestone sequences: Niobrara Formation, Western Interior Seaway, in *Stratigraphy and Paleoenvironments of the Cretaceous Western Interior Seaway*, edited by W. E. Dean and M. A. Arthur, pp. 227-255, SEPM Concepts in Sedimentology and Paleontology.

Didyk, B. M., B. R. T. Simoneit, S. C. Bassell, and G. Eglinton (1978), Organic geochemical indicators of paleoenvironmental conditions of sedimentation, *Nature 272,* 216-222.

Eglinton, G., R. J. Hamilton (1967), Leaf Epicuticular Waxes, *Science 156,* 1322-1335.

Erickson BE, Helz GR (2000), Molybdenum (VI) speciation in sulfidic waters: Stability and lability of thiomolybdates, *Geochimica et Cosmochimica Acta, 64,* 1149-1158

Ficken, K.J., Li, B., Swain, D.L., Eglinton, G. (2000), An n-alkane proxy for the sedimentary input of submerged/floating freshwater aquatic macrophytes, *Organic Geochemistry 31*, 745–749.

Freeman, K. H., J. M. Hayes, J. M. Trendel, and P. Albrecht (1990), Evidence from carbon isotope measurements for diverse origins of sedimentary hydrocarbons, *Nature 343,* 254-256.

Freeman, K. H, S. G. Wakeman, and J. M. Hayes (1994), Predictive isotopic biogeochemistry: hydrocarbons from anoxic marine basins, *Organic Geochemistry 21*, 629-644.

Goosens, H., J. W. de Leeuw, P. A. Schenck, and S. C. Brassell (1984), Tocopherols as likely precursors as likely precursors of pristane in ancient sediments and crude oils, *Nature 312,* 440-442.

Grimalt J. and Albaiges J. (1987), Sources and occurrence of C12-C22 n-alkane distributions with even carbon- number preference in sedimentary environments, *Geochimica et Cosmochimica Acta 51*, 1379-1384.

Hayes, J. M., B. N. Popp, R. Takigiku, and M. W. Johnson (1989), An isotopic study of biogeochemical relationships between carbonates and organic matter in the Greenhorn Formation, *Geochimica Et Cosmochimica Acta, 53*, 2961–2972.

Hedberg, H.D. (1968), Significance of high-wax oils with respect to genesis of petroleum, *American Association of Petroleum Geologists Bulletin 52*, 736–750.

Huang, W.-Y. and W. G. Meninshein (1979), Sterols as ecological indicators, *Geochimica et Cosmochimica Acta 43,* 739-745.

Locklair, R.E., 2007, Causes and Consequences of Marine Carbon Burial: Examples from the Cretaceous Niobrara Formation and the Permian Brushy Canyon Formation, unpublished Ph.D. thesis, Northwestern University, 515 p.

Locklair, R., B. Sageman, and A. Lerman (2011), Marine carbon burial flux and the carbon isotope record of Late Cretaceous (Coniacian-Santonian) Oceanic Anoxic Event III, *Sedimentary Geology*, *235*(1-2), 38-49.

Mackenzie, A. S., R. K. Patience, J. R. Vandenbroucke, and B. Durand (1980), Molecular parameters of maturation in the Toarcian shales, Paris Basin, France—I. Changes in the configuration of acyclic isoprenoid alkanes, steranes, and triterpanes, *Geochimica et Cosmochimica Acta 44,* 1709-1721.

Meyers, P. A. (1997), Organic geochemical proxies of paleoceanographic, paleolimnologic, and paleoclimatic processes, *Organic Geochemistry 27,* 213-250.

Meyers, P. A. (2014), Why are the δ^{13}Corg values in Phanerozoic black shales more negative than in modern marine organic matter?, *Geochemistry Geophysics Geosystems 15* (7), 3085-3106.

Meyers, S. R., B. B. Sageman, T. W. Lyons (2005), Organic carbon burial rate and the molybdenum proxy: Theoretical framework and application to Cenomanian-Turonian oceanic anoxic event 2, *Paleoceanography, 20*(2).

Miget, R. J., C. H. Oppenheimer, H. I. Kator, and D. A. Larock (1969), Microbial degradation of normal paraffin hydrocarbons in crude oil, In: *Proceedings of the Joint Conference on Prevention and Control of Oil Spills,* American Petroleum Institute, Washington DC, 327-331.

Moldowan, J. M., W. K. Seifert, and E. J. Gallegos (1985), Relationship between petroleum composition and depositional environment of petroleum source rocks, *American Association of Petroleum Geologists Bulletin 69,* 1255-1268.

Moldowan, J. M., F. J. Fago, C. Y. Lee (1990), Sedimentary 24-*n*-propylcholestanes, molecular fossils diagnostic of marine algae, *Science 247,* 309-312.

Nishimura M. and Baker E. W. (1986), Possible origin of n-alkanes with a remarkable even-to-odd predominance in recent marine sediments, *Geochimica et Cosmochimica Acta 50*, 299-305.

Peters, K.E., Walters, C. C., Moldowan, J.M. (2005), The Biomarker Guide: Volume 2 Biomarkers and Isotopes in Petroleum Exploration and Earth History, Prentice Hall, Englewood Cliffs, NJ.

Pirnick, M. P., R. Atlas, and R. Bartha (1974), Hydrocarbon metabolism by *Brevibacterium erythrogenes:* normal and branched alkanes, *Journal of Bacteriology 119,* 868-878,

Powell, T. G. and D. M. McKirdy (1973), Relationship between ratio of pristane to phytane, crude oil composition and geological environments in Australia, *Nature 243,* 37-39.

Pratt, L. M., M. A. Arthur, W. E. Dean, P. A. Scholle (1993), Paleo-oceanographic Cycles and Events during the Late Cretaceous in the Western Interior Seaway of North America, in *Evolution of the Western Interior Basin*, edited by W. G. E. Caldwell and E. G. Kauffman, pp. 333-354, GAC Special Paper.

Pratt, L. M. (1984), Influence of paleoenvironmental factors on the preservation of organic matter in middle Cretaceous Greenhorn Formation near Pueblo, Colorado, *American Association for Petroleum. Geologists Bulletin, 68*, 1146–1159.

Roberts, L. N. K., Mark A. (1995), Paleogeography and the Late Cretaceous of the Western Interior of middle North America; coal distribution and sediment accumulation, edited by United States Geological Society.

Scanlan, R. S. and J. E. Smith (1970) An improved measure of the odd-to-even predominance in the normal alkanes of sediment extracts and petroleum, *Geochimica et Cosmochimica Acta 34*, 611-620.

Schlanger, S. O., and H. C. Jenkyns (1976), Cretaceous Oceanic Anoxic Events: Causes and consequences, *Geologie en Mijnbouw*, *55*(3-4), 179-184.

Seifert, W. K. and J. M. Moldowan (1986), Use of biological markers in petroleum exploration, In: *Methods in Geochemistry and Geophysics,* Vol 24, R. B. Johns, eds., Elsevier, Amsterdam, 261-290.

Ten Haven, H. L., J. W. de Leeuw, J. Rullkotter, and J. A. Sinninghe Damste (1987), Restricted utility of the pristane/phytane ratio as a paleoenvironmental indicator, *Nature 330,* 641-643.

Tessin, A., I. Hendy, N. Sheldon, B. Sageman (2015), Redox-controlled preservation of organic matter during "OAE 3" within the Western Interior Seaway, *Paleoceanography 30* (6), 702-717.

Tissot, B. (1979), Effects on prolific petroleum source rocks and major coal deposits caused by sea-level changes *Nature 277*, p. 463-465.

Viso, A. C., and Marty, J. C. (1993), Fatty acids from 28 marine microalgae, *Phytochemistry 34*, 1521–1533.

Volkman, J.K., Farrington, J.W. and Gagosian, R.B. (1987), Marine and terrigenous lipids in coastal sediments from the Peru upwelling region at 15ºS: Sterols and triterpene alcohols, *Organic Geochemistry 11*, 463-477.

Volkman, J.K. (2003), Sterols in microorganisms, *Applied Microbiology and Biotechnology 60*, 495-506.

Williams, P., Lyle, D. (2011), Bring in the Rig, in Estes-Jackson, J.E., Anderson, D.S., ed., in *Revisiting and Revitalizing the Niobrara in the Central Rockies*: Denver, CO, Rocky Mountain Association of Geologists, p. 33-40.

Winters, J. C. and J. A. Williams (1969), Microbiological alteration of crude oil in the reservoir, *American Chemical Society, Division of Petroleum Chemistry, New York Meeting Preprints 14,* E22-E31.

Chapter 4

Iron limitation in the Western Interior Seaway during the Late Cretaceous OAE 3
and its role in phosphorus recycling and enhancing organic matter preservation

4.0 Abstract

The sedimentary record of the Coniacian-Santonian Oceanic Anoxic Event 3 (OAE 3) in

the North American Western Interior Seaway is characterized by a prolonged period of enhanced

organic carbon (OC) burial. This study investigates the role of Fe in enhancing organic matter

preservation and maintaining elevated primary productivity to sustain black shale deposition

within the Coniacian-Santonian-aged Niobrara Formation in the USGS #1 Portland core. Iron

speciation results indicate the development of a reactive Fe limitation coeval with reduced

bioturbation and increased organic matter preservation, suggesting that decreased sulfide

buffering by reactive Fe may have promoted enhanced organic matter preservation at the onset of

OAE 3. An Fe limitation would also provide a feedback mechanism to sustain elevated primary

productivity through enhanced phosphorus recycling. Additionally our results demonstrate

inconsistencies between Fe-based and trace metal redox reconstructions. Iron indices from the

Portland core indicate a single stepwise change, whereas the trace metal redox proxies indicate

fluctuating redox conditions during and after OAE 3. Using Fe speciation to reconstruct past

redox conditions may be complicated by a number of factors, including Fe sequestration in

diagenetic carbonate phases and efficient sedimentary pyrite formation in a system with limited

Fe supply and high levels of export production.

4.1 Introduction

Iron availability in marine systems can significantly influence organic carbon (OC)

accumulation in sediments by affecting rates of both primary productivity and organic matter

preservation. In the modern ocean, increased Fe delivery or "fertilization" is known to enhance

primary productivity in high nutrient, low chlorophyll regions (e.g. Boyd et al., 2000). In

sediments, the availability and early diagenesis of Fe are known to play complex roles in OC

accumulation by inducing changes in C, P, and S cycling (Canfield, 1989; Raiswell and Canfield,

1996). For example, Meyers (2007) outlined the role of Fe in the "sulfide buffer and phosphorus

trap hypothesis," where reactive Fe minerals (especially Fe (oxyhydr)oxides) act to buffer sulfide

buildup within porewaters through formation of Fe-sulfide mineral phases (FeS, FeS_2). Once all

available reactive Fe is sulfidized, free sulfide accumulates in porewaters, which promotes P

recycling in the absence of Fe (oxyhydr)oxides and reduces bioturbation and organic matter

oxygen exposure time (Canfield, 1989; Raiswell and Canfield, 1996; Meyers, 2007; Tribovillard

et al., 2015).

As some of the most dramatic examples of OC burial in the geologic record, Mesozoic

Oceanic Anoxic Events (OAEs) provide unique opportunities for studying OC burial processes

as each event varied in duration and geographic extent. The Cenomanian-Turonian OAE 2, for

example, is characterized by widespread black shale deposition (Schlanger et al., 1987; Tsikos et

al., 2002), and a distinctive and relatively short-lived (~600 ka: Sageman et al., 2006) positive

carbon isotope excursion (Arthur et al., 1987; Jenkyns, 2010). In contrast, OC-rich sedimentation during the Coniacian-Santonian OAE 3 was restricted to the equatorial Atlantic and adjacent continental shelves and seaways (e.g., März et al., 2008; Locklair et al., 2011; Wagreich, 2012), including the North American Western Interior Seaway (WIS). Due to the long duration (>3 Myrs) and higher rates of OC burial in some locations as compared to OAE 2, OAE 3 represents an important perturbation to the global carbon cycle. Irrespective of its exact geographic extent, OC burial during OAE 3 was elevated, widespread, and prolonged, and must have required internal oceanic feedback mechanisms.

This study investigates Fe speciation before, during and after OAE 3 in the WIS to understand its role in prolonged OC burial. A comparison of these results with S concentrations and previously published records of bioturbation (Savrda, 1998) and organic matter quality (Tessin et al., 2015) is used to assess how fluctuations in Fe availability can affect "sulfide buffering" and OC preservation, particularly at the onset of enhanced OC burial. Evolution of Fe speciation is also compared to TOC/P and P/Al ratios to evaluate how changes in Fe chemistry affected "P trapping" before, during, and after OAE 3. Finally, comparison of Fe speciation with redox sensitive trace metals provides a opportunity to test whether Fe-based redox reconstructions are supported by other redox proxies in highly productive sedimentary systems where pyrite formation may be Fe limited.

4.2 Background

4.2.1 Western Interior Seaway
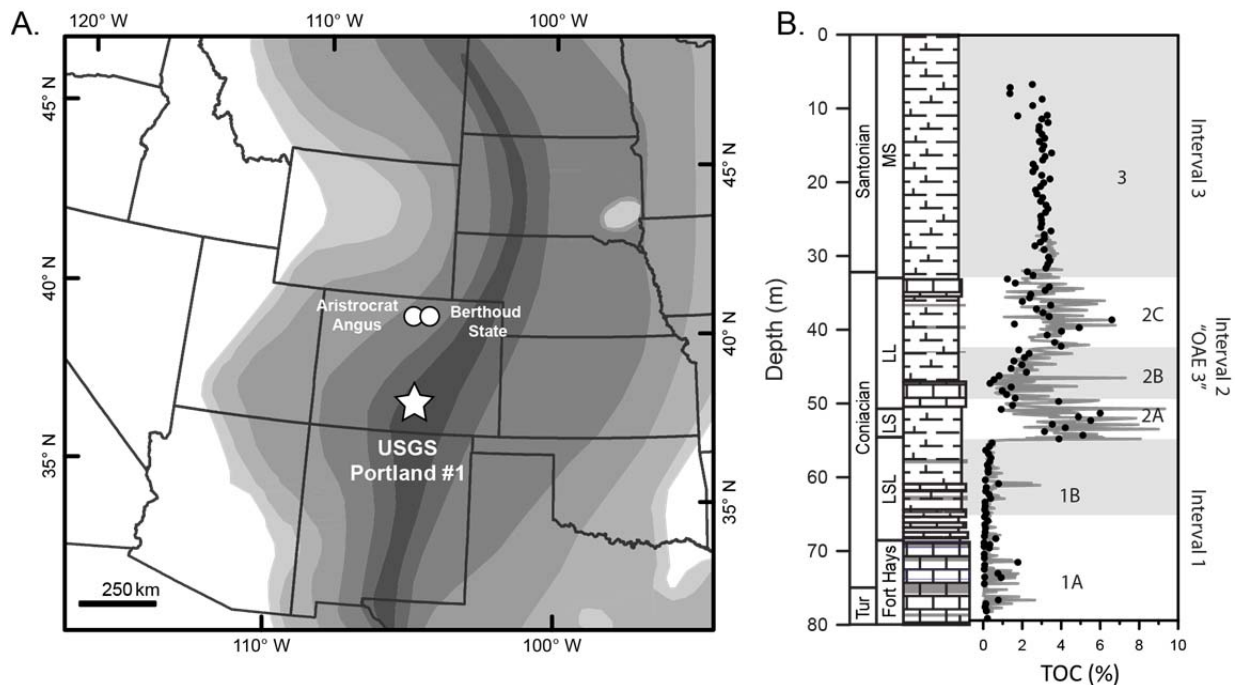
Figure 4.1

(a) Map of the Cretaceous Western Interior Seaway (WIS) with Turonian paleobathymetry estimates (adapted from Sageman and Arthur, 1995). Darker colors represent relatively deeper depths. The USGS #1 Portland core location is marked with a star. Circles denote the Aristocrat Angus and Berthoud State cores. (b) Stratigraphy and total organic carbon (TOC) for the USGS Portland core with adapted intervals from Tessin et al. (2015). Gray bars denote Intervals 1b, 2b, and 3.

During maximum transgression, the WIS extended from the Gulf of Mexico to the Arctic Ocean and from central Utah to central Iowa (Fig. 4.1). The sedimentary record of the WIS includes episodic deposition of OC-rich shales and chalks, including those recorded during the two maximum transgressions, the Greenhorn and the Niobrara Transgressions. The Niobrara Formation was deposited during the latter transgression from the Late Turonian to the Early Campanian (Scott and Cobban, 1964; Locklair et al., 2011) and is formally divided into two members: the basal Fort Hays Limestone and the overlying Smoky Hill Chalk (Fig. 4.1). Previous research has identified OAE 3 in the Smoky Hill Chalk based on a positive δ^{13}C excursion and elevated OC concentrations (e.g. Locklair et al., 2011; Tessin et al., 2015).

84

Paleontological and sedimentary evidence indicates that in western Kansas and central Colorado, the Fort Hays was initially deposited in water depths of 15–50 m and that the water column progressively deepened to water depths of 150–300 m during Smoky Hill deposition (Hattin, 1982). The focus of this study, the USGS Portland core, was located in the deepest portion of the WIS during the Late Cretaceous (Fig 4.1; Sageman and Arthur, 1994). During maximum transgression, the influx of Tethyan water from the south may have delivered nutrients, including reactive Fe into the WIS (e.g. Meyers et al., 2005). Other sources of Fe and nutrients to the seaway include continental runoff from the Sevier Highlands (e.g. Flögel et al., 2009) and volcanic ash falls, which are recorded as numerous bentonite layers.

4.2.2 Trace metal and iron redox proxies

Trace metal concentrations in ancient sediments and rocks allow for the reconstruction of marine redox conditions (Tribovillard et al., 2006). Cadmium and zinc accumulate in sediments under sulfidic conditions. Cadmium exhibits a nutrient-like behavior and is delivered to sediments with OM (Piper and Perkins, 2004). Zinc is delivered to the sediments via organic acid complexes or through adsorption on Fe-Mn oxyhydroxides (Fernex et al., 1992; Algeo and Maynard, 2004). During early diagenesis, Cd and Zn are released to porewaters from organic matter and are authigenically enriched in sediments as CdS and ZnS in the presence of free sulfide (Huerta-Diaz and Morse, 1992). Sedimentary Mo accumulation is thought to require a threshold concentration of H_2S for molybdate to be transformed to the particle reactive thiomolydbate (i.e. the thiomolybdate switch) and subsequently scavenged by OM and Fe – S mineral phases (Erickson and Helz, 2000; Chappaz et al., 2014). Thus, more sulfidic conditions are thought to be required for Mo accumulation than for Cd and Zn accumulation. Rhenium also

accumulates in reducing sediments but unlike Mo, Zn, and Cd, sedimentary enrichment is not thought to require the presence of free H_2S (Crusius et al., 1996).

Iron speciation has also been used as a redox proxy to distinguish oxic, ferruginous or euxinic conditions in ancient black shales. This approach is based on the observation that Fe, particularly highly reactive Fe (Fe_{HR}), is enriched in sediments deposited beneath an anoxic water column (e.g. Raiswell and Anderson, 2005; Lyons and Severmann, 2006). Therefore, Fe_T/Al ratios of >0.5 and Fe_{HR}/Fe_T of >0.38 are indicative of an anoxic water column (e.g. Poulton and Canfield, 2005; Lyons and Severmann, 2006). Studies of modern euxinic basins (e.g. Black Sea, Cariaco Basin) have identified the source of Fe enrichment in anoxic basins as reactive Fe shuttled from suboxic shallow shelf sediments and subsequently precipitated within the water column in the deeper euxinic basin (Lyons and Severmann, 2006; Severmann et al., 2010). The ratio of Fe_{py}/Fe_{HR} can be further used to distinguish between euxinic and non-euxinic anoxic systems because significant sulfidization of the Fe_{HR} pool (>0.7–0.8) has been used to indicate the presence of dissolved H_2S in the water column (Raiswell and Canfield, 1998; März et al., 2008; Poulton and Canfield, 2011; Poulton et al., 2015).

Certain factors, including basin geometry, high sedimentation rates, and low Fe export efficiency from the shelves, are known to complicate the interpretation of Fe-speciation results by decreasing Fe_{HR}/Fe_T and Fe_{py}/Fe_{HR} values (Raiswell and Canfield 1998; Anderson and Raiswell 2004; Raiswell and Anderson 2005; Lyons and Severmann, 2006). These complications are generally thought to obscure the signal of anoxic conditions rather than erroneously indicate anoxic/euxinic conditions. Basin geometry, in particular the shelf to basin ratio, is of interest in the current study because "shelf" settings are defined as <200 m water depth, which means that most, if not all, of the WIS is considered to be a shelf and not deep basin setting.

4.3 Methods and materials

The USGS #1 Portland core was drilled and continuously cored near Cañon City, CO (Dean and Arthur, 1998). The 75-m thick Late Cretaceous Niobrara Formation section of the Portland core was sampled at 0.5 m resolution at the USGS Core Research Center in Denver, CO (Fig. 4.1). Chemostratigraphy for the core is based on carbon isotope and total organic carbon records presented in Tessin et al. (2015), which was used to identify pre-OAE, OAE, and post-OAE intervals. In Fig. 4.1, the three defined intervals from Tessin et al. (2015) are further divided. The pre-OAE Interval (Interval 1) has been partitioned into Interval 1a, which includes the Fort Hays Limestone and Interval 1b, which includes the lower shale limestone member of the Smoky Hill Chalk (Scott and Cobban, 1964). The OAE Interval (Interval 2) is divided into 2a, 2b, and 2c based on previously published total organic carbon (TOC) values (Tessin et al., 2015; Fig. 4.1). Intervals 2a and 2c are defined by TOC values >3%. The post-OAE Interval (Interval 3) was not subdivided.

Samples analyzed for bulk elemental concentrations (Al, Fe, S, P, Mo, Re, Cd, and Zn) were ground to <75 μm and homogenized in an alumina shatterbox to minimize trace element contamination. Analyses were completed at ALS Laboratories in Vancouver, BC. Whole rock samples were digested with perchloric, hydrofluoric, nitric, and hydrochloric acids. Concentrations were determined by inductively coupled plasma-atomic emission spectrometry (ICP-AES) and inductively coupled plasma-mass spectrometry (ICP-MS). GBM908-10, GBM908-5, OREAS 90 and MRGeo08 standards were used to verify elemental concentrations. Accuracy and precision are reported in Table D.1.

Sequential iron extractions were completed following Poulton and Canfield (2005), and

pyrite Fe extractions following Canfield et al. (1986). The pyrite iron fraction is stoichiometrically determined following precipitation of chromium reducible sulfide as ZnS (Canfield et al., 1986). Carbonate-associated Fe (Fe_{carb}), magnetite Fe (Fe_{mag}), and Fe (oxyhydr)oxides (Fe_{ox}) are considered highly reactive (HR) because these phases react with sulfide on timescales of months to years (Poulton and Canfield, 2005). The Fe_{HR} pool also includes pyrite Fe (Fe_{py}), which represents Fe that has reacted with sulfide in the water column or during early diagenesis in the sediments (Raiswell and Canfield, 1998; Poulton and Raiswell, 2002). The Fe_{HR} pool is thus defined as $Fe_{carb} + Fe_{ox} + Fe_{mag} + Fe_{py}$ and poorly and non-reactive Fe ($Fe_{NR/PR}$) is calculated as $Fe_T - Fe_{HR}$. Concentrations of Fe_{carb}, Fe_{ox}, and Fe_{mag} were measured on ICP-MS (Thermo iCAP Q) within the STARLAB at Central Michigan University. Analytical precision and accuracy, determined from replicate analyses (n = 21) of a certified standard (SCP Science) were better than 5%. Calculated pyrite Fe concentrations generally replicated with <5% precision. All geochemical data discussed in this paper are archived in Pangaea (www.pangaea.de).

4.4 Results

4.4.1 Iron

The different Fe phases identified by sequential extractions and pyrite Fe measurement are plotted in Fig. 4.2. Carbonate-associated Fe (Fe_{carb}) is generally elevated during Interval 1, with concentrations up to 0.2 wt. %, whereas during Intervals 2 and 3, Fe_{carb} concentrations are consistently < 0.05 wt. %. Iron (oxyhydr)oxides (Fe_{ox}) consistently accounts for between 0.01–0.1 wt. % throughout the Portland record. Magnetite-associated Fe (Fe_{mag}) is generally low but varies throughout the three intervals. During Interval 1, Fe_{mag} concentrations range from 0.01–
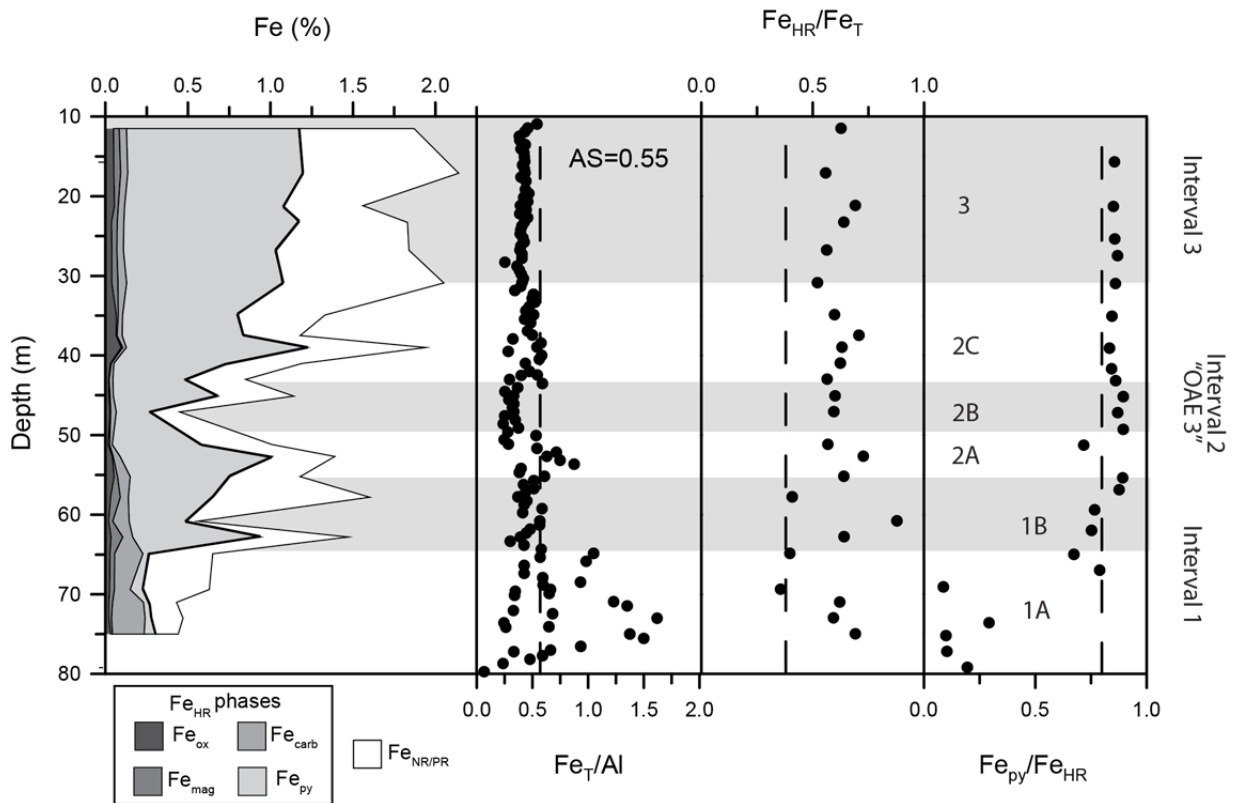
Figure 4.2

Iron concentrations and speciation results from the Portland core (a) Fe phases measured by sequential extractions (Fe_{carb}, Fe_{ox}, and Fe_{mag}), Fe_{py}, and $Fe_{NR/PR}$. The thick line indicates Fe_T (wt. %). (b) Weight % ratios of Fe_T/Al. Dashed line indicates the average Fe_T/Al shale value of 0.55. (c) Fe_{HR}/Fe_T, with the anoxic threshold of 0.38 indicated by the dashed line. (d) Fe_{py}/Fe_{HR}, with the euxinic Fe_{py}/Fe_{HR} threshold of 0.7 designated by a dashed line. Gray bars denote Intervals 1b, 2b, and 3.

0.07 wt. %. Concentrations of Fe_{mag} are consistently <0.01 wt. % during Interval 2 and range between 0.02–0.04 wt.% during Interval 3. Pyrite-associated Fe (Fe_{py}) increases notably leading into Interval 2 to concentrations of between 0.2–1.1 wt.%. During Intervals 2 and 3, an average of 88% of Fe_{HR} is in the form of Fe_{py}.

The Fe_T/Al values are the most variable and elevated during Interval 1, with values ranging from 0.07 to 1.60 (Fig. 4.2). During Intervals 2 and 3, Fe_T/Al values average 0.51 and 0.46, respectively. Values of Fe_T/Al are elevated during Intervals 2a and slightly elevated during Interval 2c. Values of Fe_{HR}/Fe_T range between 0.36 and 0.88 with an average value of 0.60

throughout the record. The lowest values (0.12 and 0.33) of Fe_{py}/Fe_{HR} occur during Interval 1a. Values of Fe_{py}/Fe_{HR} increase abruptly in Interval 1b with values ranging between 0.71 and 0.93 for the remainder of the record.

4.4.2 Trace metals

Trace metal/Al ratios are plotted as ppm (Mo, Cd, Zn) or ppb (Re) to weight % ratios and compared to previously published Mo and TOC concentrations from Tessin et al. (2015) in Fig. 4.3. The records of Mo concentrations and Mo/Al exhibit similar patterns throughout the Portland core, and generally follow the TOC record (Fig. 4.3). Interval 1 is characterized by low Mo concentrations (an average of 0.3 ppm) and Mo/Al ratios (an average of 0.2). Interval 2 exhibits the most variable Mo and Mo/Al values, with two peak periods of elevated Mo
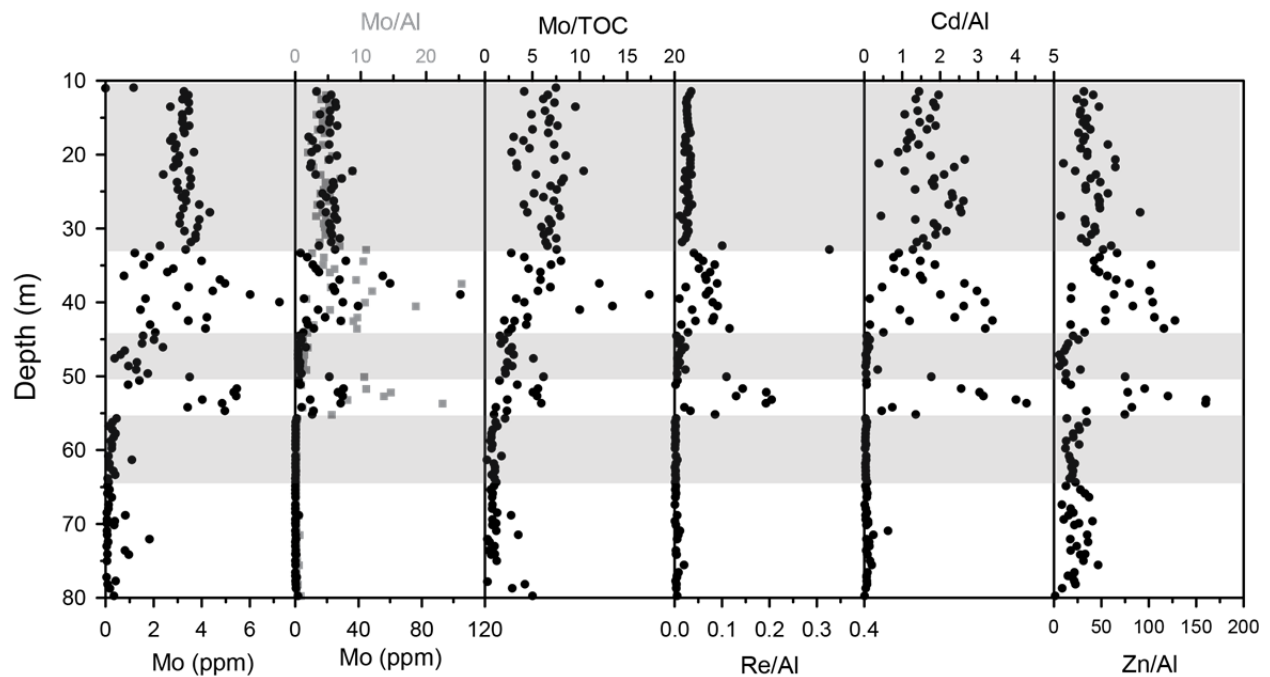
Figure 4.3

Total organic carbon (TOC) and trace metal records (Mo/Al (ppm/wt. %), Mo (ppm), Mo/TOC (ppm/wt. %), Re/Al (ppb/wt. %), Cd/Al (ppm/wt. %), and Zn/Al (ppm/wt. %)) from the USGS Portland core. Gray bars denote Intervals 1b, 2b, and 3. TOC and Mo (ppm) records are from Tessin et al. (2015).

concentrations during Intervals 2a and 2c separated by low concentrations during Interval 2b. During Interval 3, Mo concentrations and Mo/Al values become more stable, ranging from 8.5– 36 ppm and 1.9–10.8, respectively. The record of Mo/TOC exhibits similar trends to the Mo and Mo/Al record, with the lowest values recorded during Interval 1 (1.0). Within Interval 2, Mo/TOC concentrations are elevated during Intervals 2a and 2c, with low values recorded during Interval 2b. However, unlike the Mo and Mo/Al records, Mo/TOC values within Interval 3 are elevated and variable, ranging from 2.8–40.9.

Rhenium, Cd, and Zn behave similarly to Mo in the Portland core (Fig 4.3). Throughout Interval 1, Re/Al, Cd/Al, and Zn/Al values are generally low (an average of 3.8, 0.08, and 27, respectively). The highest Re/Al, Cd/Al, and Zn/Al values occur during Intervals 2a and 2c, whereas Interval 2b exhibits values similar to Interval 1. During Interval 3, values remain elevated and range between 7–85, 0.4–3.1, and 7–91, respectively.

4.4.3 Sulfur and Phosphorus

Sulfur results are compared to previously published TOC, bioturbation, and Rockeval results from Tessin et al. (2015) and Savrda (1998) in Fig. 4.4. Bioturbation derived Interpreted Oxygenation Curves (IOC) from Savrda (1998) are based on the vertical distribution of laminites and oxygen-related ichnocoenoses. The IOC record has been smoothed by integrating data to 0.5 m resolution to match the resolution of the geochemical data. IOC values generally decrease throughout Interval 1, with the lowest values recorded within Interval 2, indicating reduced bioturbation during the OAE (Savrda, 1998). Hydrogen and oxygen index values, produced through RockEval pyrolysis, are proxies for the hydrogen- and oxygen-richness of organic matter. Hydrogen index values are markedly elevated in Interval 2, as compared to Interval 1,

91
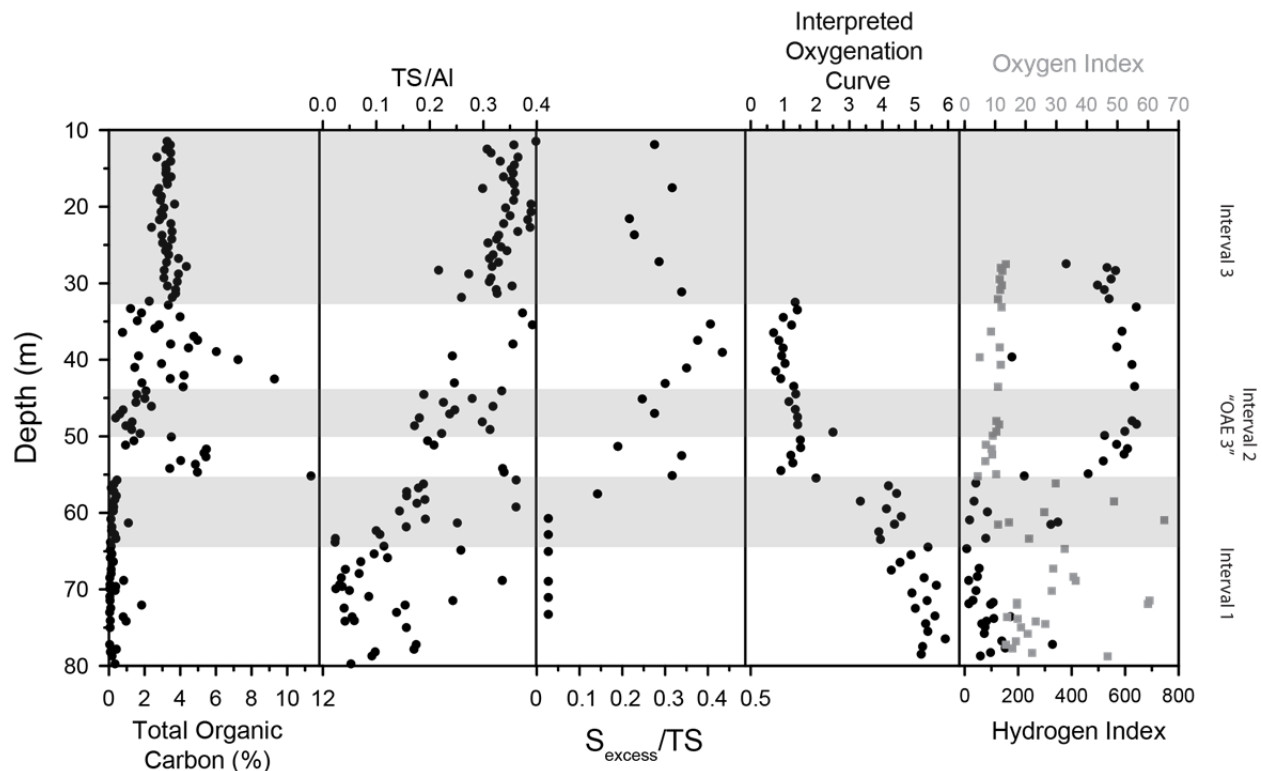
Figure 4.4

Total organic carbon (TOC), Total Sulfur (TS)/Al (wt. % ratios), S_{excess}/TS, ichnofacies-derived interpreted oxygenation curve (IOC; smoothed to 0.5 m resolution), and Oxygen Index and Hydrogen Index values. Gray bars denote Intervals 1b, 2b, and 3. TOC and RockEval results are from Tessin et al. (2015). IOC record is adapted from Savrda (1998).

highlighting an increase in the hydrogen-richness of organic matter. Conversely, oxygen index values are elevated in Interval 1 as compared to Interval 2, indicating a decrease in the oxygen-richness of organic matter (Tessin et al., 2015).

Weight % ratios of TS/Al indicate increasing S accumulation within the sediments throughout the record (Fig 4.4). During Interval 1, TS/Al averages 0.13 compared to an average of 0.51 and 0.38 during Intervals 2 and 3. Excess S/TS records (calculated as (TS-CRS)/TS) illustrate that between 13 and 44% of TS is non-CRS (Fig 4.5). Due to low concentrations of S and CRS in samples between 58 and 78 m in the core, errors on S_{excess}/TS increase but values are near 0%.
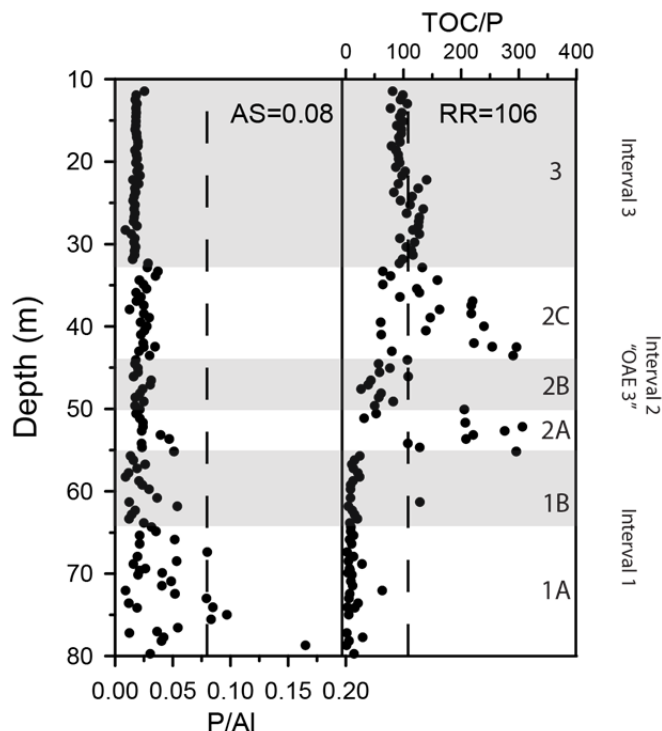
Figure 4.5

P/Al (weight % ratios) and TOC/P (molar ratios) records from the USGS Portland core. Dashed lines indicate the average shale P/Al ratio of 0.08 and the Redfield C:P ratio of 106:1. Gray bars denote Intervals 1b, 2b, and 3.

Phosphorus values are plotted as P/Al and TOC/P ratios in Figure 4.5. Trends in P geochemistry are based on total P and rather than organic or reactive P because it has been observed that P speciation records can be significantly altered by sample handling and diagenesis and that P_T/Al and TOC/P are the most reliable records of changes in P geochemistry in black shales (Algeo and Ingalls, 2007; Kraal et al., 2010). Calculations of P/Al ratios are shown as weight % ratios, while TOC/P values are calculated as molar ratios. During Interval 1, P/Al are highly variable, ranging between 0.009 and 0.170, with an average value of 0.04. During Intervals 2 and 3, P/Al values become less variable and average 0.025 and 0.018, respectively. TOC/P values are low throughout Interval 1, with an average molar ratio of 15. Molar ratios of TOC/P range between 26 and 306 during Interval 2. During Interval 3, TOC/P molar ratio values stabilize with an average value of 99.

4.5 Discussion

4.5.1 Fe speciation and limitation

Comparison of Fe speciation and trace metal concentrations throughout the Portland record suggests that changes in Fe speciation and abundance are decoupled from redox conditions. During Interval 1a, the Fe_T/Al record exhibits significant variability (Fig. 4.2). Elevated Fe_T/Al (>1) and Fe_{HR}/Fe_T ratios (>0.38) both indicate sedimentary Fe enrichments. Samples enriched in Fe_{HR} are characterized by low Al_T (0.29–0.37 wt. %) and Fe_T (0.43–0.5 wt. %) concentrations, as well as high carbonate concentrations (94.8–96.7 wt. %; Table D.2). While elevated Fe_T/Al and Fe_{HR}/Fe_T ratios could be interpreted as an indicator of periodic deposition under an anoxic water column, this interpretation is inconsistent with trace metal results. No enrichments in trace metals (Mo, Re, Cd, or Zn) are observed during Interval 1 (Fig. 4.3). This interval is also characterized by significant bioturbation and the presence of benthic macrofossils, both of which support well-oxygenated conditions (Savrda, 1998).

It has been shown in modern, carbonate-rich sediments that anomalously high Fe_T/Al values can occur when Fe_T is <0.5 wt. % due to incorporation of Fe^{2+} from anoxic porewaters into early diagenetic carbonate cements (Clarkson et al., 2014). Samples in the Portland core with <0.5 wt. % Fe, generally exhibit elevated Fe_T/Al ratios (>1) and have large contributions of carbonate-associated Fe (>40% of total Fe), whereas carbonate-associated Fe comprises less than 8% of total Fe in samples with >1 wt. % Fe (Fig. 4.2). The significant increase in Fe_{carb} suggests early diagenetic transformations of Fe within the sediments and pyrite formation limited by sulfide supply (Raiswell et al., 2011). The latter is also supported by the S excess/TS data, showing that all available sulfide has been sequestered into pyrite. Our results agree with the

modern compilation of Clarkson et al. (2014) that suggests that Fe speciation from carbonate-rich samples <0.5 wt. % Fe may not accurately record redox conditions.

During Interval 1b, Fe_{py}/Fe_{HR} values increase abruptly and remain elevated throughout the remainder of the record, suggesting efficient sulfidization of reactive Fe preceding, during and after the OAE (Fig. 4.2). This transition marks a shift from sulfide limited to reactive Fe limited pyrite formation in WIS sediments. Ratios of Fe_{HR}/Fe_T consistently falling above the anoxic threshold value of 0.38 and elevated Fe_{py}/Fe_{HR} values suggest water column precipitation of Fe^{2+} via pyrite formation under euxinic conditions preceding, during, and after the OAE (Fig. 4.2). However, persistent euxinia is inconsistent with trace metal distributions and biotic evidence, which indicate fluctuating redox conditions (Savrda, 1998). Redox sensitive trace metals (Mo, Re, Cd, and Zn) all exhibit consistent patterns throughout the Portland record, wherein trace metal accumulations track TOC concentrations. In particular, during Intervals 1b and 2b, low trace metal concentrations indicate relatively well-oxygenated conditions, despite consistently elevated Fe_{py}/Fe_{HR}. Additionally, Intervals 1b and 2b are associated with increased bioturbation, which is inconsistent with persistent euxinia (Savrda, 1998). Conversely, during Intervals 2a and 2c, elevated Mo, Cd, Re, and Zn concentrations and dominantly laminated (not bioturbated) sediments (Savrda, 1998) support the presence of euxinic conditions indicated by elevated Fe_{py}/Fe_{HR} and Fe_{HR}/Fe_T ratios.

The differences between Fe_{py}/Fe_{HR} and Mo, two proxies for euxinia, are highlighted in Fig. 4.6. Based on modern observations, Scott and Lyons (2012) proposed that Mo enrichment levels can be correlated with specific redox conditions: oxic (up to 2 ppm), anoxic (chemocline located within sediment, 2–25 ppm), intermittently euxinic conditions (chemocline located within water column, 25–100 ppm), and permanently euxinic (>100 ppm). However, Mo
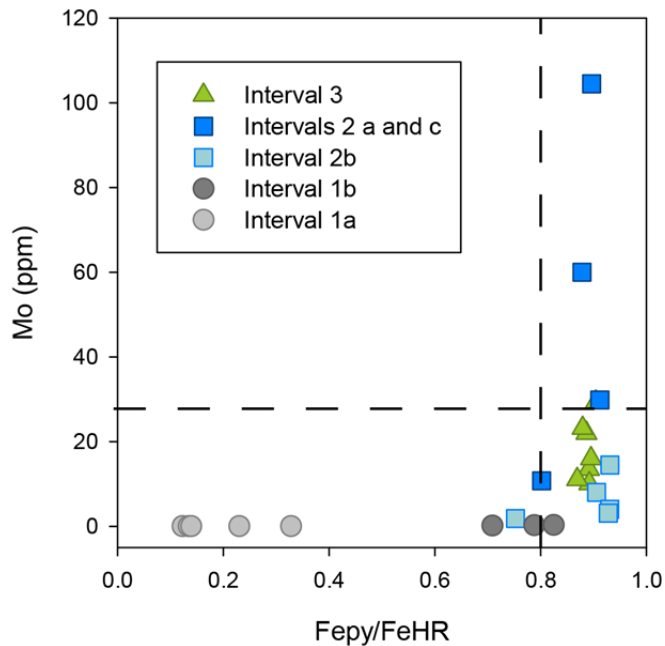
Figure 4.6

Crossplot of Fe_{py}/Fe_{HR} and Mo (ppm; Tessin et al. 2015). Gray circles indicate samples from Interval 1; blue squares indicate samples from Interval 2 and green triangles indicate samples from Interval 3. Dashed lines indicate interpreted euxinic conditions for Mo concentrations (Scott and Lyons, 2012) and Fe_{py}/Fe_{HR} (März et al., 2008; Poulton and Canfield, 2011).

concentrations >25 ppm are only recorded within Intervals 2a and 2c, despite Fe_{py}/Fe_{HR} values >0.7 throughout Intervals 1b, 2, and 3.

Changes in the trace metal inventory of the ocean, particularly within a partially restricted basin, could affect interpretation of trace metal redox proxies. Low Mo/TOC values in the Niobrara Formation relative to modern marine sediments indicate significant basin restriction and/or a reduced global Mo seawater budget (Tessin et al., 2015). However, variability in the Mo/TOC record, specifically higher Mo/TOC values coeval with elevated Mo and TOC concentrations, suggests that Mo is not being forced by changes in the Mo budget of the ocean (Fig. 4.3). Additionally, the consistency of trends across all trace metals, paired with biological evidence, demonstrates that the trace metal distributions are likely primarily controlled by redox conditions. Therefore, the lack of variability in Fe_{py}/Fe_{HR} values suggests that this proxy may

have been insensitive to redox fluctuations displayed by trace metal enrichments during and after OAE 3 in the WIS (Fig. 4.6).

The disagreement between the trace metal distributions and the Fe speciation could be explained by either significant porewater sulfidization of reactive Fe or downward moving sulfidization fronts. Elevated TOC concentrations during Intervals 2 and 3 indicate a significant increase in organic matter flux to the sediments, which would result in elevated sedimentary sulfate reduction, increased porewater H_2S concentrations, and enhanced porewater sulfidization of reactive Fe. While it is generally assumed that water column sulfide is required to scavenge Fe^{2+} and produce elevated Fe_{py}/Fe_{HR} and Fe_{HR}/Fe_T ratios, a recent study from the Peel-Harvey Estuary in Australia illustrated that significant Fe sulfidization in sediments can occur despite deposition under a <2m deep, oxic water column (Kraal et al., 2013). The Peel-Harvey estuary sediments similarly exhibit large Fe_{HR} enrichments despite the absence of an anoxic water column. Efficient Fe sulfidization has also been recorded within the surface sediments of the highly productive Achterwasser lagoon in the SW Baltic Sea, despite oxic conditions at the sediment-water interface (Neumann et al., 2005). These observations of significant early diagenetic sulfidization of reactive Fe within the surface sediments of modern sites support the possibility of pore water, rather than water column, sulfidization of reactive Fe within the WIS.

Downward moving sulfidization fronts associated with peak export productivity during Intervals 2a and 2c could also have pyritized reactive Fe deposited in the underlying Intervals 1b and 2b. Trace metal and TOC results indicate that sediments in Intervals 1b and 2b were deposited under conditions characterized by enhanced oxygenation and/or reduced export productivity. Enhanced levels of sulfate reduction under elevated export productivity during Intervals 2a and 2c could have led to porewater H_2S accumulation (for example, around a

sulfate-methane transition zone), which could "burn down" into underlying organic- and Fe-poor sediments, sulfurizing any available Fe_{HR}. Diagenetic sulfidization of reactive Fe in sediments underlying high TOC sediments has been recorded in a number of modern settings including the Black Sea, Kau Bay, and the Arabian Sea OMZ (Neretin et al., 2004; Middelburg, 1991; Schenau et al., 2002) and also occurred below Mediterranean sapropels (Passier et al., 1996). These sulfidization processes occur far below the sediment-water interface, and are not associated with any OC or trace metal enrichments, which could explain the discrepancy between trace metal, TOC, and Fe results within Intervals 1b and 2b.

Reactive Fe consumption within sediments, whether through early diagenetic sulfidization near the surface sediment or through post-depositional sulfide burn down, could occur more readily under low Fe availability. Despite elevated Fe_{HR}/Fe_T ratios, the Fe_T/Al record rarely shows Fe enrichments after Intervals 1a (Fig. 4.2). A marked increase in Fe_T/Al during Interval 2a (up to 0.88) and a more modest increase during Interval 2c (up to 0.58) paired with elevated Fe_{HR}/Fe_T and Fe_{py}/Fe_{HR} values (>0.38; >0.7) are consistent with pyrite formation in a euxinic water column. In general, however, the majority of Fe_T/Al ratios from Intervals 1b to 3 are below the average shale value of 0.55, strongly supporting that Fe could be the limiting pyrite formation in the WIS.

Although Fe_T/Al values are relatively low, a significant portion of this Fe is Fe_{HR}. Potential sources of reactive Fe to the deep basin of the WIS include Fe shuttled from the shallower to the deeper parts of the basin, the influx of nutrient-rich Tethyan water to the WIS during the Niobrara transgression, and Fe associated with volcanic ash. Regardless of the relative influence of these Fe sources, Fe_T/Al ratios generally suggest that, especially during Intervals 1b, 2b, and 3, Fe delivery to the sediments is low, which could promote porewater sulfide

accumulation and reactive Fe consumption. While Fe speciation has not been measured elsewhere in the WIS during OAE 3, in depth analysis of Fe-S-C relationships in the Berthoud State #4 core indicated that, similar to the Portland core, pyrite formation was reactive Fe limited during deposition of the Niobrara Formation (Dean and Arthur, 1989; Fig. 4.1). Furthermore, average Fe_T/Al ratios within the Berthoud and the Aristocrat Angus cores are 0.39 and 0.38, respectively, within the Niobrara subunits that are equivalent to our OAE and post-OAE intervals (Dean and Arthur, 1998; Locklair et al., 2011; Table D.2; Fig.4.1). Ratios of Fe_T/Al below crustal values (0.55) at all three sites support the conclusion that low Fe delivery was a persistent phenomenon throughout the deep basin in central Colorado during and after OAE 3. Efficient Fe retention in shallower, nearshore sediments due to expansion of sedimentary sulfidic conditions could limit Fe shuttling, reducing the supply of reactive Fe to the deepest regions of the WIS. Recent work by Scholz et al. (2014) demonstrates that a relatively narrow window of redox conditions that promote Fe release exists, such that slightly more reducing conditions on the "shelf" could limit Fe supply to the deepest portions of the basin.

Our results suggest that Fe limitation, paired with either elevated early diagentic sulfidization of reactive Fe in surface sediments or downward moving sulfidization fronts, can lead to significant porewater pyrite formation, suggesting that particular attention should be taken when applying the Fe_{py}/Fe_{HR} proxy to reconstruct water column redox at sites characterized by low Fe availability and elevated export productivity.

4.5.2 Implications of low Fe availability

The ability of Fe to buffer porewater sulfide has been proposed as a mechanism to decrease organic matter preservation in sediments (e.g. Meyers et al., 2005; Meyers, 2007;

Tribovillard et al., 2015). When reactive Fe is readily available, it can buffer porewater H_2S accumulation via Fe-sulfide formation. Conversely, when reactive Fe is limited, H_2S can accumulate in porewaters more rapidly (Meyers et al., 2005). Resulting high porewater H_2S concentrations create inhospitable conditions for infauna and, subsequently, can reduce the degree of bioturbation (Meyers et al., 2005; Meyers 2007). A reduction in bioturbation and bioirrigation, in turn, influences the composition of the porewater and solid constituents in sediments because infaunal organisms ventilate the substrate with oxygen-rich waters, stimulating microbial activity and reducing sedimentary organic matter preservation (Aller, 1978; Kristensen, 2000; Zonneveld et al., 2010).

During the Coniacian-Santonian, a strong relationship is found between S concentrations, bioturbation-derived IOC, and TOC in the Portland core (Fig. 4.4). Interval 1a is highly bioturbated and characterized by low TOC, indicating that burrowing organisms and the associated oxidative processes resulted in near complete OC loss from the sediments. When oxygen limitation reduces macrofaunal activity, beginning at the end of Interval 1, the reduction in bioturbation reduced sedimentary ventilation and oxygen exposure time. The increase in Fe_{py}/Fe_{HR}, S_{excess}/TS, and TS/Al ratios near the end of Interval 1 (Figure 4.2) suggests that a drawdown of reactive Fe by H_2S consumption is coeval with the observed onset of reduced benthic activity. Coeval changes in Hydrogen Index and Oxygen Index (HI and OI) values indicate enhanced preservation of hydrogen-rich, oxygen-poor organic matter in laminated or microbioturbated sediments. These combined results support that a reactive Fe limitation led to increased porewater sulfide concentrations, reduced bioturbation and bioirrigation, and increased organic matter preservation. Changes in organic matter composition (HI and OI) occur alongside

significant increases in measured TOC concentrations, highlighting the importance of changes in

organic matter preservation during periods of enhanced OC burial.

Another consequence of a reactive Fe limitation is the possible sulfurization of organic

matter (Zaback et al., 1993; Meyers, 2007; Tribovillard et al., 2015). Organic matter

sulfurization occurs when excess sulfide (not reacted with Fe) modifies organic matter functional

groups, such as lipids and carbohydrates. During and after OAE 3, 20–45% of S is in excess of

pyrite S and S_{excess} generally tracks TOC, indicating that excess S may be associated with organic

matter accumulation (Fig. 4.4). Sulfurization would make organic matter more resistant to

degradation, further promoting organic matter preservation throughout Intervals 2 and 3.

By reducing sedimentary P sequestration (the so called "Phosphorus Trap"), an Fe

limitation could also directly impact nutrient recycling within sediment porewaters, helping to

sustain elevated levels of primary production throughout the prolonged interval of black shale

deposition. Iron speciation is known to control benthic P recycling and can therefore impact the

return of nutrients buried with organic matter to the photic zone. Generally, as organic matter

degrades in surface sediments, phosphate (PO_4^{3-}) is released to porewaters where it can be

adsorbed on Fe oxyhydroxides, providing an efficient sedimentary sink for P. However, under

O_2 depleted conditions, Fe oxyhydroxides are dissolved and thus, P adsorption is limited (Rozan

et al., 2002). In the presence of free H_2S, Fe will precipitate as Fe-sulfides (e.g. FeS and FeS_2),

which have a low affinity for PO_4^{3-} (Krom and Berner, 1980). Enhanced P recycling in the

presence of sulfide has been suggested as a means to sustain primary productivity (Van

Cappellen and Ingall, 1994), indicating that a change in how nutrients are recycled from the

sediments could be as important as changes in external nutrient input for nutrient dynamics and

primary productivity in the WIS.

Elevated P/Al and low TOC/P values during Interval 1 indicate P sequestration in sediments. Conversely, during Intervals 2 and 3, P/Al values decrease and TOC/P values increase suggesting that P is no longer efficiently sequestered in the sediments (Fig. 4.5). Changes in P burial are coeval with increased pyrite abundance and low siderite, magnetite, and Fe (oxyhydr)oxides abundances (Figure 4.2), indicating that increased sedimentary P release is caused by Fe sulfidization. Our results support enhanced P recycling during the OAE and post-OAE intervals because (1) TOC/P records are consistently elevated during Intervals 2 and 3, as compared to Interval 1, and (2) P/Al ratios are very low compared to average shale values, despite significant increases in organic matter deposition during Intervals 2 and 3, which would deliver P to the sediments.

4.5.3 Implications for the development of OAEs

Elevated Fe delivery was proposed to be a primary control on low OC accumulation within the WIS during OAE 2 by reducing organic matter preservation and enhancing sedimentary phosphate burial (Meyers, 2007). Our results indicate that, during OAE 3, Fe cycling had the opposite effect and promoted prolonged black shale deposition both during and after the OAE. Efficient organic matter preservation and P recycling during the Coniacian-Santonian could provide a feedback mechanism that explains the prolonged duration of black shale deposition during OAE 3 within the WIS as compared to OAE 2.

The role of P release from sediments during Cretaceous OAEs has been the focus of recent work in other ocean basins. Geochemical evidence of enhanced sedimentary P recycling during OAE 2 has been found from the Tethys, WIS, and proto-Atlantic Ocean (Mort et al., 2007; Tsandev and Slomp, 2009; Kraal et al., 2010). Furthermore, the termination of OAE 2 is

associated with an increase in sedimentary P sequestration, indicating that P burial was a possible control on the duration of the event (Kraal et al., 2010). Conversely, sustained sedimentary P recycling in the WIS could have prolonged OC burial after the OAE 3 interval if remineralized P was returned to the photic zone.

Phosphorus recycling in the WIS appears to be distinct from the Proto-Atlantic during OAE 3. Previous work on OAE 3 from the Demerara Rise indicated that fluctuating ferruginous and euxinic conditions caused periods of massive P deposition that probably decreased levels of primary productivity (März et al., 2008). While the samples in our study were collected at a lower resolution than the Demerara Rise study, our results do not provide similar evidence of P burial during OAE 3, even during better oxygenated periods such as Interval 2b. Specifically, the new results indicate that reactive Fe, not sulfate, was consistently limiting within the WIS throughout Intervals 1b, 2, and 3, thereby, inhibiting P burial throughout OAE 3 and afterwards. The ferruginous/euxinic fluctuations observed at the Demerara Rise, but not the WIS, could be attributed to either periodic influence of oxic South Atlantic water masses at the Demerara Rise or sulfate drawdown in the restricted Proto-Atlantic (März et al., 2008).

Similar ferruginous/euxinic redox fluctuations associated with variable continental Fe delivery were observed in OAE 2 deposits from Tarfaya, Morocco; however, efficient P recycling was also observed throughout OAE 2 (Poulton et al., 2015). Further detailed and high-resolution geochemical work is, therefore, necessary to look for relationships between Fe speciation and enhanced P recycling at other Cretaceous sites that experienced prolonged periods of black shale deposition. Additionally, the relationship between changes in organic matter composition, bioturbation and Fe speciation should be determined during OAEs to evaluate

whether an Fe limitation was important to OAE development in other regions, or only within the WIS.

4.6 Conclusions

Iron speciation results from OAE 3 suggest that a reactive Fe limitation may have stimulated and maintained enhanced OC burial after the initial development of anoxia within the WIS by increasing organic matter preservation in sediments and enhancing nutrient recycling. Preceding the onset of increased OC burial, Fe speciation results record a shift from predominantly non-sulfide Fe phases (carbonate, (oxyhydr)oxides, and magnetite) to predominantly sulfide Fe phases. Intervals 2 and 3 are characterized by stable, elevated pyrite formation despite other proxies recording significant redox variability, suggesting efficient Fe sulfidization, either within surface sediments or due to downward migration of sulfidization fronts. Significant sulfidization of Fe, paired with low Fe_T/Al ratios, indicates that reactive Fe may be limiting sedimentary pyrite formation.

Our results highlight two complications for using Fe as a redox proxy on geologic timescales: (1) similar to modern observations, reactive Fe is sequestered in early diagenetic carbonate phases during Interval 1a producing anomalously elevated Fe_T/Al values independent of redox conditions, and (2) efficient sulfidization of reactive Fe within the Fe-limited WIS, obscured redox variability before, during and after the OAE.

A reactive Fe limitation could promote organic matter preservation in sediments because the amount of reactive Fe was insufficient to buffer porewater H_2S concentrations through Fe-sulfide formation. Coeval changes in Fe, S, bioturbation and organic matter composition support that changes in Fe availability reduced the sedimentary "sulfide buffer," reducing bioturbation

104

and producing conditions more conducive to organic matter preservation. During Interval 1a, the availability of non-sulfide Fe phases promoted P sequestration. However, as porewater H_2S accumulation increased, sulfidization of reactive Fe phases promoted P release from the sediments. This change in phosphate cycling could have prolonged enhanced OC burial during and after OAE 3 by stimulating enhanced primary productivity in the WIS, helping to extend the duration of OAE 3 as compared to OAE 2.

Distinct C-S-P cycling in the WIS during the Coniacian-Santonian, as compared to the Proto-Atlantic, during supposedly stable and widespread anoxic periods in the Late Cretaceous oceans, indicates that there was a significant amount of spatial variability between open shelf settings, continental margins, and epicontinental seas such as the WIS. Detailed studies of stratigraphically equivalent sediment intervals in high resolution, using a range of sedimentological and geochemical tools will enable a more complete understanding of the biogeochemical cycles of the Cretaceous greenhouse ocean.

4.8 References

Algeo, T., E. Ingall (2007), Sedimentary C_{org}:P ratios, paleocean ventilation, and Phanerozoic atmospheric O_2, *Palaeogeography Palaeoclimatology Palaeoecology 256*, 130-155.

Algeo, T., J.B. Maynard (2004), Trace-element behavior and redox facies in core shales of Upper Pennsylvanian Kansas-type cyclothems, *Chemical Geology, 206*, 289-318.

Anderson, TF, Raiswell, R (2004) Sources and mechanisms for the enrichment of highly reactive iron in euxinic Black Sea sediments , *American Journal of Science, 304*, 203-233.

Arthur, M. A., S.O. Schlanger, and H.C. Jenkyns (1987), The Cenomanian-Turonian Oceanic Anoxic Event, II, Paleoceanographic controls on organic matter production and preservation, in Marine Petroleum Source Rocks, Geological Society of London Special Paper, edited by J. a. A. F. Brooks, pp. 401-420.

Boyd, P. W., et al. (2000), A mesoscale phytoplankton bloom in the polar Southern Ocean stimulated by iron fertilization, *Nature, 407*, 695-702.

Canfield, D.e. (1989), Reactive iron in marine sediments, *Geochimica et Cosmochimica Acta, 53*, 619-623.

Canfield DE, Raiswell R, Westrich JT, Reaves CM, Berner RA (1986), The use of chromium reduction in the analysis of reduced inorganic sulfur in sediments and shales, *Chemical Geology 54*,149–155.

Chappaz, A., T. Lyons, D. Gregory, C. Reinhard, B. Gill, C. Li, R. Large (2014), Does pyrite act as an important host for molybdenum in modern and ancient sediments?, *Geochimica et Comsmochimica Acta, 126*, 112-122.

Clarkson, M., S. Poulton, R. Wood, R. Guilbaud (2014), Assessing the utility of Fe/Al and Fe-speciation to record water column redox conditions in carbonate-rich sediments, *Chemical Geology 382*, 111-122.

Crusius, J., S. Calvert, T. Pedersen, and D. Sage (1996), Rhenium and molybdenum enrichments in sediments as indicators of oxic, suboxic and sulfidic conditions of deposition, *Earth and Planetary Science Letters, 145*(1-4), 65-78.

Dean, W.E., M. A. Arthur (1989), Iron-sulfur-carbon relationships in organic-carbon-rich sequences: Cretacesou Western Interior Seaway, American Jounal of Science, 289 (6), 708-743.

Dean, W. E., M. A. Arthur (1998), Geochemical expressions of cyclicity in Cretaceous pelagic limestone sequences: Niobrara Formation, Western Interior Seaway, in *Stratigraphy and Paleoenvironments of the Cretaceous Western Interior Seaway*, edited by W. E. a. M. A. A. Dean, pp. 227-255, SEPM Concepts in Sedimentology and Paleontology.

Erickson BE, Helz GR (2000), Molybdenum (VI) speciation in sulfidic waters: Stability and lability of thiomolybdates, *Geochimica et Cosmochimica Acta, 64*, 1149-1158

Fernex, F., Février, G., Benaïm, J., Arnoux, A. (1992), Copper, lead and zinc trapping in Mediterranean deep-sea sediments: probable coprecipitation with manganese and iron, *Chemical Geology, 98*, 293–308.

Floegel, S., W. W. Hay, R. M. DeConto, and A. N. Balukhovsk (2005), Formation of sedimentary bedding couplets in the Western Interior Seaway of North America - implications from climate system modeling, *Palaeogeography Palaeoclimatology Palaeoecology 218*(1-2), 125-143.

Hattin, D.E., 1982. Stratigraphy and depositional environment of Smoky Hill Chalk Member, Niobrara Chalk (Upper Cretaceous) of the type area, Western Kansas. Kansas Geological Society Bulletin 225, 108 p.

Huerta-Diaz, M.A., Morse, J.W. (1992), Pyritisation of trace metals in anoxic marine sediments, *Geochimica et Cosmochimica Acta, 56*, 2681–2702.

Jenkyns, H. C. (2010), Geochemistry of oceanic anoxic events, *Geochemistry Geophysics Geosystems*, *11*.

Kraal, P., E. Burton, R. Bush (2013), Iron monosulfide accumulation and pyrite formation in eutrophic estuarine sediments, *Geochimica et Cosmochimica Acta, 122*, 75-88.

Kraal, P., C. P. Slomp, A. Forster, M. M. M. Kuypers (2010), Phosphorus cycling from the margin to abyssal depths in the proto-Atlantic during oceanic anoxic event 2, *Palaeogeography, Palaeoclimatology, Palaeoecology 295* (1), 42-54.

Krom, M., R. Berner (1980), Adsorption of phosphate in anoxic marine sediments, *Limnology and Oceanography, 25*(5), 797-806.

Locklair, R., B. Sageman, and A. Lerman (2011), Marine carbon burial flux and the carbon isotope record of Late Cretaceous (Coniacian-Santonian) Oceanic Anoxic Event III, *Sedimentary Geology 235*(1-2), 38-49.

Lyons TW, Severmann S (2006), A critical look at iron paleoredox proxies: new insights from modern euxinic marine basins, *Geochimica Et Cosmochim Acta 70*, 5698–5722

März, C., S. W. Poulton, B. Beckmann, K. Kuester, T. Wagner, and S. Kasten (2008), Redox sensitivity of P cycling during marine black shale formation: Dynamics of sulfidic and anoxic, non-sulfidic bottom waters, *Geochimica Et Cosmochimica Acta*, *72*(15), 3703-3717.

Meyers, S.R., Sageman, B.B., and Lyons, T. (2005), Organic carbon burial rate and the molybdenum proxy: Theoretical framework and application to Cenomanian-Turonian OAE II, *Paleoceanography*, PA2002, doi:10.1029/2004PA001068.

Meyers, S.R. (2007), Production and preservation of organic matter: The significance of iron: *Paleoceanography 22*, PA4211, doi:10.1029/2006PA001332.

Middelburg, J. (1991), Organic carbon, sulfur, and iron in recent semi-euxinic sediments of Kau Bay, Indonesia, *Geochimica et Cosmochimica Acta 55*, 815-828.

Neretin, L., M. Bottcher, B. Jorgensen, I. Volkov, H. Luschen, K. Hilgenfeldt (2004), Pyritization processes and greigite formation in advancing sulfidization front in the Upper Pleistocene sediments of the Black Sea, *Geochimica et Cosmochimica Acta 68*(9), 2081-2093.

Neumann, T., N. Rausch, T. Leipe, O. Dellwig, Z. Berner, M. Bottcher (2005), Intense pyrite formation under low-sulfate conditions in the Achterwasser lagoon, SW Baltic Sea, *Geochimica et Cosmochimica Acta 69*(14), 3619-3630.

Mort, H. P., T. Adatte, K. B. Follmi, G. Keller, P. Steinmann, V. Matera, Z. Berner, and D. Stuben (2007), Phosphorus and the roles of productivity and nutrient recycling during oceanic anoxic event 2, *Geology 35,* 483–486.

Passier, H., J. Middelburg, B. van Os, G. De Lange (1996), *Geochimica et Cosmochimica Acta 60*(5), 751-763.

Piper, D.Z., Perkins, R.B. (2004), A modern vs. Permian black shale— the hydrography, primary productivity, and water-column chemistry of deposition, *Chemical Geology, 206*, 177–197.

Poulton SW, Canfield DE (2005), Development of a sequential extraction procedure for iron: implications for iron partitioning in continentally derived particulates, *Chemical Geology 214*, 209–221

Poulton, SW, Raiswell, R (2002) The low-temperature geochemical cycle of iron: From continental fluxes to marine sediment deposition, *American Journal of Science, 302,* 774-805.

Poulton SW, Fralick PW, Canfield DE (2004), The transition to a sulphidic ocean 1.84 billion years ago, *Nature 431*, 173–177

Poulton, S., S. Henkel, C. Marz, H. Urquhart, S. Floegel, S. Kasten, J. Sinninghe Damste, T. Wagner (2015), A continental-weathering control on orbitally driven redox-nutrient cycling during Cretaceous Oceanic Anoxic Event 2, *Geology, 43* (11), 963-966.

Raiswell R, Anderson TF (2005), Reactive iron enrich- ment in sediments deposited beneath euxinic bottom waters: constraints on supply by shelf recycling, *Geological Society of London Special Publications 248*, 179–194

Raiswell, R, Canfield, DE (1996) Rates of reaction between silicate iron and dissolved sulfide in Peru Margin sediments, *Geochimica et Cosmochimica Acta, 60*, 2777-2787.

Raiswell, R; Canfield, DE (1998) Sources of iron for pyrite formation in marine sediments, *American Journal of Science*, *298*, 219-245.

Raiswell, R., Reinhardt, C.T., Derkowski, A., Owens, J., Bottrell, S.H., Anbar, A.D., Lyons, T.W. (2011) Formation of syngenetic and early diagenetic iron minerals in the late Archean Mt. McRae Shale, Hamersley Basin, Australia: new insights on the patterns, controls and paleoenvironmental implications of authigenic mineral formation. *Geochimica Cosmochimica Acta, 25*, 1072-1087.

Rozan, T, M. Taillefert, R. Trouwborst, B. Glazer, S. Ma, J. Herszage, L. Valdes, K. Price, G. Luther III (2002), Iron-sulfur-phospohorus cycling in the sediment of a shallow coastal bay: Implications for sediment nutrient release and benthic macroalgal blooms, *Limnology and Oceanography 47*(5), 1346–1354.

Sageman, B., M. Arthur (1994), Early Turonian paleogeographic/paleobathymetric map, Western Interior, US *in* Caputo, M. V., Peterson J. A., and Franczyk, K.J., eds., Mesozoic Systems of the Rocky Mountain Region, USA: SEPM, Rocky Mountain Section, 457-470.

Sageman, B. B., S. R. Meyers, M. A. Arthur (2006), Orbital time scale and new C-isotope record for Cenomanian-Turonian boundary stratotype, *Geology, 34* (2), 125-128.

Savdra, C. E. (1998), Ichnocoenoses of the Niobrara Formation: Implications for benthic oxygenation histories, in *Stratigraphy and Paleoenvironments of the Cretaceous Western Interior Seaway*, edited by W. E. a. M. A. A. Dean, pp. 227-255, SEPM Concepts in Sedimentology and Paleontology.

Schenau, S.J., Reichart, G.J. and De Lange, G.J. (2002), Oxygen minimum zone controlled Mn redistribution in Arabian Sea sediments during the late Quaternary, *Paleoceanography 17*.

Schlanger, S. O., M. A. Arthur, H. C. Jenkyns, P. A. Scholle (1987), The Cenomanian-Turonian Oceanic Anoxic Event, I. Stratigraphy and distribution of organic carbon-rich beds and the marine $\delta13C$ excursion, *Geological Society, London, Special Publications 26* (1), 371-399.

Scholz, F., J. McManus, A. Mix, C. Hensen, R. Schneider (2014), The impact of ocean deoxygenation on iron release from continental margin sediments, *Nature Geoscience 7*, 433-437.

Scott, C., and T. W. Lyons (2012), Contrasting molybdenum cycling and isotopic properties in euxinic versus non-euxinic sediments and sedimentary rocks: Refining the paleoproxies, *Chemical Geology 324*, 19-27.

Scott, G. R., and W. A. Cobban (1964), Stratigraphy of the Niobrara Formation at Pueblo, Colorado, *Professional Papers US Geological Survey*, *454-L*, L1-L30.

Severmann, S., J. McManus, W. Berelson, D. Hammond (2010), The continental shelf benthic iron flux and its isotope composition, *Geochimica et Cosmochimica Acta 74*, 3984-4004.

Tessin, A., I. Hendy, N. Sheldon, B. Sageman (2015), Redox-controlled preservation of organic matter during "OAE 3" within the Western Interior Seaway, *Paleoceanography 30* (6), 702-717.

Tribovillard, N., T. Algeo, T. Lyons, A. Riboulleau (2006), Trace metals as paleoredox and paleoproductivity proxies: an update, *Chemical Geology, 232*, 12-32.

Tribovillard, N., E. Hatem, O. Averbuch, F. Barbecot, V. Bout-Roumazeilles, A. Trentesaux (2015), Iron availability as a dominant control on the primary composition and diagenetic overprint of organic-matter-rich rocks, *Chemical Geology 401*, 67-82.

Tsandev, I., C. P. Slomp (2009), Modeling phosphorus cycling and carbon burial during Cretaceous Oceanic Anoxic Events, *Earth and Planetary Science Letters 286* (1), 71-79.

Tsikos, H., H.C. Jenkyns, B. Walsworth-Bell, M. R. Petrizzo, A. Forster, S. Kolonic, W. Erba, I. Premoli Silva, M. Baas, T. Wagner, J. Sinninghe Damste (2004) Carbon-isotope stratigraphy recorded by the Cenomanian-Turonian oceanic anoxic event: correlation and implications based on three key-localities, *Journal of the Geological Society, 161*, 711-720.

Van Cappellen P. and Ingall E (1994), Benthic phosphorus regeneration, net primary production, and ocean anoxia: A model of the coupled marine biogeochemical cycles of carbon and phosphorus, *Paleoceanography 9*, 677-692.

Wagreich, M. (2012), "OAE 3" --regional Atlantic organic carbon burial during the Coniacian-Santonian, *Climate of the Past*, 8, 1447-1455.

Zaback, D.A., Pratt, L.M., Hayes, J.M. (1993), Transport and reduction of sulphate and immobilisation of sulphide in marine black shales, *Geology 21*, 141–144.

Zonneveld, K. A. F., et al. (2010), Selective preservation of organic matter in marine environments; processes and impact on the sedimentary record, *Biogeosciences 7*, 483–511.

Chapter 5

Paleoredox reconstructions from the Carlile and Niobrara Formations in southern
Alberta: Implications for the Late Cretaceous Oceanic Anoxic Event 3

5.0 Abstract

Deposition of fine-grained, organic carbon-rich rocks within the Cretaceous Western

Interior Seaway (WIS) has been the focus of decades of research. The Coniacian-Santonian

Oceanic Anoxic Event 3 represents a significant interval of prolonged organic carbon burial

within the WIS. While the importance of changing redox conditions on organic carbon burial has

been illustrated, the primary driver for the development of anoxia remains debated. However,

most of the existing research on redox conditions in the WIS during the Coniacian-Santonian

and, subsequently the driving mechanisms of enhanced organic carbon burial comes from cores

taken within Colorado, making it impossible to evaluate seaway-wide trends. In this study, we

use redox sensitive trace metals (Re, Cd, and Mo) and Fe speciation to reconstruct paleoredox

changes within the Niobrara Formation in southern Alberta. These results are then compared to

paleoredox records from Colorado in order to evaluate temporal and spatial trends of anoxia in

the WIS. These results suggest that three intervals of oxygen limitation occurred coeval with

elevated organic carbon burial. The first of these, in the lower Verger Member, precedes carbon

burial in Colorado and is likely caused by significant local volcanic activity. The two remaining

intervals, the upper Verger Member and the First White Specks Member, are both associated

with sea-level rise and incursion of Tethyan water into the WIS. The influence of Tethyan water could drive the development of anoxia and enhanced organic carbon burial by increasing primary productivity in nutrient-rich waters and/or through the development of density stratification. Our results point to sea level as the primary driver for the development of anoxia and enhanced organic carbon burial, which explains many of the complexities in identifying a global OAE 3.

5.1 Introduction

The deposition of fine-grained, organic carbon-rich rocks within the North American Western Interior Seaway (WIS) during the Late Cretaceous is of widespread interest, both due to their potential as petroleum source rocks and as an archive of marine carbon cycling under a greenhouse climate. Particular attention has been focused on the Cenomanian to Campanian sedimentary record in the WIS, as this interval includes Oceanic Anoxic Events 2 and 3 (e.g. Nielsen et al., 2008; Schröder-Adams et al., 2012; Du Vivier et al., 2014; Eldrett et al., 2014, Zhou et al., 2015; Tessin et al., 2015). Oceanic Anoxic Events (OAEs) are globally recognized intervals of widespread ocean anoxia and enhanced organic carbon burial (e.g. Schlanger and Jenkyns, 1976; Jenkyns, 2010). The Cenomanian-Turonian OAE 2 is the canonical example of these events. It is associated with a distinct, short-lived (<0.5 Ma) positive isotope excursion and black shale deposition in many regions around the world (e.g., Arthur et al., 1987; Schlanger et al., 1987; Tsikos et al., 2002; Jenkyns, 2010). Conversely, the Coniacian-Santonian OAE 3 is identified globally by a muted carbon isotope plateau and is of a prolonged duration (~3 Ma; Locklair et al., 2011; Wagreich, 2012). Black shale deposition during OAE 3 only occurs in shallow and restricted marine environments. However, in contrast to the oxic conditions

112

observed in the WIS during OAE 2, significant evidence of anoxia is recorded in the WIS during OAE 3 (Locklair et al., 2011; Tessin et al., 2015).

The development of anoxia and subsequent changes in organic matter preservation has been identified as the primary control on organic carbon burial within the WIS (e.g. Locklair, 2007; Tessin et al., 2015; Tessin et al., 2016). However, the driver of the anoxia is less clear. Oxygen consumption may occur in response to either decreased ventilation of subsurface waters or increased oxidant demand under elevated photic zone primary productivity. Decreased ventilation could occur as a response to changing circulation patterns and water mass dynamics or the development of stratification due to a fresh water lid from continental runoff (e.g. Kauffman, 1975; Pratt, 1981; Barron et al., 1985; Hattin, 1985). Contrasting circulation patterns have been suggested for the WIS, including those suggesting dominantly Tethyan-sourced surface waters (Slingerland et al., 1996) or dominantly Arctic-sourced surface waters (Watkin, 1986; Poulsen et al., 1999; Coulson et al., 2011). The incursion of Tethyan-sourced waters has additionally been suggested as a source of nutrient-rich, oxygen-poor waters to the WIS (Leckie et al., 1998; Meyers et al., 2001; Arthur and Sageman, 2005). In this regard, high sea level would lead to more Tethyan water bathing the WIS, fueling oxygen consumption through enhanced surface productivity.

While black shale deposition occurred episodically throughout the WIS during the Coniacian-Santonian, information about evolving paleoredox conditions and mechanisms to explain changing organic carbon deposition under changing paleoredox conditions, comes largely from a series of cores in Colorado (Dean and Arthur, 1998, Locklair et al., 2011; Tessin et al., 2015). In order to evaluate the proposed mechanisms that drove the development of anoxia and increased organic carbon burial, paleoredox records from other regions of the seaway are

required. In this study, we present trace metal and Fe speciation records from southeastern Alberta in order to evaluate changes in oxygen availability throughout deposition of the Coniacian-Santonian Niobrara Formation. By comparing redox results from southeastern Alberta to the well-documented trends in Colorado, different hypotheses about the primary driver for the development of anoxia and the nature of "OAE 3" in the WIS can be evaluated.

5.2 Study Site

The Colorado Group in the United States and Canada includes two second order sea level cycles: the Greenhorn Cycle of the Lower Colorado Group and the Niobrara Cycle of the Upper Colorado Group (e.g. Kauffman, 1967; McNeil and Caldwell, 1981; Caldwell et al., 1993). The Carlile Formation represents the final regression of the Greenhorn Sea and is overlain by the Niobrara Formation, which includes the entire transgressive phase of the Niobrara Cycle (Nielsen et al., 2003). The Niobrara Formation is subdivided into three formal members: the Verger, Medicine Hat, and First White Specks members, which are overlain by the regressive Milk River Formation in southern Alberta. Intervals of elevated organic carbon burial have been identified within the Niobrara Formation in both the Sweetgrass Arch and Cold Lake regions (Fig. 5.1; Nielsen et al., 2008; Schröder-Adams et al., 2014).

The Colorado Group was deposited in the Canadian Western Interior Seaway (CWIS), an asymmetrical foreland basin (e.g. Plint et al., 1993; Bloch et al., 1993; Leckie et al., 1994; Kreitner and Plint, 2006). Maximum subsidence and sediment input from the Cordillera to the west produced a clastic wedge that thins to the east (e.g. McNeil and Caldwell, 1981; Shurr and Rice, 1986; Leckie et al., 1994). The study area is locally complicated by the Sweetgrass Arch, which divides the CWIS into the Alberta Basin to the west and the Williston Basin to the east

(Nielsen et al., 2008).
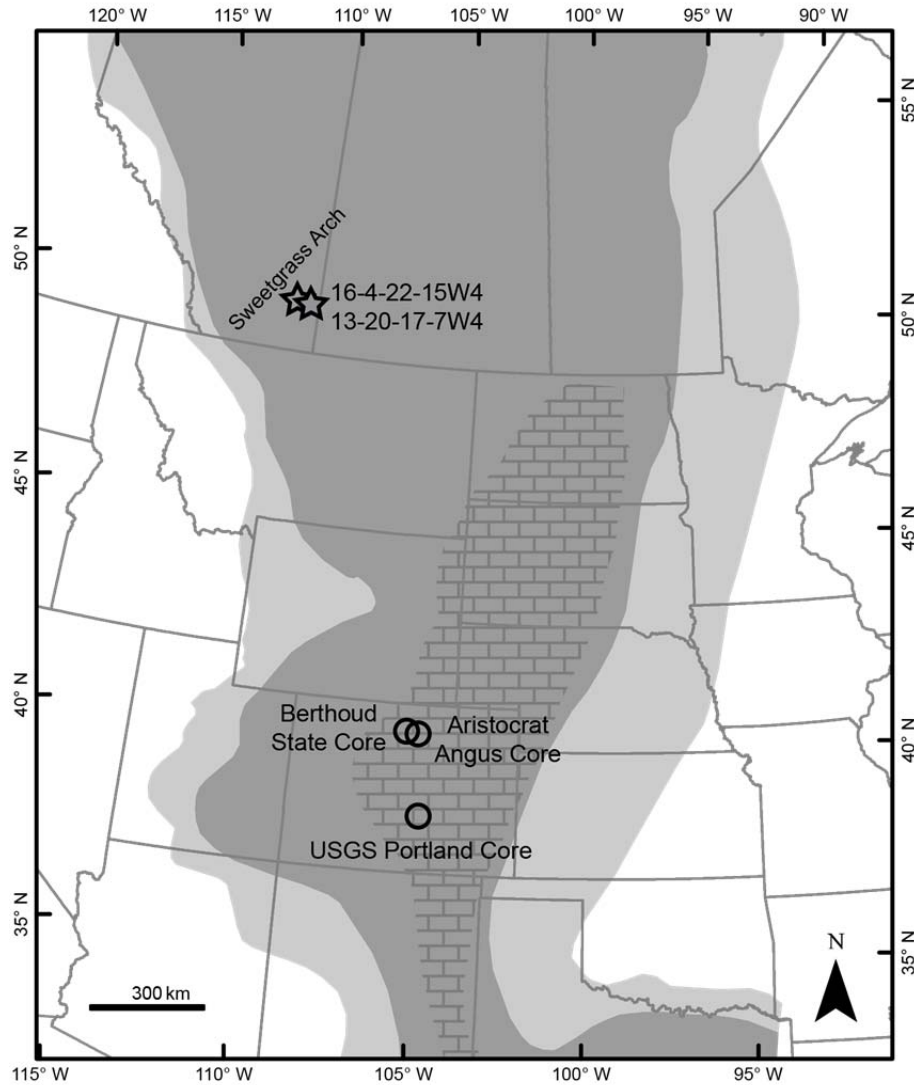
Figure 5.1

Map of the Western Interior Seaways (adapted from Roberts and Kirshbaum, 1995) indicating seaway extent and distribution of lithologies during the Coniacian. The star designates the location of cores 16-4-22-15W4 and 13-20-17-7W4. Circles designate cores from the central Western Interior Seaway (USGS Portland, Berthoud State, and Aristocrat Angus) for comparison.

5.3 Methods and Materials

The Niobrara Formation was sampled from two reference cores from wells from the

Sweetgrass Arch region, 13-20-17-7W4 and 16-4-22-15W4 (Fig. 5.1). The former core is the

reference core for the Carlile-Niobrara formational contact and the latter is the reference core for

the three members of the Niobrara Formation. Core 13-20-17-7W4 includes the lower portion

and 16-4-22-15W4 records the upper portion of the Verger Member (Nielsen et al., 2003). The

wells are ~60 km apart, with the more distal site (13-20-17-7W4) located to the southeast. Cores

were sampled at 30 cm to 1 m intervals with increased sampling frequency near lithological

boundaries and in critical intervals.

Samples were prepared for foraminiferal analysis according to the standard methods of Then

and Dougherty (1983). Relative foraminiferal abundance is expressed in three categories: rare for

samples with less than 15 specimens, common for samples with 15 to 30 specimens, and

abundant for samples with over 30 specimens (Nielsen et al., 2003).

Samples for major and trace element geochemistry were ground to <75 μm and

homogenized in an alumina shatterbox to minimize trace element contamination. Elemental

analysis was completed on samples from the Portland core at ALS Laboratories in Vancouver,

BC. Whole rock samples were digested with perchloric, hydrofluoric, nitric, and hydrochloric

acids. Concentrations were determined by inductively coupled plasma-atomic emission

spectroscopy (ICP-AES) and inductively coupled plasma-mass spectroscopy (ICP-

MS). GRM908, OREAS 90 and MRGeo08 standards were used to verify elemental

concentrations. In order to compare results to other seaway localities, enrichment factors (EF)

are calculated based on the trace metal (TM) to aluminum (Al) ratio of the sample as compared

to the average shale value:

$$EF = \frac{(\frac{TM}{Al})_{sample}}{(\frac{TM}{Al})_{avg.\ shale}}$$

Separation of iron phases for iron speciation was completed following Poulton and Canfield

(2005), and pyrite Fe extractions following Canfield et al. (1986). Carbonate-associated Fe

(Fe_{carb}), magnetite Fe (Fe_{mag}), and Fe (oxyhydr)oxides (Fe_{ox}) are considered highly reactive (HR) because these phases react with sulfide on timescales of months to years (Poulton and Canfield, 2005). These three phases were separated using the following sequential extraction: Fe_{carb} phase was extracted in 10 mL 1 M Na-acetate (pH 4.5; shake for 48 hours), the Fe_{ox} phase was extracted in 10 mL of citrate-buffered Na-dithionite (pH 4.8; shake for 2 hours), and the Fe_{mag} phase was extracted in 10 mL ammonium oxalate (pH 3.2, shake for 6 hours). Concentrations of Fe_{carb}, Fe_{ox}, and Fe_{mag} were measured on ICP-MS (Thermo iCAP Q) within the STAR LAB at Central Michigan University. Analytical precision and accuracy, determined from replicate analyses (n = 21) of a certified standard (SCP Science) were better than 5%.

The Fe_{HR} pool also includes pyrite Fe (Fe_{py}), which represents Fe that has reacted with sulfide in the water column or during early diagenesis in the sediments (Raiswell and Canfield, 1998; Poulton and Raiswell, 2002). The pyrite fraction is stoichiometrically determined following precipitation of chromium reducible sulfide as Ag_2S. Calculated pyrite Fe concentrations generally replicated with <5% precision. The Fe_{HR} pool is thus defined as $Fe_{carb} + Fe_{ox} + Fe_{mag} + Fe_{py}$ and poorly reactive Fe (Fe_{PR}) is calculated as $Fe_T - Fe_{HR}$.

5.4 Results

5.4.1 Foraminiferal Assemblages

The Carlile Formation is represented by the *Trochammina* sp. 1 Zone. The three members of the Niobrara Formation can be recognized by four foraminiferal zones; these are the *Marssonella oxycona* Zone in the lower Verger Member, the *Bullopora laevis* Zone in the upper Verger Member, the *Gavelinella henbesti* Zone in the Medicine Hat Member and the *Glogiberinelloides/Heterohelix* cf. *reussi* Zone in the First White Specks Member (Nielsen, et al., 2008). Detailed zonal species compositions for both wells discussed here
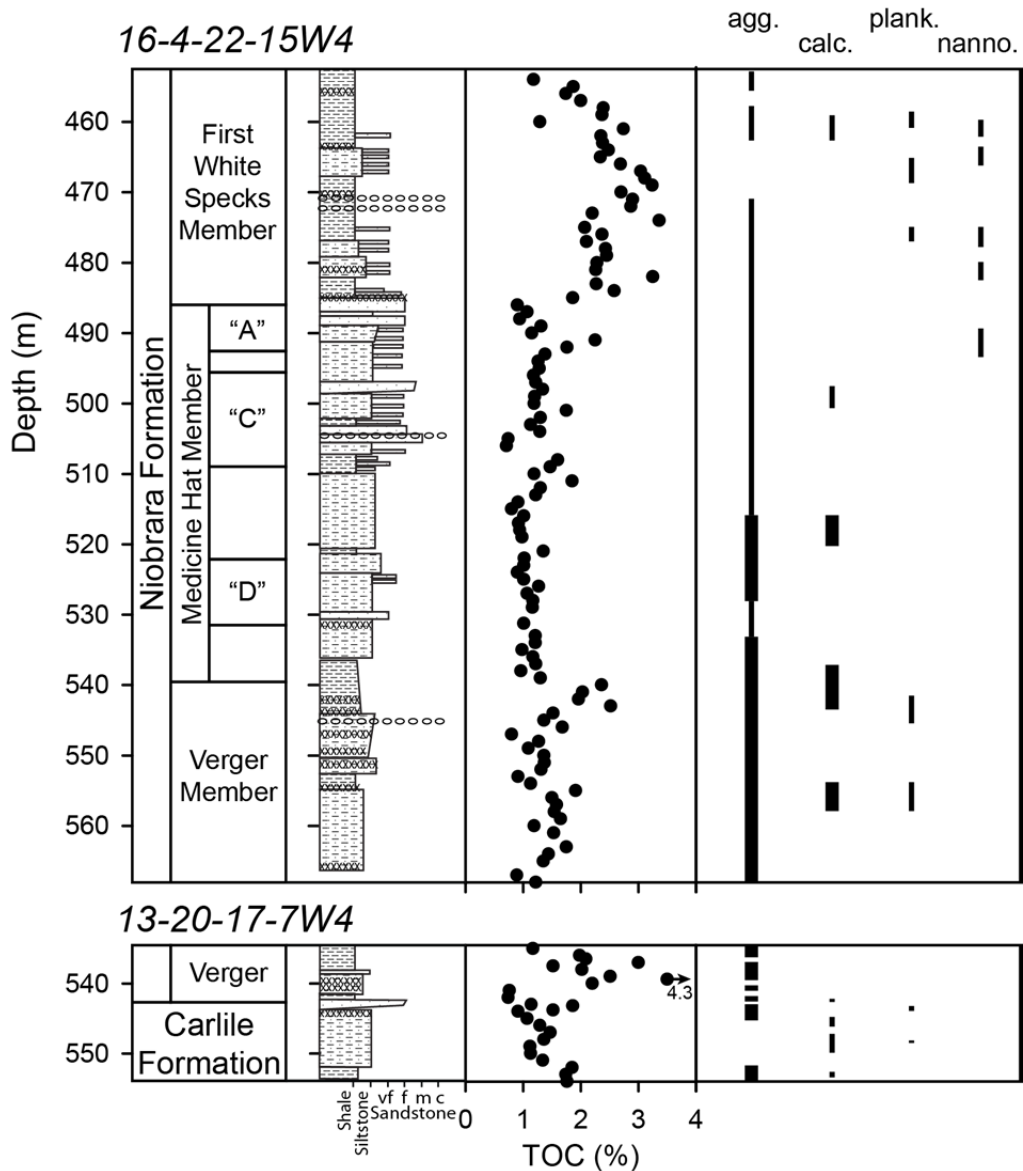
Figure 5.2

Statigraphy, total organic carbon, and micropaleontology from cores 16-4-22-15W4 and 13-20-17-7W4. Presence of agglutinated and calcareous benthic foraminifera, planktonic foraminifera, and nannofossils are indicated by lines. No line indicates absent, a thin line indicates presence and a thick line indicates abundant.

were provided by Elberdak (2004). The Carlile Formation is characterized by a dominantly

agglutinated assemblage with two short-live appearances of calcareous species (Fig. 5.2).

The Verger Member is barren of benthic foraminifera in its basal that is marked by a

bentonite swarm. Benthic foraminifera as observed in the 16-04-22-15W4 well are

common to abundant throughout the upper Verger to the base of the C Sandstone of the

Medicine Hat Member. The remaining Niobrara Formation from the C Sandstone up to the top to the Milk River Formation is marked only by rare benthic foraminifera (Fig. 5.2). Calcareous benthic species occur sporadically and planktic species occur with rare to common numbers in the upper Verger and First White Specks members (Elberdak, 2004). The relatively poor planktic foraminiferal assemblage on the north flank of the Sweetgrass Arch (Nielsen et al., 2008) contrasts much richer planktic assemblages as observed eastwards in cores of Saskatchewan penetrating the First White Specks Member (e.g. Schröder-Adams et al., 1996).

5.4.2 Inorganic chemistry

Trace metals (Mo, Re, U, V, Cd, and Zn) within southeastern Alberta cores show enrichment factors that indicate trace metal enrichments (>3) with enrichment factors >10 in Mo, Re, and Cd (Table 1). In core 16-4-22-15W4, Mo concentrations range from 0.25—33.1 (Fig. 5.3). Molybdenum concentrations average 2.3 ppm and 2.8 ppm in the Verger and Medicine Hat Members, increasing to an average of 17.1 ppm in the First White Specks Member before decreasing in the overlying Milk River Formation to an average of 1.2 ppm (Fig. 5.3). Rhenium concentrations in the Niobrara Formation of core 16-4-22-15W4 range from 2–87 ppb, with the highest Re concentrations occurring within the Verger and First White Specks Members (average of 15 and 30 ppb, respectively) and lower concentrations (averaging 10 ppb) in the intervening Medicine Hat Member (Fig. 5.3). Cadmium concentrations range from 0.05–2.24 ppm in the Niobrara interval of core 16-4-22-15W4, with the lowest concentrations of Cd within the sandstones of the Medicine Hat Member and the highest concentrations during the First White Specks Member (average 0.9 ppm). Iron speciation results from core 16-4-22-15W4 are plotted
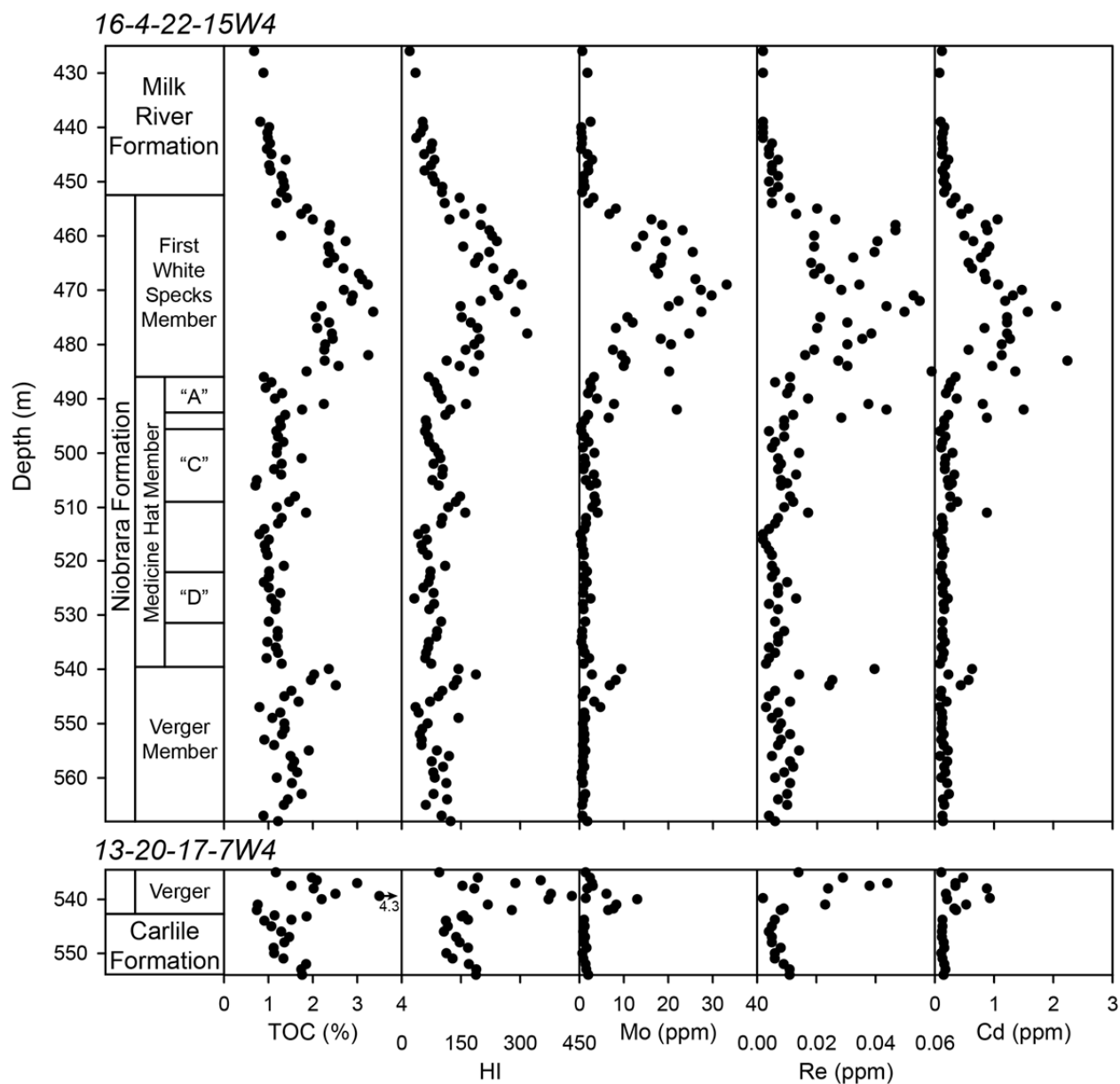
Figure 5.3

Trace metal concentrations (Re, Cd, and Mo) from cores 16-4-22-15W4 and 13-20-17-7W4, compared to previously published total organic carbon (TOC) and hydrogen index (HI) values (Nielsen et al., 2008).

as Fe phases, Fe_T/Al, Fe_{HR}/Fe_T, and Fe_{py}/Fe_{HR} in Figure 5.4. Ratios of Fe_T/Al range from 0.23–

7.4 within the Niobrara section of the core with average values for each member of 0.41, 0.43,

and 0.49 respectively. Ratios of Fe_{HR}/Fe_T range from 0.21–0.68, with the highest values

occurring within the First White Specks Member and the lowest values occurring in the Milk

120
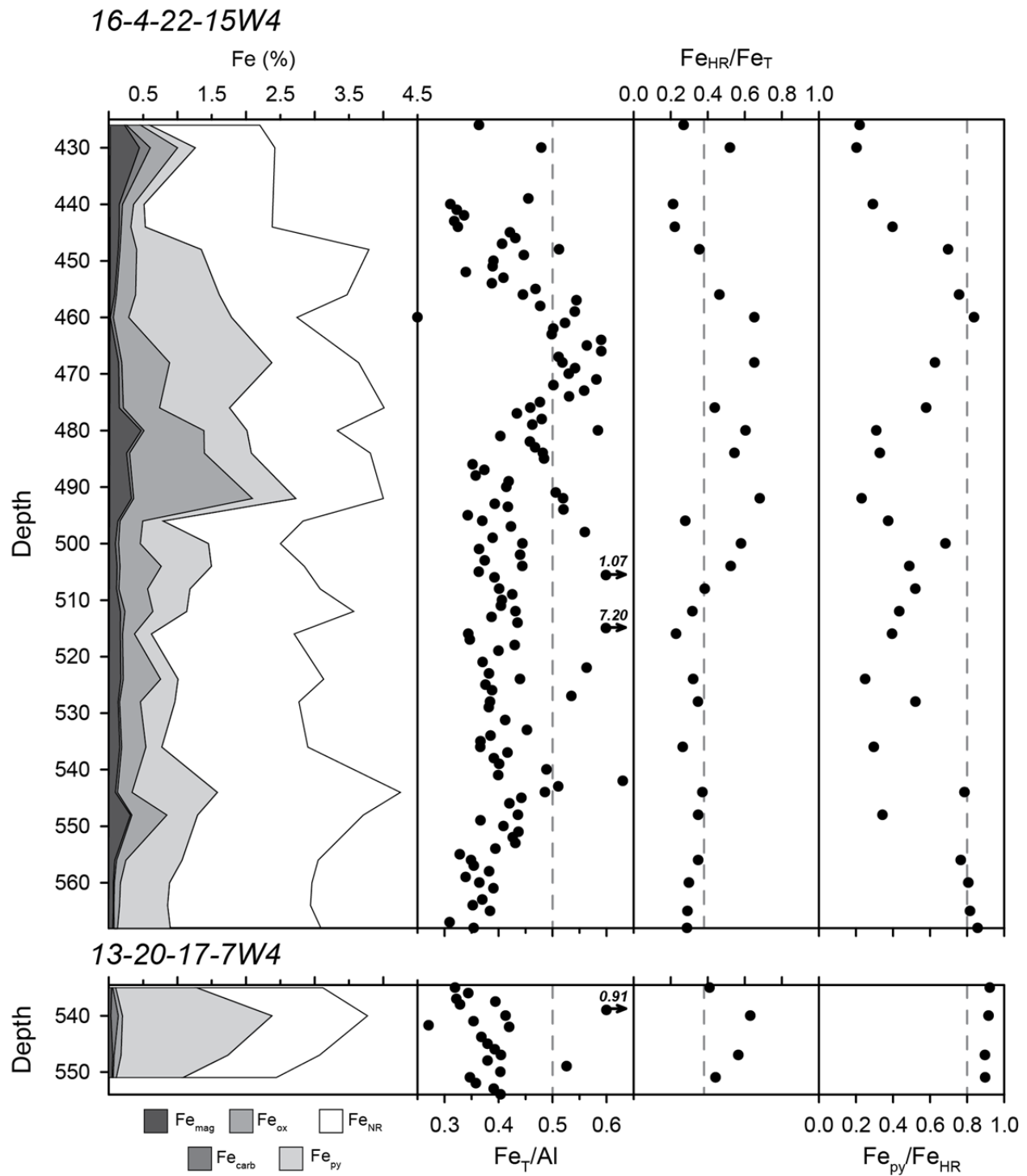
Figure 5.4

Iron speciation results from cores 16-4-22-15W4 and 13-20-17-7W4. (a) Fe phases measured by sequential extractions (Fe_{carb}, Fe_{ox}, and Fe_{mag}), $Fe_{py,}$ Fe_{PR}, and Fe_T. (b) Weight % ratios of Fe_T/Al. Dashed line indicates the average shale value of Fe_T/Al of 0.55. (c) Fe_{HR}/Fe_T, with the anoxic threshold of 0.38 indicated by the dashed line. (d) Fe_{py}/Fe_{HR}, with the euxinic Fe_{py}/Fe_{HR} threshold of 0.8 designated by a dashed line.

River Formation (Fig. 5.3). Values of Fe_{py}/Fe_{HR} range from 0.20–0.86 in core 16-4-22-15W4. The highest values of Fe_{py}/Fe_{HR} (>0.8) occur within the middle Verger Member and First White Specks Member (Fig. 5.4).

Trace metal concentrations from core 13-20-17-7W4 are plotted in Figure 5.3 and Fe speciation results are plotted in Figure 5.4. The concentrations of each trace metal generally increase across the Carlile-Niobrara boundary. Molybdenum concentrations range from 0.7–13 ppm, Re concentrations range from 2–87 ppb, and Cd concentrations range between 0.11–0.93 ppm (Fig. 5.2). Ratios of Fe_T/Al average 0.39 within the core, ranging from 0.35–0.53 in the Carlile Formation and from 0.24–0.91 in the Verger member (Fig. 5.3). The record of Fe_{HR}/Fe_T varies from 0.41–0.63 and Fe_{py}/Fe_{HR} are consistently elevated above those found in core 16-4-22-15W4, with ratios from 0.90–0.92 (Fig. 5.4).

5.5 Discussion

5.5.1 Redox conditions within the Canadian Basin

The Carlile Formation was deposited during the regression of the Greenhorn Sea (Nielsen et al., 2008). The faunal assemblage in the upper Carlile Formation, which includes few to locally abundant agglutinated, monospecific benthic calcareous, and rare planktic foraminifera, confirms deposition within a shallow, slightly brackish, but oxygenated shallow water paleoenvironment (Fig. 5.2; Nielsen et al., 2008). The elemental composition of organic matter indicates a mix of hydrogen-poor, oxygen-rich Type III organic matter, likely derived from terrestrial higher plants, and hydrogen-rich, oxygen-poor Type II organic matter, likely derived from marine zooplankton, phytoplankton, and bacterial debris (Fig. 5.3; Nielsen et al., 2008).

Within the upper Carlile Formation, the average concentrations of Re (6.9 ppb), Cd (.14

ppm), and Mo (1.2 ppm) are within error of average shale concentrations (10 ppb, 0.13 ppm, 1 ppm; Wedepol, 1971; 1991). Each of these trace metals is known to accumulate in sediments under reducing porewater conditions (Table 1). The lack of elevated trace metal concentrations during deposition of the upper Carlile Formation suggests deposition under a relatively well-oxygenated water column, as also confirmed by relatively low TOC values (Fig. 5.3).

Low Fe_T/Al ratios (0.27–0.42) and elevated Fe_{HR}/Fe_T values (0.44–0.56) are recorded within the upper Carlile Formation (Fig. 5.4). Low Fe_T/Al values, paired with low trace metal concentrations, indicate sedimentary Fe loss under oxic to suboxic sedimentary conditions (Table 2). Well-oxygenated conditions are further supported by intense bioturbation and abundant benthic foraminifera (Fig. 5.2; Pemberton et al., 1992; Nielsen et al., 2008). In contrast, Fe_{HR}/Fe_T and Fe_{py}/Fe_{HR} values would suggest more reducing conditions (Table 2), but likely reflect elevated sedimentary pyrite formation instead (Fig. 5.4).

The basal Verger Member records the initial transgression of the Niobrara Sea (Kauffman and Caldwell, 1993). Trace metal concentrations are generally low throughout the Verger, suggesting relatively oxic conditions, with the exception of two periods of elevated values (Fig. 5.3). The first increase occurs within a ~5 m interval in the lower Verger Member in core 13-20-17-7W4, during which Re and Cd increase to maximum values of 87 ppb and 0.93 ppm respectively. Molybdenum concentrations of up to 13 ppm suggest the development of sulfidic conditions within the sediments. The presence of sulfidic conditions is supported by elevated Fe_{py}/Fe_{HR} values (Fig. 5.4). Organic carbon accumulation is elevated at this time (values >4%) and high hydrogen-index values document more significant contribution of marine organic matter (Fig. 5.3; Nielsen et al., 2008). Increases in the accumulation of marine organic matter indicate that the development of sedimentary sulfidic conditions were likely in response to

123

elevated primary productivity and subsequent respiration of organic matter. The frequent ash falls during this time might have acted as fertilizer of the ocean increasing plankton productivity. However, sulfidic conditions resulted in complete lack of benthic foraminifera (Fig. 5.2).

The second increase in trace metal concentrations occurs at the top of the Verger Formation, within the 16-4-22-15W4 core (Fig. 5.3). Trace metal concentrations increase above background values within the top 6 m of the Verger Formation, with Mo concentrations of up to 10 ppm. The development of more reducing conditions is supported by coeval increases in sedimentary Fe accumulations, with Fe_T/Al values of up to 0.92. Despite increases in total Fe, Fe_{HR}/Fe_T values remain relatively low throughout (<0.38; Fig. 5.4). Similar to the oxygen depleted interval in the lower Verger, elevated trace metal concentrations are coeval with increased concentrations of TOC and preservation of more hydrogen-rich, Type II organic matter, suggesting increased levels of marine productivity and delivery of algal organic matter to the sediments increased TOC values occur above pebble lags that are interpreted as the result of transgressive ravinement of older deposits (Nielsen et al., 2008). This interval is associated with a diverse and abundant floral and faunal assemblage, including agglutinated, benthic calcareous and planktic foraminifera, ostracodes, and nannofossils, which indicate a fully marine environment as Tethyan waters enter the region (Nielsen et al., 2008; Fig. 5.2).

The Medicine Hat Member consists of alternating sandstones, shales, and siltstones (Fig. 5.2). The fine-grained sandstones of the Medicine Hat Member were deposited in a moderate energy environment along the flanks of the Sweetgrass Arch as isolated shelf sandstones not connected to the coeval shoreline (Nielsen et al., 2008). The extensive isolated sandstones (1000 to 3000 km^2) are unusual and without many ancient or modern analogues (Swift et al., 1976, 1986; Swift and Rice, 1984; Rice, 1984; Galloway, 2002). The best explanation for their

deposition is that shallow-water geostrophic currents distributed sediments along the shallow, subtle arch (Fig. 5.1; Stow et al., 1998).

Trace metal concentrations remain relatively low throughout deposition of the Medicine Hat Member indicating generally oxidizing conditions, likely due to increased mixing under higher energy conditions (Fig. 5.3). Relatively oxic conditions are supported by relatively low Fe_T/Al and Fe_{HR}/Fe_T values (Fig. 5.4). Trace metal concentrations are slightly elevated within the shales as compared to the sandstone intervals of the Medicine Hat Formation (Fig. 5.3), which is consistent with more abundant and diverse ichnofossils found within the sandstones (Nielsen and Schröder-Adams, 1999; Nielsen et al., 2003). Furthermore, the shales are characterized by elevated TOC values and significant Type II organic matter influence, whereas sandstone facies are dominated by Type III organic matter (Nielsen et al., 2008). This indicates that the reconstructed differences in redox conditions between shales and sandstones may be caused by elevated marine productivity during shale deposition associated with lower energy conditions or by differences in turbidity, which would exert a strong control on habitability for plankton.

An abrupt sedimentological change occurs at the boundary between the Medicine Hat and First White Specks members that is attributed to a renewed transgression of the Niobrara Sea (Fig. 5.2; Kauffman, 1984; Caldwell et al., 1993). It is not until this transition that there is evidence for more permanent oxygen limitation within the Niobrara Sea. Throughout the 30 m thick First White Specks Member, trace metals are consistently elevated with Re concentrations between 15 and 60 ppb, Cd concentrations from 0.5–2.5 ppm, and Mo concentrations between 5 and 33 ppm (Fig. 5.3). Anoxic conditions are further supported by sedimentary Fe enrichments, as indicated by Fe_T/Al values >0.5 and Fe_{HR}/Fe_T >0.38 (Fig. 5.4). Elevated Mo concentrations and Fe_{py}/Fe_{HR} values of ~0.8 suggest consistently sulfidic conditions, at least within the

sediments. Reducing conditions are also indicated by absent bioturbation within the generally

finely laminated First White Specks Member (Nielsen et al., 2008). Similar to the upper Verger

Member, total organic carbon increases across the Medicine Hate-First White Specks boundary

and is accompanied by an increase in marine-derived organic matter (Nielsen et al., 2008).

Facies associations within the First White Specks Member indicate that it represents the

most distal, low energy environment since the peak Greenhorn transgression recorded in the

Second White Specks Formation (Nielsen et al., 2008). Faunal and floral assemblages include

both planktic foraminifera and nannofossils, suggesting the greatest Tethyan influence during the

Niobrara Formation, similar to conditions during peak Greenhorn transgression (Fig. 5.2).

Finally, the overlying sandstone-rich Milk River Formation records the regression of the

Niobrara Sea. Within this unit, trace metal concentrations decrease to the lowest values recorded

within the two cores, indicating a return to more oxygenated conditions (Fig. 5.3). Additionally,

low Fe_T/Al and Fe_{HR}/Fe_T values support oxic to suboxic sedimentary conditions (Fig. 5.4).

Benthic foraminifera remained in low numbers, but with retreating Tethyan watermass influence

planktic foraminifera disappeared.

5.5.2 Seaway-wide trends in redox and organic carbon burial

In order to compare trends in redox conditions between southeast Alberta and Colorado,

macrofossil biozones were used to correlate between the southeastern Alberta cores (16-4-22-

15W4 and 13-20-17-7W4) and the Aristocrat Angus core (Fig. 5.5). Foraminiferal biozones were

determined (Nielsen et al., 2008) in cores 16-4-22-15W4 and 13-20-17-7W4 and correlated to

macrofossil zones following Caldwell et al., (1978), while in the Aristocrat Angus core (and
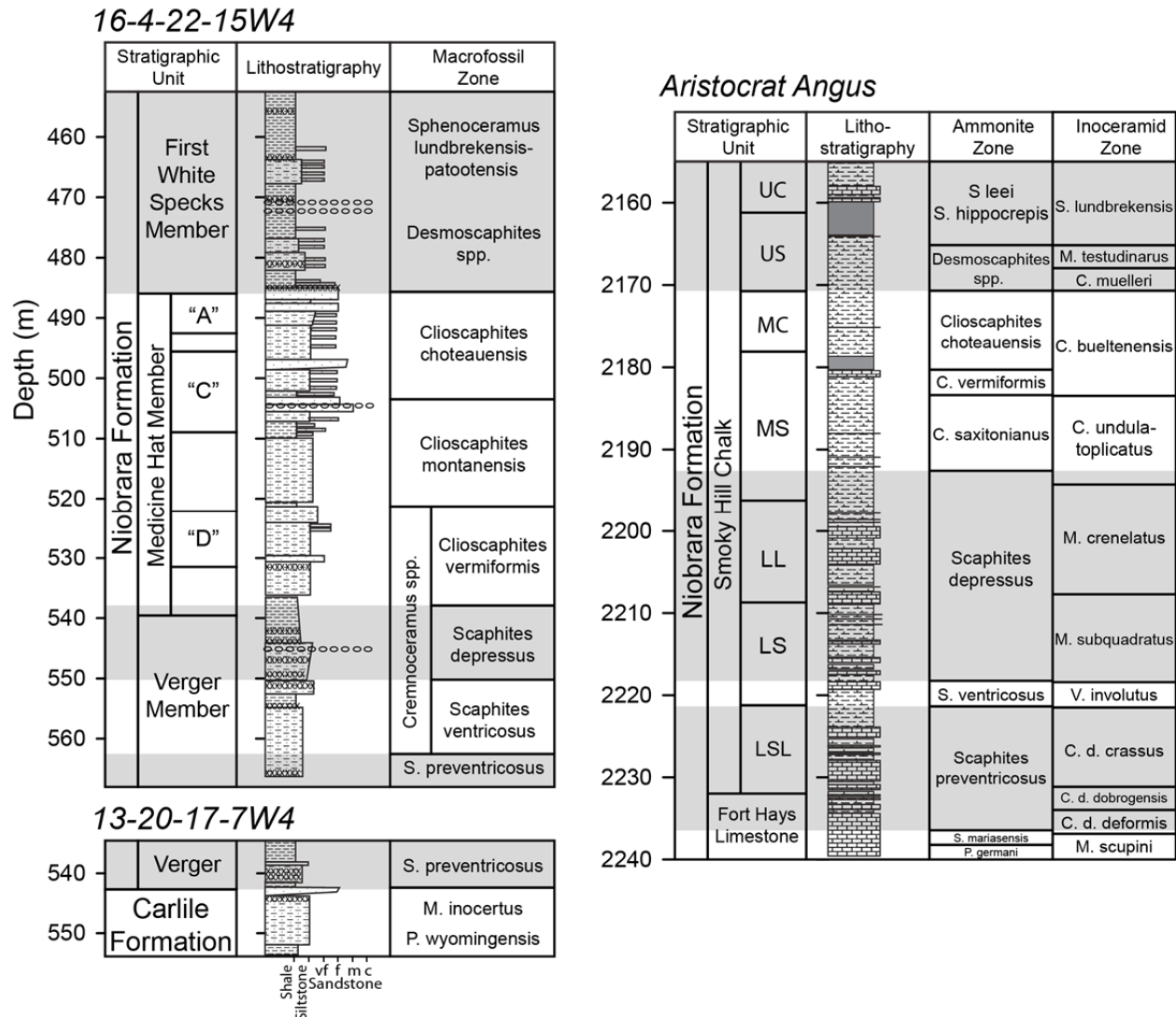
Figure 5.5

Macrofossil biozones and stratigraphic columns from cores 16-4-22-15W4 and 13-20-17-7W4 and a representative central WIS section (the Aristocrat Angus core). Correlations are made based on the following biozones (a) *Scaphites preventicosus*, (b) *Scaphites venticosus*, (c) *Scaphites depressus*, (d) *Clioscaphites* spp., and (e) *Sphenoceramus lundbrekensis* and *Desmoscaphitess* spp.

lithologically correlated Berthoud State and Portland cores), the biostratigraphy follows the

scheme of Cobban et al. (2006).

In southeastern Alberta, the Niobrara Formation includes three low oxygen intervals

associated with enhanced sedimentary organic carbon accumulation. The first instance of anoxia

occurs within the *Scaphites preventicosus/Scaphites ventricosus* biozone of the lower Verger

member, which are found within the Fort Hays Limestone and lower shale limestone unit of the

Smoky Hill Chalk in Colorado (Fig. 5.6). Deposition within these units occurred under well-

oxygenated conditions in Colorado, suggesting that anoxia in Alberta was associated with local

environmental and oceanographic conditions. This interval of elevated trace metal concentrations

occurs within a ~5 m interval in the *Scaphites preventicosus* biozone and is coeval with abundant

bentonites (up to 20 in 3 m of shale; Nielsen et al., 2003). Frequent ashfalls may have created

inhospitable conditions for both planktic and benthic foraminifera, which are rare in bentonite-

rich intervals (Nielsen et al., 2008). However, increased TOC during this period suggests that the

ashfalls produced conditions that were generally conducive to the production of marine organic

matter, possibly in form of phytoplankton due to surface water nutrient input, which in turn
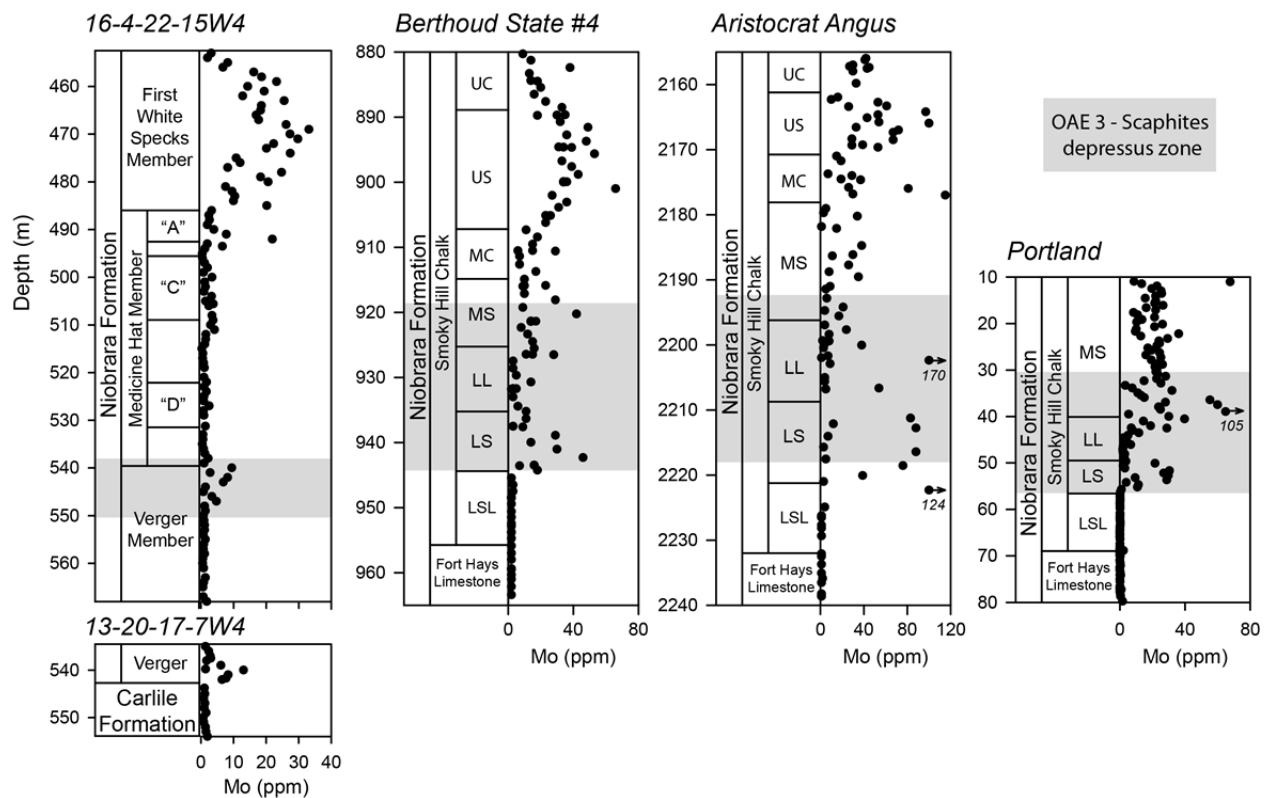
Figure 5.6

Lithostratigraphy and Mo concentrations from cores 16-4-22-15W4 and 13-20-17-7W4 and the central
WIS cores (USGS Portland, Berthoud State, and Aristocrat Angus). Gray bars are used to indicate
correlations based on biostratigraphy. The *Scaphites despressus* biozone correlates to the previously
identified OAE 3.

fueled the development of benthic anoxia. Higher organic carbon deposition likely lead to increased oxidant demand in sediments that further fueled the development of local anoxia.

Unlike the reducing conditions during the lower Verger, the two other oxygen-limited intervals in southeastern Alberta have corresponding intervals of elevated trace metal accumulation in Colorado (Fig. 5.6). In both Alberta and Colorado, the interval between these latter two reducing periods contains evidence for more-oxygenated conditions. The trace metal results from southeastern Alberta highlight that the development of anoxia is coeval with incursion of Tethyan water, based on the appearance of planktic foraminifera and nannoplankton (Fig. 5.2). These results indicate that the two primary intervals of organic carbon burial within the Coniacian-Santonian in the WIS are forced by sea level transgression and the resulting water mass interactions. Nutrient-rich, oxygen-poor water from the Tethys would fuel both elevated primary productivity and promote the development of anoxia through subsequent respiration. Additionally, the incursion of Tethyan water could promote oxygen limitation and enhanced organic matter preservation due to enhanced stratification as warmer, more saline water from the south encounters northern-sourced cooler, brackish water from the Cretaceous Polar Sea (e.g. Caldwell et al., 1993; Nielsen et al., 2008).

Trace metal enrichments can be used to determine the relative degree of anoxia between the central seaway and the Canadian Basin. While enrichment factors within the southeastern Alberta cores indicate trace metal enrichments (defined as >3; Brumsack, 2006), enrichment factors are consistently higher in the central seaway. Based on data available for comparison, Figure 5.7 illustrates the temporal changes in enrichment factors of Mo, a sulfidic indicator, and V+Cr, a suboxic indicator. These results demonstrate that not only did consistent anoxia develop later in the Canadian Basin than in the central seaway, but also that anoxia was consistently less

129
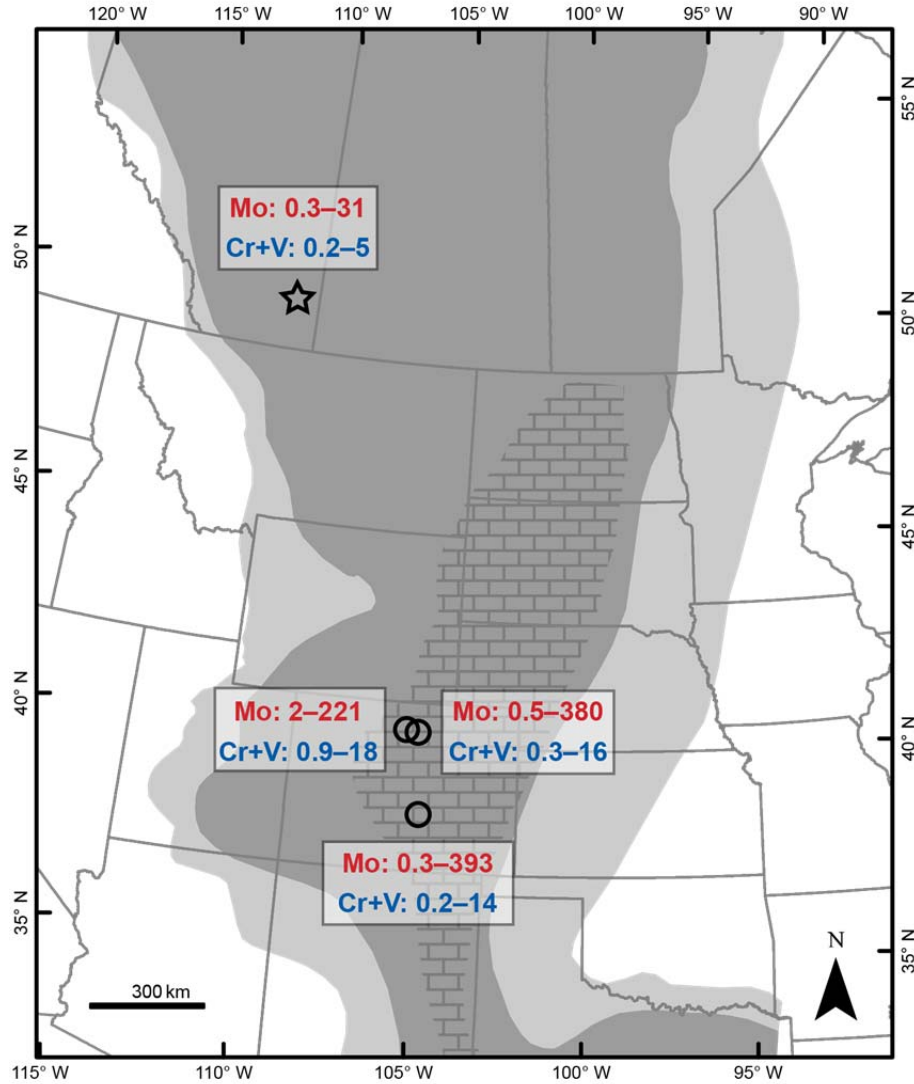
Figure 5.7

Map of the Western Interior Seaway (adapted from Roberts and Kirshbaum, 1995) with Mo and V+Cr enrichment factors for cores 16-4-22-15W4 and 13-20-17-7W4, USGS Portland, Berthoud State, and Aristocrat Angus.

extreme once oxygen limitation did occur.

The less intense anoxia and organic carbon burial observed within the Canadian Basin may be due to shallow depth of sites in Alberta relative to those in Colorado. During high sea level, water depth at the southeastern Alberta core sites is thought to be approximately 50–100 m, with depths of 10–30 m during periods of low sea level (Nielsen et al., 2008). Conversely, during maximum transgression, the water depth in Colorado is estimated to be ~150–300 m

(Hattin, 1982; Tessin et al., 2015). The influence of wind mixing within a shorter water column, particularly due to the influence of the Sweetgrass Arch (Fig. 5.1), could inhibit the development of stable stratification at the Alberta sites.

Additionally, the shallow water depth might affect the scale of Fe and trace metal accumulations within the sediments due to scavenging integrated over a shorter water column. Another possible explanation for the greater intensity of carbon burial and anoxia observed in Colorado is the proximity to the southern sill of the seaway. If changing paleoceanographic conditions are primarily forced by increased Tethyan influence, the location of the sites in Colorado are better situated to receive a significant influence from the nutrient-rich, oxygen-poor Tethyan water mass. The Tethyan influence in the south is indicated by the distribution of lithofacies between the southern and northern portions of the seaway (e.g. Nielsen et al., 2008). For example, within Kansas and Colorado, deposition is dominated by chalk deposition, due to the abundance of calcareous plankton, whereas calcareous plankton are never as abundant in Alberta (Fig. 5.2).

5.5.3 Implications for Oceanic Anoxic Event 3

Based on carbon isotope stratigraphy and total organic carbon concentrations in multiple cores from Colorado, OAE 3 has been identified within the middle Coniacian (specifically, the *Scaphites despressus* biozone; Locklair et al., 2011; Joo and Sageman, 2014; Tessin et al., 2015; Sageman et al., 2015), which corresponds to a moderate, short-lived increase in trace metal accumulations within the upper Verger member in southeastern Alberta. Conversely, at Cold Lake in east-central Alberta, OAE 3 was identified as Late Santonian in age based on elevated TOC values within the First White Specks Member (Schröder-Adams et al., 2012). The organic

carbon isotope record from Cold Lake indicates an abrupt decrease in $\delta^{13}C_{org}$ at this time, possibly caused by local changes in organic matter source (Schroder-Adams et al., 2012).

An interval of anoxia and organic carbon burial within the upper Niobrara Formation in Colorado is generally time equivalent to the increased TOC and anoxia recorded in Cold Lake and during the First White Specks Member. However, these changes occur after the "OAE 3" $\delta^{13}C$ excursion recorded in the Aristocrat Angus and Portland cores. This highlights the difficulty in defining a single OAE 3 interval within the WIS during a period of time characterized by multiple intervals of anoxia and carbon burial. The proposed timing of OAE 3 has been contentious because organic carbon-rich sedimentation occurs during the Coniacian at some locations and during the Santonian in others (Jarvis et al., 2006; Locklair et al., 2011), or as the WIS records indicate, an interval in the Coniacian and Santonian.

The difficulty in identifying a single OAE 3 event highlights the need to better understand the mechanisms driving carbon burial during the Coniacian-Santonian in order to determine if there is a global signal of the OAE 3 and if so, can it be recognized with the WIS. Paired paleontological and geochemical evidence suggest that intervals of anoxia and elevated organic carbon burial within the WIS are caused by sea-level transgressions and incursion of Tethyan waters into the WIS (Figs. 5.2–5.4). Sea level control of organic carbon burial during the Coniacian-Santonian explains widespread black shale deposition in shallow and restricted marine environments including the WIS, which will be sensitive to sea-level change, while deeper, open marine environments remain well-oxygenated during OAE 3. A sea level driver for OAE 3, additionally explains the complexities in correlating the event in the WIS to other shallow, restricted marine regions where the amplitude and timing of sea-level change is controlled both by eustatic and local tectonic forcing.

Within the WIS, high sea level alone does not explain the difference between OAE 2 and OAE 3, as both the Cenomanian-Turonian (OAE 2) Greenhorn and the Coniacian-Santonian (OAE 3) Niobrara formations were deposited during sea-level highstands. However, anoxia does not develop immediately in the WIS in response to marine transgression during the Cenomanian-Turonian. Within the Niobrara Formation in Colorado, the transgressive Fort Hays Limestone records carbonate-rich deposition under well-oxygenated conditions, similar to the Greenhorn Limestone, and anoxia develops within the overlying Smoky Hill Chalk. Similarly, in the latter part of OAE 2, organic carbon accumulation does increase. Arthur (1998) proposed that advection of deep Arctic and Tethyan water masses caused either a pulse of marine algal productivity or enhanced organic matter preservation due to low oxygen in the advected water. This suggests that anoxia and organic carbon burial occur significantly (~1 Ma) after initial seaway transgression, which is why the Greenhorn Limestone records predominantly oxic and low TOC deposition. Additionally, different global ocean circulation patterns may have affected the initial nutrient and oxygen composition of Tethyan waters entering the seaway between the two intervals.

5.6 Conclusions

Trace metal and Fe speciation records from the Niobrara Formation in southern Alberta indicate three intervals of reducing bottom conditions. The first interval, in the lower Verger Member, precedes black shale deposition in Colorado and the identified OAE 3 intervals in both Colorado and Alberta. The lower Verger interval is coeval with frequent bentonite layers, suggesting that anoxia developed locally in response to significant volcanic ashfall that fertilized surface waters. The second interval occurs within the upper Verger Member and corresponds to

the identified OAE 3 event in Colorado. However, the upper Verger Member records only a short-lived, minor enrichment in trace metals, unlike the significant enrichments in Colorado. It is not until the First White Specks Member that trace metal enrichment and Fe speciation indicate the development of prolonged anoxia coeval with sea-level highstand supported by paleontological and sedimentological evidence. Rising sea level allowed incursion of Tethyan waters that bathed the WIS in nutrient-rich, oxygen-poor waters and increased density stratification.

New trace metal results demonstrate that a single, distinct anoxic event does not define OAE 3 within the WIS during the Coniacian-Santonian. While OAE 3 has been identified in the Coniacian *Scaphites depressus* biozone in Colorado, significant oxygen limitation and organic carbon burial does not occur within Alberta until the Santonian. Both intervals of reducing conditions in Alberta and Colorado (the Coniacian and Santonian) occur alongside evidence for sea level highstands and, importantly, greater influence of Tethyan waters. A sea level control of Coniacian-Santonian anoxia and organic carbon burial may explain why "OAE 3" is only identified in shallow and restricted marine environments, as well as the diachronous timing of the event in different regions.

5.7 Acknowledgements

5.8 References

Arthur, M. A., S.O. Schlanger, and H.C. Jenkyns (1987), The Cenomanian-Turonian Oceanic
Anoxic Event, II, Paleoceanographic controls on organic matter production and
preservation, in *Marine Petroleum Source Rocks, Geological Society of London Special
Paper*, edited by J. a. A. F. Brooks, pp. 401-420.

Arthur, M.A., and Sageman, B.B. (2005), Sea Level Control on Source Rock Development:
Perspectives from the Holocene Black Sea, the mid-Cretaceous Western Interior Basin of
North America, and the Late Devonian Appalachian Basin, In Harris, N.B. (ed.), *The
Deposition of Organic Carbon-rich Sediments: Models, Mechanisms and Consequences,*
SEPM Special Publication No. 82, p. 35-59.

Bloch, J., Schröder-Adams, C.J., Leckie, D.A., McIntyre, D.J., Craig, J., Staniland, M. (1993),
Revised stratigraphy of the lower Colorado Group (Albian to Turonian), Western
Canada, *Bulletin of Canadian Petroleum Geology 41* (3), 325–348.

Brumsack, H. J. (2006), The trace metal content of recent organic carbon-rich sediments:
Implications for Cretaceous black shale formation, *Palaeogeography Palaeoclimatology
Palaeoecology*, *232*(2-4), 344-361.

Caldwell, W.G.E., Diner, R., Eicher, D.L., Fowler, S.P., Stelck, C.R., von Holdt Wilhelm, L.
(1993), Foraminiferal biostratigraphy of Cretaceous marine cyclothems. In: Caldwell,
W.G.E., Kauffman, E.G. (Eds.), *Evolution of the Western Interior Basin*, Special Paper,
vol. 39, Geological Association of Canada, pp. 477–520.

Canfield, D. E. (1994), Factors influencing organic carbon preservation in marine sediments,
Chemical Geology, 114, 315–329.

Chappaz, A., T. Lyons, D. Gregory, C. Reinhard, B. Gill, C. Li, R. Large (2014), Does pyrite act
as an important host for molybdenum in modern and ancient sediments?, *Geochimica et
Comsmochimica Acta, 126*, 112-122.

Coulson, A. B., M. J. Kohn, and R. E. Barrick (2011), Isotopic evaluation of ocean circulation in
the Late Cretaceous North American seaway, *Nature Geoscience*, *4*(12), 852-855.

Crusius, J., S. Calvert, T. Pedersen, and D. Sage (1996), Rhenium and molybdenum enrichments
in sediments as indicators of oxic, suboxic and sulfidic conditions of deposition, *Earth
and Planetary Science Letters*, *145*(1-4), 65-78.

Dean, W. E. a. M. A. A. (1998), Geochemical expressions of cyclicity in Cretaceous pelagic limestone sequences: Niobrara Formation, Western Interior Seaway, in *Stratigraphy and Paleoenvironments of the Cretaceous Western Interior Seaway*, edited by W. E. Dean and M. A. Arthur, pp. 227-255, SEPM Concepts in Sedimentology and Paleontology.

Du Vivier, A. D. C., D. Selby, B. B. Sageman, I. Jarvis, D. R. Groecke, and S. Voigt (2014), Marine Os-187/Os-188 isotope stratigraphy reveals the interaction of volcanism and ocean circulation during Oceanic Anoxic Event 2, *Earth and Planetary Science Letters*, *389*, 23-33.

Eldrett, J., D. Minisini, and S. Bergman (2014, Decoupling of the carbon cycle during Ocean Anoxic Event 2, Geology 42 (7), 567-570.

Erickson BE, Helz GR (2000), Molybdenum (VI) speciation in sulfidic waters: Stability and lability of thiomolybdates, *Geochimica et Cosmochimica Acta, 64*, 1149-1158

Galloway, W.E. (2002), Paleogeographic setting and depositional architecture of a sand dominated shelf depositional system, Miocene Utsira Formation, North Sea Basin, *Journal of Sedimentary Research 72* (4), 476–490.

Hattin, D.E., 1982. Stratigraphy and depositional environment of Smoky Hill Chalk Member, Niobrara Chalk (Upper Cretaceous) of the type area, Western Kansas. *Kansas Geological Society Bulletin* 225, 108 p.

Huerta-Diaz, M.A., Morse, J.W. (1992), Pyritisation of trace metals in anoxic marine sediments, *Geochimica et Cosmochimica Acta, 56*, 2681–2702.

Jarvis, I., A. S. Gale, H. C. Jenkyns, and M. A. Pearce (2006), Secular variation in Late Cretaceous carbon isotopes: a new delta C-13 carbonate reference curve for the Cenomanian-Campanian (99.6-70.6 Ma), *Geological Magazine*, *143*(5), 561-608.

Jenkyns, H. C. (2010), Geochemistry of oceanic anoxic events, *Geochemistry Geophysics Geosystems*, *11*.

Joo, Y. J., and B. B. Sageman (2014), Cenomanian to Campanian carbon isotope chemostratigraphy from the Western Interior Basin, USA, *Journal of Sedimentary Research*, *84*(7), 529-542.

Kauffman, E. G. (1977), Geological and biological overview: Western Interior Cretaceous Basin, in *Cretaceous Facies, Faunas and Paleoenvironments across the Western Interior Basin*, edited by E. G. Kauffman, pp. 75-99, Mountain Geologist.

Kauffman, E.G. (1984), Paleogeography and evolutionary response dynamic in the Cretaceous Western Interior Seaway of North America. In: Westerman, G.E.G. (Ed.), *Jurassic–Cretaceous Biochronology and Paleogeography of North America,* Special Paper, vol. 27, Geological Association of Canada, pp. 273–306.

Kauffman, E. G., and W. G. E. Caldwell (1993), The Western Interior basin in space and time, in *Evolution of the Western Interior Basin*, edited by W. G. E. Caldwell and E. G. Kauffman, pp. 1 – 30, Geological Association of Canada, Toronto, Ontario.

Kreitner, M.A., Plint, A.G. (2006), Allostratigraphy and paleogeography of the upper Cenomanian, lower Kaskapau Formation in subsurface and outcrop, Alberta and British Columbia, *Bulletin of Canadian Petroleum Geology 54* (2), 110–137.

Leckie, D.A., Bhattacharya, J.P., Bloch, J., Gilboy, C.F., Norris, B. (1994), Cretaceous Colorado/Alberta Group of the Western Canada Sedimentary Basin, *Geological Atlas of the Western Canada Sedimentary Basin* (compiled by Mossop,G. and Shetson, I.), Canadian Society of Petroleum Geologists and the Alberta Research Council, pp. 335–352.

Leckie, R.M., Yuretich, R.F.,West, O.L.O., Finkelstein, D., Schmidt,M. (1998), Paleoceanography of the southwesternwestern interior sea during the time of the Cenomanian–Turonian boundary (Late Cretaceous). In: Dean, W.E.Walter, Arthur,M.A. (Eds.), *Stratigraphy and Paleoenvironments of the Cretaceous Western Interior Seaway, USA*, SEPM Concepts in Sedimentology and Paleontology, vol. 6, pp. 101–126.

Locklair, R., B. Sageman, and A. Lerman (2011), Marine carbon burial flux and the carbon isotope record of Late Cretaceous (Coniacian-Santonian) Oceanic Anoxic Event III, *Sedimentary Geology*, *235*(1-2), 38-49.

Lyons TW, Severmann S (2006), A critical look at iron paleoredox proxies: new insights from modern euxinic marine basins, *Geochimica Et Cosmochim Acta 70*, 5698–5722

McNeil, D.H., Caldwell, W.G.E. (1981), Cretaceous rocks and their foraminifera in the Manitoba Escarpment, *Geological Association of Canada Special Paper*, vol. 21.

Meyers, S., Sageman, B., and Hinnov, L. (2001), Integrated quantitative stratigraphy of Cenomanian- Turonian Bridge Creek Limestone Member using Evolutive Harmonic Analysis and stratigraphic modeling, *Journal of Sedimentary Research*, v. 71, p. 628-644.

Meyers, S. R., B. B. Sageman, T. W. Lyons (2005), Organic carbon burial rate and the molybdenum proxy: Theoretical framework and application to Cenomanian-Turonian oceanic anoxic event 2, *Paleoceanography, 20*(2).

Nielsen, K.S., Schröder-Adams, C.J., Leckie, D.A. (2003), A new stratigraphic framework for the Upper Colorado Group (Cretaceous) in southern Alberta and southwestern Saskatchewan, *Canada Bulletin of Canadian Petroleum Geology 51* (3), 304–346.

Nielsen, K.S., Schröder-Adams, C.J., Leckie, D.A., Haggart, J.W., Elderbak, K (2008), Turonian to Santonian paleoenvironmental changes in the Cretaceous Western Interior Sea: The Carlile and Niobrara formations in southern Alberta and southwestern Saskatchewan, Canada, *Palaeogeography, Palaeoclimatology, Palaeoecology 270*, 64-91.

Piper, D.Z., Perkins, R.B. (2004), A modern vs. Permian black shale— the hydrography, primary productivity, and water-column chemistry of deposition, *Chemical Geology, 206*, 177–197.

Plint, A.G., Hart, B.S., Donaldson, W.S. (1993), Lithospheric flexure as a control on stratal geometry and facies distribution in Upper Cretaceous rocks of the Alberta foreland basin, *Basin Research 5*, 69–77.

Poulsen, C. J., E. J. Barron, W. H. Peterson, P. A. Wilson (1999), A reinterpretation of mid-Cretaceous shallow marine temperatures through model-data comparison, *Paleoceanography 14* (6), 679-697.

Poulton SW, Canfield DE (2005), Development of a sequential extraction procedure for iron: implications for iron partitioning in continentally derived particulates, *Chemical Geology 214*, 209–221

Poulton, SW, Raiswell, R (2002) The low-temperature geochemical cycle of iron: From continental fluxes to marine sediment deposition, *American Journal of Science, 302,* 774-805.

Raiswell, R; Canfield, DE (1998) Sources of iron for pyrite formation in marine sediments, *American Journal of Science, 298,* 219-245.

Reinhard, C.T., Lyons, T.W., Rouxel, O., Asael, D., Dauphas, N., Kump, L.R. (2013) Iron speciation and isotope perspectives on Paleoproterozoic water column chemistry. *In* Melezhik, V.A., Fallick, A.E., Kump, L., Lepland, A., Prave, A.R., Strauss, H. (*eds.*), *Reading the Archive of Earth's Oxygenation,* 3, 1483-1492, Springer.

Rice, D.D. (1984), Widespread, shallow-marine, storm-generated sandstone units in the Upper Cretaceous Mosby Sandstone, CentralMontana. In: Tillman, R.W., Seimers, C.T. (Eds.), *Siliciclastic Shelf Sediments,* Special Publication, vol. 34, Society of Economic Paleontologists and Mineralogists, pp. 143–161.

Roberts, L. N. K., Mark A. (1995), Paleogeography and the Late Cretaceous of the Western Interior of middle North America; coal distribution and sediment accumulation, edited by United States Geological Society.

Sageman, B. B. S., B. S.; Meyers, S. R.; Siewart, S. E.; Walaszczyk, I.; Condon, D. J.; Jicha, B. R.; Obradovich, J. D.; Sawyer, D. A. (2014), Integrating 40Ar/39Ar, U-Pb, and astronomical clocks in the Cretaceous Niobrara Formation, Western Interior Basin, USA, *Geological Society of America Bulletin, 7-8*, 956-973.

Schlanger, S. O., and H. C. Jenkyns (1976), Cretaceous Oceanic Anoxic Events: Causes and consequences, *Geologie en Mijnbouw, 55*(3-4), 179-184.

Schlanger, S. O., M. A. Arthur, H. C. Jenkyns, P. A. Scholle (1987), The Cenomanian-Turonian Oceanic Anoxic Event, I. Stratigraphy and distribution of organic carbon-rich beds and the marine $\delta^{13}C$ excursion, *Geological Society, London, Special Publications 26* (1), 371-399.

Schröder-Adams, C.J., Herrle, J.O., and Tu, Q. (2012), Albian to Santonian carbon isotope excursions and faunal extinctions in the Canadian Western Interior Sea: recognition of eustatic sea-level controls on a forebulge setting. *Sedimentary Geology 281*, p. 50-58.

Severmann, S., J. McManus, W. Berelson, D. Hammond (2010), The continental shelf benthic iron flux and its isotope composition, *Geochimica et Cosmochimica Acta 74*, 3984-4004.

Shurr, G.W., Rice, D.D. (1986), Paleotectonic controls on deposition of the Niobrara Formation, Eagle Sandstone, and equivalent rocks (Upper Cretaceous), Montana and South Dakota. In: Peterson, J.A. (Ed.), *Paleotectonics and sedimentation in the Rocky Mountain region*, Memoir, vol. 41, American Association of Petroleum Geologists, pp. 193–211.

Slingerland, R., Kump, L.R., Arthur, M.A., Fawcett, P.J., Sageman, B.B., Barron, E.J., (1996), Estuarine circulation in the Turonian Western Interior Seaway of North America, *Geological Society of America Bulletin 108* (7), 941–952.

Stow, D.A.V., Faugeres, J., Viana, A., Gonthier, E. (1998), Fossil contourites: a critical review, *Sedimentary Geology 115*, 3–331.

Swift, D.J.P., Rice, D.D. (1984), Sand bodies on Muddy shelves: a model for sedimentation in the Western Interior Cretaceous Seaway, North America. In: Tillman, R.W., Seimers, C.T. (Eds.), *Siliciclastic Shelf Sediments*, Special Publication, vol. 34, Society of Economic Paleontologists and Mineralogists, pp. 25–37.

Swift, D.J.P., Thorne, J., Oertel, G.F., 1986. Fluid processes and sea-floor response on a modern storm-dominated shelf: Middle Atlantic shelf of North America. Part II: Response of the shelf floor. In: Knight, R.J., McLean, J.R. (Eds.), Shelf Sands and Sandstones. Memoir, vol.11. Canadian Society of Petroleum Geologists, pp.191–213.

Swift, J.P., Freeland, G.L.,Gadd, P.E.,Han,G., Lavell, J.W., Stubblefield,W.L. (1976), Morphologic evolution and coastal sand transport, *New York–New Jersey Shelves*, Middle Atlantic Continental Shelf and the New York Bight Special Symposia, vol. 2, pp. 69–89.

Tessin, A., I. Hendy, N. Sheldon, B. Sageman (2015), Redox-controlled preservation of organic matter during "OAE 3" within the Western Interior Seaway, *Paleoceanography 30* (6), 702-717.

Tessin, A., N. Sheldon, I. Hendy, and A. Chappaz. Iron limitation in the Western Interior Seaway during the Late Cretaceous OAE 3 and its role in phosphorus recycling and enhancing organic matter preservation. In revision for *Earth and Planetary Science Letters*.

Tsikos, H., H.C. Jenkyns, B. Walsworth-Bell, M. R. Petrizzo, A. Forster, S. Kolonic, W. Erba, I. Premoli Silva, M. Baas, T. Wagner, J. Sinninghe Damste (2004) Carbon-isotope stratigraphy recorded by the Cenomanian-Turonian oceanic anoxic event: correlation and implications based on three key-localities, *Journal of the Geological Society, 161,* 711-720.

Wagreich, M. (2012), "OAE 3" --regional Atlantic organic carbon burial during the Coniacian-Santonian, *Climate of the Past*, *8*, 1447-1455.

Watkins, D. K. (1986), Calcareous nannofossil paleoceanography of the Cretaceous Greenhorn Sea, *Geological Society of America Bulletin 97*, 1239-1249.

Wedepohl, K.H. (1971), Environmental influences on the chemical composition of shales and clays, *in* L.H. Ahrens, F. Press, S.K. Runcorn, and H.C. Urey, (eds.) *Physics and Chemistry of the Earth*: Oxford (Pergamon) Press, Oxford, England, v. 8, p. 307-331.

Wedepohl, K.H. (1991), The composition of the upper earth's crust and the natural cycles of selected metals: metals in natural raw materials, natural resources, *in* E. Merian, (ed.), *Metals and their Compounds in the Natural Environment*: Weinhein (VCH- Verlagsges), Germany, p. 3-17.

Zhou, X., Jenkyns, H.C., Owens, J.D., Junium, C.K., Zheng, X., Sageman, B.B., Hardisty, D.S., Lyons, T.W., Ridgwell, A., and Lu, Z. (2015)**,** The I/Ca proxy and upper ocean oxygenation dynamics during the Cenomanian–Turonian OAE 2, *Paleoceanography*.

Chapter 6

Conclusions

This chapter summarizes the major results of each data chapter (2–5), provides a synthesis of the contributions to our understanding of shallow marine carbon cycling and OAE 3, and proposes future directions based on this work.

6.1 Results summary and conclusions

In **Chapter 2**, I use paired organic and metal redox proxies to evaluate redox-controlled changes in organic matter preservation. Metal redox reconstructions document a gradual drawdown of oxygen leading into the abrupt onset black shale deposition associated with OAE 3. The elemental composition of organic matter (Hydrogen-Index, Oxygen-Index, and Carbon:Nitrogen ratios) documents preferential preservation of hydrogen-rich, nitrogen-poor organic matter under reducing conditions. Changes in $\Delta^{13}C$ ($\delta^{13}C_{carb}$ - $\delta^{13}C_{org}$) mirror changes in the elemental composition of organic matter, suggesting that post-depositional redox conditions altered primary $\delta^{13}C_{org}$ records through preferential preservation of ^{13}C depleted, hydrogen-rich organic matter. Decreased O_2 availability coeval with significant changes in organic matter elemental composition highlight that redox controlled changes in organic matter preservation for black shale deposition within the Niobrara Formation. Increased export productivity and basin

stagnation are both possible mechanisms for the development of anoxia within the WIS. The importance of bottom water circulation restriction associated with changes in sea level is indicated by sea level reconstructions, $\delta^{18}O$ results, and Mo/total organic carbon (TOC) ratios.

In **Chapter 3**, I expand on the results from Chapter 2 with lipid biomarker and compound specific carbon isotope analyses. Based on the alkane, sterane, and hopane distributions, we conclude that the samples are thermally immature and appropriate for organic geochemical analysis. Biomarkers demonstrate that sedimentary organic matter is dominated by marine algal and bacterial sources. Additionally, biomarker results indicate that the onset of OAE 3 is associated with a significant increase in the contribution of marine algal organic matter, either due to elevated productivity or enhanced preservation.

Chapter 4 focuses on the role of changing Fe chemistry in increased nutrient cycling and organic matter preservation. Low total Fe (Fe_T) concentrations and Fe_T/Al ratios paired with efficient Fe pyritization, independent of evidence for euxinic conditions, indicate that highly reactive iron (Fe_{HR}) became limiting at the onset of OAE 3 in the WIS. The Fe limitation was coeval with reduced bioturbation, elevated sulfide accumulation within sediments, and enhanced organic matter preservation, indicating that low Fe availability played an important role in black shale deposition. Reduced P sequestration in sediments suggests that the Fe limitation also provided a feedback mechanism to sustain elevated OC production through enhanced phosphorus recycling, which provided nutrients for further marine productivity. The comparison of trace metal redox reconstructions to the Fe geochemistry indicates that Fe-based redox proxies may be complicated in high-productivity, shallow marine settings and care needs to be taken when solely relying on Fe geochemistry for redox reconstructions.

The results of **Chapters 2–4** illustrate that oxygen and reactive iron limitations drove enhanced organic carbon burial within the shallow WIS. These results are particularly relevant to future warming as ocean anoxia is currently expanding in response to modern greenhouse warming and enhanced nutrient input into coastal zones (e.g. Diaz and Rosenberg, 2008; Stramma et al., 2010; Stramma et al., 2012). Evidence of similar Fe chemistry has been observed in the modern Peel Harvey estuary, a shallow (~2 m), eutrophic environment in southwest Western Australia (Kraal et al., 2013). Based on my results, I would expect these modern changes in Fe and O_2 cycling to enhance organic carbon burial in shallow marine environments, and therefore, potentially drive elevated CO_2 sequestration in the future.

While Chapters 2–4 focus on the USGS Portland #1 core in Colorado, **Chapter 5** presents redox reconstructions from the Sweetgrass Arch region to evaluate the temporal and spatial variability in environmental conditions in the WIS during the Coniacian-Santonian. Three intervals of oxygen-limited conditions are identified in the Sweetgrass Arch region. The first interval, in the lower Verger Member, precedes black shale deposition in Colorado and the identified OAE 3 intervals in both Colorado and Alberta. The lower Verger interval contains many bentonite layers, suggesting that anoxia developed locally in response to significant volcanic ashfall, which fueled enhanced algal productivity based on paleontological results. The second interval occurs within the upper Verger Member and corresponds to the identified OAE 3 event in Colorado. However, the upper Verger Member records only a short-lived, minor enrichment in trace metals, unlike the significant enrichments in Colorado. It is not until the First White Specks Member that trace metal enrichment and Fe speciation indicate the development of prolonged anoxia coeval with sea level highstands supported by paleontological and sedimentological evidence. This change in environmental conditions is coeval with greater

Tethyan influence and an increase in accumulation of marine-sourced organic matter. The influx of Tethyan water could have promoted black shale deposition through increased productivity fueled by the nutrient-rich composition of southern sourced waters. Conversely, black shale deposition could have resulted from the interaction of brackish, polar water with saline Tethyan water creating strong water column stratification between buoyant surface waters and dense bottom waters, thereby enhancing organic matter preservation through reduced ventilation of bottom waters.

The results presented in **Chapter 5** highlight the complex nature of OAE 3. These results indicate that in order to understand marine carbon cycling under greenhouse climate conditions, it is necessary to focus on the regional responses during different OAEs. The results of Chapter 5 additionally indicate that sea level changes and the resulting water mass interactions were of primary importance during the Coniacian-Santonian. With sea level expected to rise between 0.98–1.31 m before 2100 (IPCC, 2013; DeConto and Pollard, 2016), understanding the drivers of marine organic carbon burial in shallow marine environments during sea level transgressions will be important when predicting how the global carbon cycle will respond to future sea level rise.

6.2 Future work

The work completed in this dissertation has raised a series of new research questions. These ongoing and future research directions are outlined below.

(1) **What is the relative influence of biological vs. physical drivers in the development of O_2-limited conditions in the Late Cretaceous WIS?** The results of this dissertation highlight the importance of changing O_2 and Fe conditions in enhanced organic carbon burial that were likely

forced by the coincident incursion of Tethyan water. However, the relative contributions of biological (primary productivity) and physical (water column stratification) factors are unclear, as incursion of Tethyan water could have produced either or both. Additionally, the increased influence of nutrient-rich Tethyan water could have enhanced primary productivity rates. . Greater interaction of warm-salty Tethyan water with continental runoff and fresher-polar sourced waters could also have promoted density stratification in the WIS, reducing bottom water ventilation. Moving forward, it will be important to assess these two factors independently.

New proxies, specifically metal isotopes, are promising for further elucidating independently evaluating changes in primary productivity. Cadmium isotopes, for example, have been suggested as a proxy for nutrient utilization (e.g. Georgiev et al., 2015), which would allow changes in nutrient delivery and subsequent increases in primary productivity to be directly assessed. The importance of new proxies or multi-proxy approaches is highlighted by the results from Chapter 4, in which iron and trace metal proxies produced contrasting redox reconstructions.

(2) How heterogeneous was geochemical cycling in the Late Cretaceous WIS? Comparison of results between central Colorado and southwestern Alberta was necessary in order to discern that the primary driver of organic carbon burial during OAE 3 in the WIS was a sea level transgression. The addition of more study sites, specifically those closer to the northern and southern sills and to the western sedimentary source, are needed to build-on and refine this finding. Recent WIS drill cores have focused on capturing the Cenomanian-Turonian OAE 2 interval. In order to produce a more complete view of conditions during the Coniacian-Santonian and to allow for comparison to OAE 2, new cores are needed that target Niobrara-aged rocks.

Specifically, drilling efforts should focus on the Austin Chalk in Texas, the Niobrara Formation in northern Alberta, and the Mancos shale in western Colorado and Utah.

(3) Were the changes in WIS ocean chemistry during the Coniacian-Santonian related to other regions where OAE 3 black shale deposition is identified? Oceanic Anoxic Event 3 has proven enigmatic (e.g. Locklair et al., 2011; Wagreich, 2012), particularly when studied through the lens of other OAEs, specifically OAE 2. The results presented in this dissertation indicate that within the WIS, Coniacian-Santonian black shale deposition was controlled by sea level change and water mass interactions. While it is likely that these factors played a role in organic carbon burial in other shallow and restricted marine environments, a strong influence of cyclic terrigenous input on black shale deposition has been identified in Venezuela and the Ivory Basin (Wagner et al., 2004; Rey et al., 2004). Determining the relative influence of weathering and sea level in different regions will require further study. In addition to further geochemical and paleoceanographic analyses, improved age constraints are required to accurately correlate between different regions. Recent efforts in bio- and chrono-stratigraphy have led to anomalously good age constraints in the Late Cretaceous WIS (e.g. Joo and Sageman, 2013; Sageman et al., 2014). Improved chronology in other regions, including the Venezuela La Luna Formation, would be a significant step forward.

(4) What effects will modern climate change have on shallow marine organic carbon burial and the global carbon cycle?

The work presented in this dissertation and the ongoing research efforts aimed at understanding the factors that control enhanced marine carbon burial have important

implications for both Late Cretaceous black shale deposition and OAEs, and more broadly for improving our understanding of how the marine carbon cycle will evolve in response to anthropogenic climate change. In the future, as sea levels rise in response to melting ice sheets and coastal regions flood, an understanding of the processes controlling the shallow marine carbon cycle will be especially important. In addition to efforts focusing on modern shallow marine environments, research focusing on the sedimentary record of past warm climates must continue to improve our understanding of how shallow marine carbon cycling changed in response to past climate change.

6.3 References

DeConto, R. M., D. Pollard (2016), Contribution of Antarctica to past and future sea level rise, *Nature 531*, 591–597.

Diaz, R. J., R. Rosenberg (2008), Spreading dead zones and consequences for marine ecosystems, *Science 321,* 926–929.

Georgiev, S.V., T.J. Horner, H.J. Stein, J.L. Hannah, B. Bingen, and M Rehkämper (2015), Cadmium-isotopic evidence for increasing primary productivity during the Late Permian anoxic event, *Earth and Planetary Science Letters.*

Intergovernmental Panel on Climate Change (2013), Climate Change 2013 The Physical Science Basis, *Working Group I Contribution to the Fifth Assessment Report of the Intergovernmental Panel on Climate Change.*

Joo, Y. J., and B. B. Sageman (2014), Cenomanian to Campanian carbon isotope chemostratigraphy from the Western Interior Basin, USA, *Journal of Sedimentary Research*, *84*(7), 529–542.

Kraal, P., E. Burton, R. Bush (2013), Iron monosulfide accumulation and pyrite formation in eutrophic estuarine sediments, *Geochimica et Cosmochimica Acta, 122*, 75–88.

Locklair, R., B. Sageman, and A. Lerman (2011), Marine carbon burial flux and the carbon isotope record of Late Cretaceous (Coniacian-Santonian) Oceanic Anoxic Event III, *Sedimentary Geology*, *235*(1-2), 38–49.

Rey, O., J.A. Simo, M. Lorente (2004), A record of long- and short-term environmental and climatic change during OAE3: La Luna Formation, Late Cretaceous (Santonian-early Campanian), Venezuela, *Sedimentary Geology 170* (1), 85–105.

Sageman, B. B. S., B. S.; Meyers, S. R.; Siewart, S. E.; Walaszczyk, I.; Condon, D. J.; Jicha, B. R.; Obradovich, J. D.; Sawyer, D. A. (2014), Integrating 40Ar/39Ar, U-Pb, and astronomical clocks in the Cretaceous Niobrara Formation, Western Interior Basin, USA, *Geological Society of America Bulletin*, *7-8*, 956–973.

Stramma, L., G. C. Johnson, J. Sprintall, V. Mohrholz (2008), Expanding Oxygen-Minimum Zones in the Tropical Oceans, *Science, 320*(5876), 655–658.

Stramma, L., E. D. Prince, S. Schmidtko, J. Luo, J. P. Hoolihan, M. Visbeck, D. W. R. Wallace, P. Brandt, A. Körtzinger (2012), Expansion of oxygen minimum zones may reduce available habitat for tropical pelagic fishes, *Nature Climate Change 2*, 33–37.

Wagner, T., J. S. S. Damste, P. Hofmann, and B. Beckmann (2004), Euxinia and primary production in Late Cretaceous eastern equatorial Atlantic surface waters fostered orbitally driven formation of marine black shales, *Paleoceanography*, *19*(3).

Wagreich, M. (2012), "OAE 3" --regional Atlantic organic carbon burial during the Coniacian-Santonian, *Climate of the Past*, 8, 1447–1455.

Supplemental Figures for Chapter 2
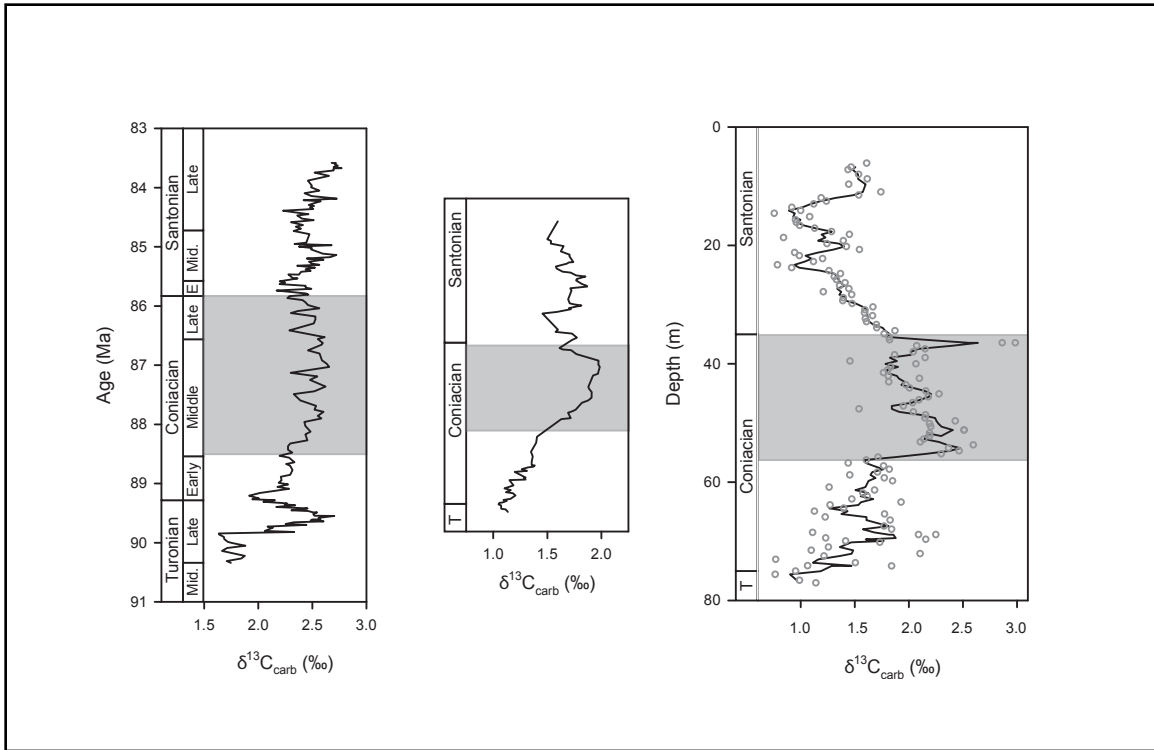
Figure A.1. $\delta^{13}C_{carb}$ isotope profiles for the Portland core, the Berthoud State core (Pratt et al., 1993), and the English Chalk composite (Jarvis et al., 2006). Grey bars designate the previously identified OAE 3 isotope plateau in the Berthoud and English Chalk records and in the new Portland record.
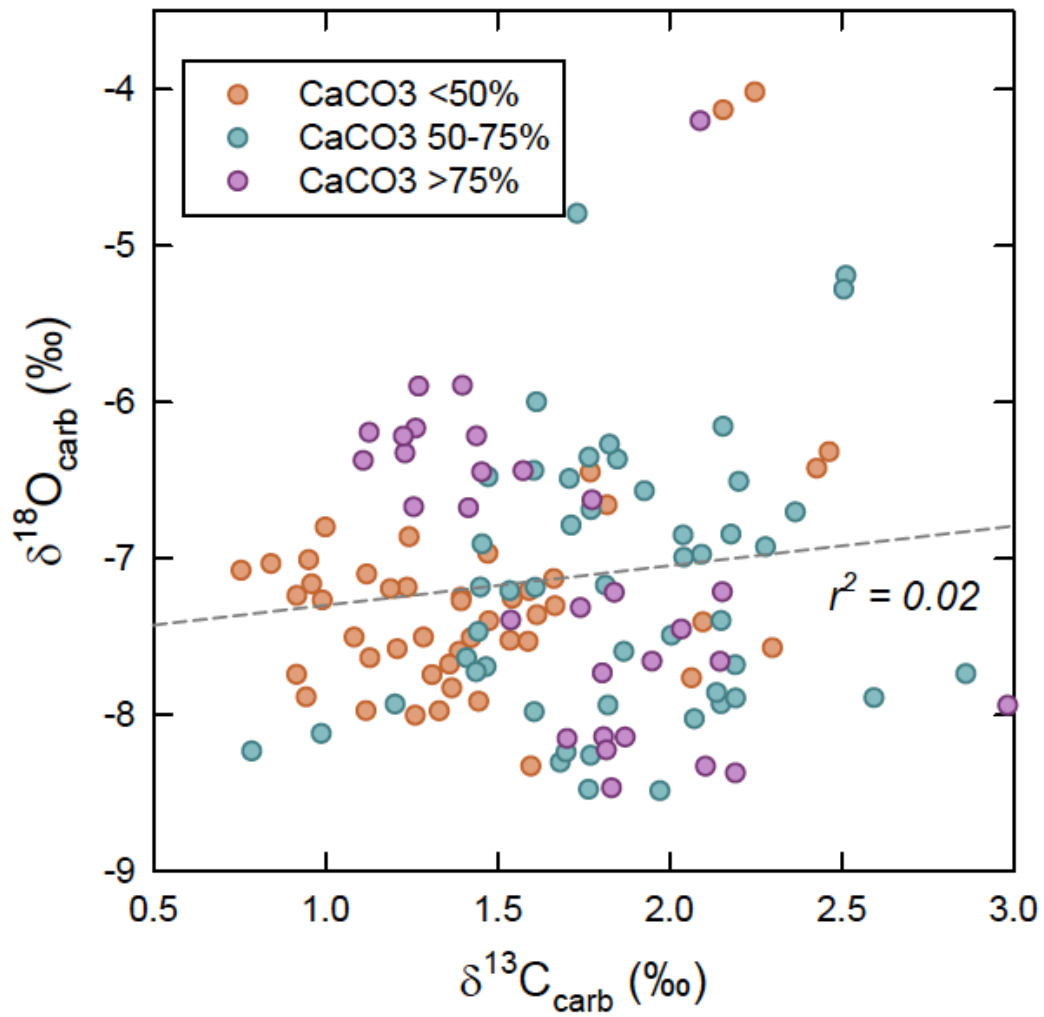
Figure A.2 . $\delta^{13}C_{carb}$ $\delta^{18}O_{carb}$ crossplot for the Portland core. Colors represent $CaCO_3$ concentrations.

Supplemental Figures for Chapter 4
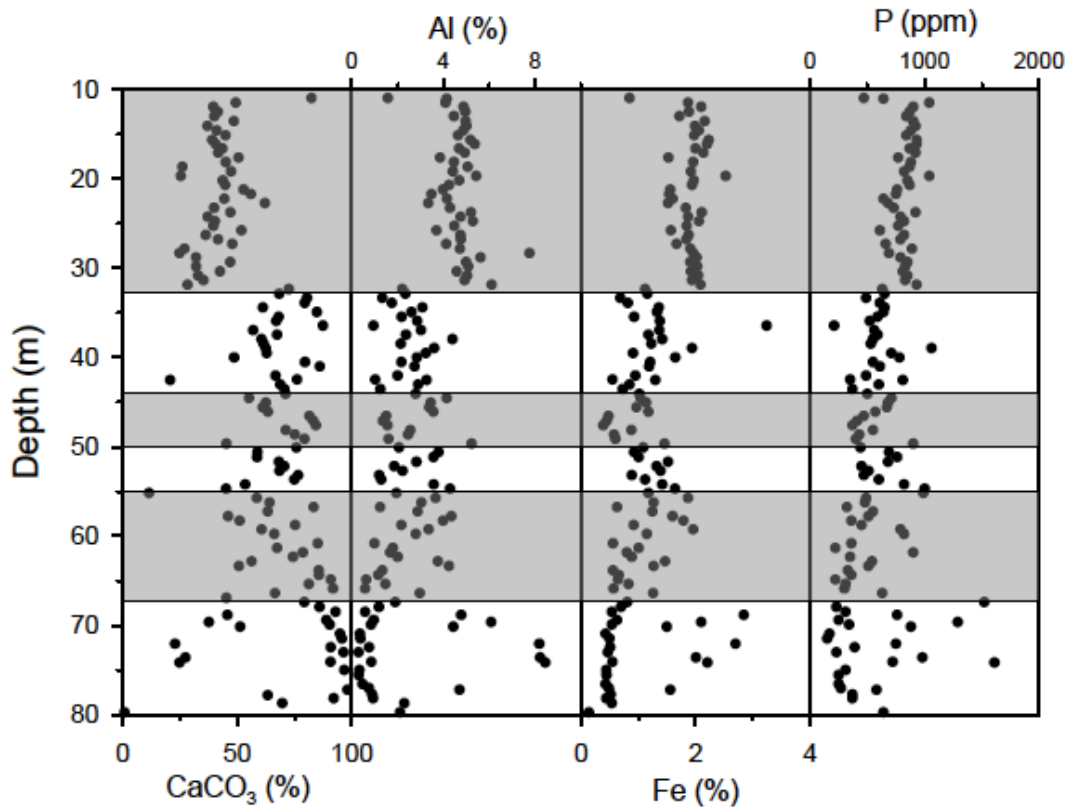
Figure B.1. Calcium carbonate, aluminum, iron and phosphorus concentrations from the USGS Portland #1 core. Gray bars indicate Intervals 1b, 2b, and 3.

Appendix C.

Data Tables for Chapter 2

Table C.1
Total organic carbon, calcium carbon, total nitrogen, and organic and inorganic isotopes
for the USGS Portland #1 core

Depth (m)	Total organic carbon (TOC %)	Calcium Carbonate (CaCO$_3$)	Total Nitrogen (N %)	$\delta^{13}C_{carb}$	$\delta^{18}O_{carb}$	$\delta^{13}C_{org}$
6.10	0.40	60.3	0.05	1.61	-7.18	
6.76	2.85	57.58	0.11	1.47	-7.69	
7.19	1.56	64.19	0.07	1.44	-7.72	
8.00	1.45	55.02	0.08	1.54	-7.20	-27.02
8.76	3.47	46.13	0.14	1.62	-7.36	
9.65	2.82	53.09	0.12	1.44	-7.47	
10.97	1.17	82.29	0.05	1.74	-7.31	
11.48	3.27	49.29	0.14	1.54	-7.52	
11.96	3.44	39.47	0.15	1.19	-7.19	
12.52	3.20	41.44	0.13	1.24	-7.18	
13.01	3.46	39.97	0.13	1.12	-7.10	
13.56	2.70	48.53	0.12	0.92	-7.24	
14.10	3.47	36.93	0.15	1.00	-6.80	
14.58	3.19	40.98	0.14	0.76	-7.07	
15.14	3.21	44.9	0.13	1.08	-7.50	-27.35
15.65	3.19	39.06	0.14	0.95	-7.01	
16.13	3.48	40.49	0.15	0.96	-7.16	
16.61	3.25	43.46	0.14	0.99	-7.26	
17.09	3.29	41.67	0.13	1.13	-7.63	
17.65	2.80	50.48	0.12	1.29	-7.50	
18.14	2.70	44.93	0.12	1.45	-7.18	
18.67	2.94	25.91	0.14	0.84	-7.03	
19.18	2.89	47.24	0.13	1.39	-7.27	
19.69	3.68	25.32	0.17	1.24	-6.86	
20.19	3.08	43.58	0.13	1.42	-7.51	
20.70	2.92	44.71	0.13	1.54	-7.25	

Depth (m)	Total organic carbon (TOC %)	Calcium Carbonate (CaCO$_3$)	Total Nitrogen (N %)	$\delta^{13}C_{carb}$	$\delta^{18}O_{carb}$	$\delta^{13}C_{org}$
21.21	3.03	52.68	0.12	0.94	-7.88	-27.25
21.72	2.83	55.82	0.11	0.99	-8.12	
22.23	3.48	44.28	0.14	1.20	-7.93	
22.73	2.40	62.09	0.10	1.12	-7.97	
23.27	3.55	39.84	0.15	0.79	-8.23	
23.75	2.98	46.95	0.13	0.92	-7.74	
24.26	3.53	37.09	0.15	1.26	-8.00	
24.77	3.01	40.23	0.14	1.37	-7.83	
25.27	3.33	39.54	0.15	1.31	-7.74	
26.29	3.36	36.21	0.15	1.41	-7.63	
26.80	3.91	41.62	0.16	1.36	-7.67	
27.31	3.24	47.76	0.13	1.45	-7.91	-27.11
28.32	3.11	24.78	0.14	1.47	-6.97	
28.83	3.91	31.95	0.16	1.39	-7.25	
29.34	3.09	46.85	0.13	1.39	-7.59	
29.82	3.83	32.08	0.16	1.48	-7.40	
30.38	3.29	42.45	0.12	1.67	-7.30	
30.86	3.75	32.87	0.14	1.59	-7.20	
31.37	3.75	35.27	0.14	1.59	-7.53	
31.88	3.55	28.23	0.14	1.66	-7.13	
32.36	2.27	72.54	0.08	1.60	-8.33	-26.63
32.87	3.33	68.22	0.10	1.61	-7.98	
33.35	1.22	80.45	0.04	1.70	-8.24	-26.53
33.91	1.83	79.43	0.06	1.70	-8.15	
34.42	4.00	61.18	0.12	1.87	-8.14	
34.93	1.59	84.72	0.05	1.77	-8.26	
35.46	2.82	68.03	0.09	1.82	-8.22	-26.25
35.94	2.57	66.99	0.10	1.82	-7.94	
36.45	0.76	87.3	0.03	2.92	-7.84	-25.50
36.96	4.77	56.85	0.17	2.07	-8.02	
37.47	4.98	67.29	0.16	2.15	-7.93	-25.69
37.97	3.46	60.5	0.13	2.04	-6.85	-25.47
38.48	4.47	61.37	0.15	1.87	-7.59	
38.96	6.02	62.32	0.20	2.15	-7.40	
39.52	1.66	62.74	0.07	1.46	-6.91	-25.99
40.01	7.24	48.56	0.23	2.06	-7.76	-26.42
40.52	2.96	79.51	0.10	1.83	-8.47	
41.02	1.45	85.98	0.05	1.81	-7.73	-26.16

Depth (m)	Total organic carbon (TOC %)	Calcium Carbonate (CaCO$_3$)	Total Nitrogen (N %)	$\delta^{13}C_{carb}$	$\delta^{18}O_{carb}$	$\delta^{13}C_{org}$
42.50	3.44	76.06	0.10	1.81	-8.14	
42.55	9.29	20.69	0.30	2.10	-7.40	-25.47
43.05	1.86	68.7	0.08	1.81	-7.17	
43.56	4.16	70.48	0.12	1.97	-8.48	-26.49
44.09	2.07	71.08	0.08	2.01	-7.49	-25.59
44.58	1.56	55.05	0.08	2.16	-6.15	-26.16
45.09	2.02	62.45	0.08	2.28	-6.92	
45.59	1.52	61.04	0.07	2.18	-6.84	-25.90
46.10	2.39	63.28	0.09	2.09	-6.97	
46.58	0.79	81.4	0.03	2.04	-7.45	-25.83
47.12	0.62	83.1	0.03	1.95	-7.66	-25.74
47.63	0.38	84.19	0.02	1.54	-7.39	
50.11	3.50	75.73	0.10	2.19	-8.37	-26.33
50.62	1.40	58.73	0.06	2.20	-6.51	
51.18	0.93	58.63	0.06	2.51	-5.23	-25.95
51.71	5.46	68.16	0.15	2.19	-7.68	-26.62
52.20	5.34	70.42	0.15	2.19	-7.89	-26.58
52.71	5.44	68.4	0.15	2.14	-7.86	-25.74
53.21	4.02	76.48	0.11	2.11	-8.33	-26.32
53.70	4.85	74.83	0.13	2.60	-7.89	
54.23	3.42	53.44	0.12	2.37	-6.70	-25.09
54.71	4.97	45.09	0.16	2.46	-6.32	-24.77
55.22	11.33	11.4	0.34	2.30	-7.57	-25.84
55.75	0.46	58.54	0.05	1.71	-6.79	
56.26	0.28	64.05	0.05	1.61	-6.44	-26.07
56.77	0.13	83.25	0.02	1.44	-6.22	
57.25	0.28	63.23	0.05	1.77	-6.35	-26.03
57.81	0.41	45.91	0.05	1.82	-6.66	
58.29	0.33	50.98	0.08	1.71	-6.49	
58.78	0.22	75.25	0.06	1.45	-6.44	
59.28	0.26	60.55	0.03	1.77	-6.69	-25.50
59.79	0.26	66.11	0.05	1.85	-6.36	
60.83	0.12	85.05	0.04	1.26	-6.16	
61.34	1.10	67.29	0.01	1.68	-8.30	-26.26
61.85	0.16	78.58	0.06	1.57	-6.44	
62.36	0.15	74.33	0.03	1.61	-6.00	
62.84	0.32	56.26	0.02	1.47	-6.48	
63.37	0.40	50.68	0.03	1.93	-6.57	
63.86	0.09	85.51	0.06	1.27	-5.90	

Depth (m)	Total organic carbon (TOC %)	Calcium Carbonate (CaCO$_3$)	Total Nitrogen (N %)	$\delta^{13}C_{carb}$	$\delta^{18}O_{carb}$	$\delta^{13}C_{org}$
64.90	0.07	90.73	0.02	1.13	-6.19	-25.84
65.38	0.16	81.23	0.02	1.78	-6.62	
65.89	0.07	91.81	0.01	1.23	-6.22	
66.42	0.25	66.41	0.02	1.83	-6.27	
66.93	0.38	45.19	0.01			
67.41	0.13	79.2	0.05	1.77	-6.45	-25.01
67.95	0.12	85.83	0.11	1.84	-7.22	
68.50	0.05	92.88	0.03	1.11	-6.37	
69.42	0.06	88.82	0.01	1.23	-6.32	-26.50
69.65	0.38	37.58	0.06	2.16	-4.13	
69.93	0.05	90.33	0.02	1.42	-6.67	
70.16	0.36	51.2	0.09	1.73	-4.79	
70.97	0.06	94.77	0.01	1.26	-6.67	
71.50	0.07	95.6	0.07	1.10	-7.28	
72.09	1.83	22.75	0.01	2.10	-5.79	
72.47	0.10	90.81	0.01	1.22	-7.54	
73.03	0.05	96.34	0.13	0.77	-7.33	
73.61	0.81	27.28	0.01	1.51	-5.36	
74.12	0.08	90.7	0.00	1.06	-7.12	
74.17	0.96	24.73	0.10	1.84	-4.99	
75.03	0.06	96.72	0.01	0.95	-6.99	-26.50
77.24	0.04	98.08	0.11	1.14	-7.28	-25.78
77.85	0.42	63.26	0.00			
78.18	0.08	92	0.00			
78.74	0.17	69.56	0.04			
79.76	0.35	0.78	0.01			
81.71	0.06	0.51	0.02			
83.82	0.07	7.13	0.03			
85.85	0.20	0.6	0.01			

Table C.2
Elemental concentrations in the USGS Portland #1 core

Depth (m)	Aluminum (%)	Manganese (ppm)	Molybdenum (ppm)	Rhenium (ppb)
6.10	3.48	86	16.55	23
6.76	3.47	100	23.10	189
7.19	2.96	93	19.80	50
8.00	3.93	111	23.60	107
8.76	4.40	115	17.90	200
9.65	3.96	121	13.10	162
10.97	1.57	95	8.72	130
11.05	4.13	27	67.80	178
11.48	4.09	119	13.50	144
11.96	4.87	119	22.80	154
12.52	4.95	124	19.65	131
13.01	4.45	133	25.40	111
13.56	4.96	137	25.70	135
14.10	5.00	136	22.00	130
14.58	4.86	139	15.65	132
15.14	4.63	138	22.10	127
15.65	5.17	133	21.50	143
16.13	5.36	133	26.60	156
16.61	4.68	131	16.25	146
17.09	4.92	135	22.00	166
17.65	3.85	139	8.46	91
18.14	4.45	129	10.95	107
18.67	5.05	120	21.40	110
19.18	4.40	131	13.60	129
19.69	5.42	123	10.35	118
20.19	4.68	123	26.30	161
20.70	4.24	124	21.40	142
21.21	3.97	137	10.10	132
21.72	3.47	131	9.54	117
22.23	4.14	115	36.20	96
22.73	3.33	119	12.90	121
23.27	4.28	114	29.40	94
23.75	5.20	124	24.00	144
24.26	4.74	112	24.40	131
24.77	5.28	133	22.80	99
25.27	4.47	117	17.20	126
25.78	3.69	110	19.55	113
26.29	4.74	125	24.40	119

Depth (m)	Aluminum (%)	Manganese (ppm)	Molybdenum (ppm)	Rhenium (ppb)
27.31	4.11	115	25.20	122
27.84	4.71	122	19.40	128
28.32	7.76	100	24.70	87
28.83	5.61	111	26.30	101
29.34	4.99	130	21.60	145
29.82	5.08	112	22.80	128
30.38	4.58	110	22.20	134
30.86	5.03	112	23.20	131
31.37	4.91	113	28.20	116
31.88	6.10	113	22.70	99
32.36	2.20	90	14.95	221
32.87	2.33	91	25.20	761
33.35	1.32	91	3.38	54
33.91	1.74	93	7.60	88
34.42	3.08	77	32.00	185
34.93	2.60	78	11.10	221
35.46	2.17	85	13.00	112
35.94	2.85	94	15.05	214
36.45	0.94	43	55.40	61
36.96	3.01	73	28.00	202
37.47	2.36	66	60.00	212
37.97	4.39	128	23.90	105
38.48	2.13	75	25.00	155
38.96	3.59	75	104.50	240
39.52	3.22	97	5.47	33
40.01	2.83	67	30.10	228
40.52	2.16	68	39.80	197
41.02	2.73	78	14.50	102
42.04	2.00	64	18.95	166
42.50	1.01	71	7.05	81
42.55	3.26	71	28.90	144
43.05	2.89	91	8.07	42
43.56	1.24	79	11.70	144
44.09	2.78	98	5.06	79
44.58	4.13	103	2.45	18
45.09	3.44	91	4.07	45
45.59	3.37	95	2.56	26
46.10	3.55	108	6.76	80
46.58	1.50	100	2.00	22
47.12	1.35	90	1.87	13

Depth (m)	Aluminum (%)	Manganese (ppm)	Molybdenum (ppm)	Rhenium (ppb)
48.64	2.45	92	2.74	17
49.15	1.60	88	2.69	37
49.66	5.22	88	3.82	30
50.11	2.05	85	21.60	225
50.62	3.78	104	2.15	24
51.18	3.56	122	3.18	9
51.71	2.81	88	30.50	404
52.20	1.85	96	27.00	358
52.71	2.21	93	29.90	287
53.21	1.19	110	9.48	244
53.70	1.28	135	28.80	247
54.23	3.57	128	3.96	74
54.71	4.28	116	11.50	144
55.22	1.94	197	10.80	166
55.75	3.65	346	0.97	12
56.26	3.03	549	0.32	4
56.77	1.23	869	0.17	3
57.25	2.87	696	0.23	4
57.81	4.34	332	0.28	10
58.29	3.98	510	0.23	7
58.78	2.16	797	0.13	6
59.28	3.35	520	0.21	5
59.79	2.79	665	0.18	4
60.83	0.99	1210	0.20	3
61.34	1.79	473	0.22	11
61.85	1.67	779	0.15	5
62.36	2.00	1060	0.16	2
62.84	3.75	803	0.34	9
63.37	4.23	476	0.29	8
63.86	1.32	1580	0.09	4
64.39	1.14	1550	0.15	2
64.90	0.62	1520	0.07	2
65.38	1.46	976	0.10	3
65.89	0.58	1300	0.06	2
66.42	2.96	964	0.19	6
67.41	1.90	1180	0.10	2
67.95	1.18	1010	0.09	<2
68.50	0.58	1690	0.07	<2
68.86	4.77	667	2.28	27
69.42	0.95	1400	0.05	<2
69.65	6.08	825	0.32	6

Depth (m)	Aluminum (%)	Manganese (ppm)	Molybdenum (ppm)	Rhenium (ppb)
70.16	4.42	852	0.28	13
70.97	0.35	993	0.07	4
71.50	0.37	885	0.24	3
72.09	8.19	177	0.47	46
72.47	0.75	880	0.05	<2
73.03	0.29	1100	0.05	<2
73.61	8.22	317	0.35	24
74.12	0.85	1020	0.08	3
74.17	8.45	342	0.63	38
75.03	0.32	1330	0.08	<2
75.57	0.30	1240	0.16	6
76.58	0.46	879	0.09	4
77.04	0.74	613	0.07	4
77.24	4.70	382	0.89	25
77.75	0.88	578	0.11	2
78.18	0.92	799	0.34	4
78.74	2.29	513	0.50	9
79.76	2.10	13	1.74	12
80.77	1.96	11	0.79	4
86.87	5.72	48	0.56	3

Appendix D.

Data Tables for Chapter 3

Table D.1
Thermal maturity biomarker results for the USGS Portland #1 core

Depth (m)	C_{27} $\alpha\beta\beta$ sterane 20S/(20S+20R)	C_{29} $\alpha\beta\beta$ sterane 20S/(20S+20R)	C_{30} moretane/ hopane	C_{31} Hopane 20S/(20S+20R)	C_{32} Hopane 20S/(20S+20R)
	<0.55	**<0.55**	**>0.05**	**<0.6**	**<0.6**
9.65	0.266	0.269	0.162	0.593	0.621
15.14	0.269	0.237	0.194		
20.19	0.229	0.233	0.175	0.561	0.518
25.27	0.261	0.256	0.182	0.586	0.522
30.38	0.249	0.247	0.189	0.555	0.498
34.93	0.280	0.301	0.174	0.565	0.537
40.01	0.293	0.311	0.180	0.559	0.665
45.09	0.311	0.284	0.102	0.565	0.595
50.11	0.307	0.302	0.157	0.588	0.610
55.22	0.273	0.267	0.182	0.583	0.550
59.79	0.152	0.257			
62.84	0.277	0.205			
68.86	0.227	0.303	0.176	0.544	0.778
70.16	0.336	0.278			
74.17	0.132	0.208	0.141	0.597	0.296

Table D.2

Most abundant compounds from the USGS Portland #1 core

Depth (m)	MAC
9.65	pristane
15.14	pristane
20.19	pristane
25.27	pristane
30.38	pristane
34.93	pristane
40.01	n-C_{22}
45.09	n-C_{22}
50.11	pristane
55.22	pristane
59.79	n-C_{22}
62.84	n-C_{22}
70.16	n-C_{23}
70.16	n-C_{23}

Table D.3
Organic matter source biomarker results for the USGS Portland #1 core

Depth (m)	Carbon Preference Index (CPI)	Odd-Even Preference (OEP$_{31}$)	Sterane 27R/29R	Sterane 28R/27R	Steranes/Hopanes
9.65	1.04	1.75	1.25	0.93	0.22
15.14	1.00	1.56	1.06	0.95	0.23
20.19	0.96	1.55	1.16	0.85	0.36
25.27	1.02	1.43	1.22	0.91	0.39
30.38	1.00	1.43	1.14	0.88	0.33
34.93	0.98	1.22	1.05	0.96	0.48
40.01	0.95	1.32	0.99	1.06	0.19
45.09	0.95	1.24	0.92	0.84	0.22
50.11	0.94	1.53	1.10	0.86	0.34
55.22	0.96	1.44	1.09	0.85	0.15
59.79	1.12	1.29	1.14	0.41	0.04
62.84	0.98	1.22		0.19	0.03
68.86	1.02	1.33	1.34	0.42	0.05
70.16	0.94	1.47	1.30	0.24	0.02
74.17	1.12	1.53	1.32	0.12	0.07

Table D.4
Pristane and phytane results for the USGS Portland #1 core

Depth (m)	Pr/Ph	Pr/n-C_{17}	Ph/n-C_{18}
9.65	2.710	1.785	0.858
15.14	2.782	1.863	0.936
20.19	2.741	1.714	0.764
25.27	2.721	2.037	0.921
30.38	3.187	1.758	0.788
34.93	1.253	0.668	0.597
40.01	1.929	1.284	0.708
45.09	2.468	1.192	0.536
50.11	3.012	1.339	0.551
55.22	2.784	1.160	0.535
59.79	2.067	0.560	0.293
62.84	1.253	0.668	0.597
68.86	3.406	0.748	0.337
70.16	0.980	0.525	0.826
74.17	1.379	0.811	0.882

Table D.5
Compound specific isotope results for the USGS Portland #1 core

Depth (m)	C_{19}	C_{20}	C_{21}	C_{22}	C_{23}	C_{24}
15.19	-31.06		-29.70		-30.35	
20.19	-30.13	-32.02	-29.30		-29.44	-28.52
25.27	-30.67		-29.81	-28.51	-29.25	-28.38
34.96	-29.86	-29.76	-29.09	-28.63	-29.13	-29.24
40.01		-30.37	-28.60	-27.88	-28.10	-29.25
45.09	-30.11	-29.39	-28.15	-28.05	-28.01	-28.16
50.11	-30.27		-29.48	-28.90	-29.18	
55.22		-29.93	-29.18	-28.44	-28.54	-28.58
59.79		-28.26	-27.68	-29.05	-29.82	
62.84		-28.94	-28.59	-28.76	-28.92	-29.74
68.86		-28.86	-28.57	-28.44	-28.90	-28.39
70.16			-28.82		-28.65	

Appendix E.

Data Tables for Chapter 4

Table E.1
Errors for ALS elemental measurements

Standard		Al	Fe	P
GBM908-10	Accuracy	0.03%	0.03%	4.06 ppm
n=18	Precision	0.04%	0.04%	4.66 ppm
GBM908-05	Accuracy	0.11%	0.04%	19.89 ppm
n=8	Precision	0.11%	0.05%	21.79 ppm
MRGeo08	Accuracy	0.05%	0.03%	6.62 ppm
n=21	Precision	0.07%	0.04%	8.18 ppm
OREAS 90	Accuracy	0.10%	0.04%	10.89 ppm
n=6	Precision	0.11%	0.05%	12.40 ppm

Table E.2

Fe$_T$/Al values for Aristocrat Angus, Berthoud State #3, and USGS Portland #1 cores

	USGS Portland #1	Berthoud State #3	Aristocrat Angus
Middle Marl	0.42 ± 0.11	0.41 ± 0.24	0.37 ± 0.15
Lower Chalk	0.42 ± 0.11	0.40 ± 0.13	0.38 ± 0.14
Lower Marl	0.50 ± 0.20	0.37 ± 0.11	0.44 ± 0.11
Total OAE and post-OAE	**0.48 ± 0.37**	**0.38 ± 0.12**	**0.39 ± 0.14**
Fort Hays	0.65 ± 0.43	0.77 ± 0.42	0.79 ± 0.40

Table E.3
Fe speciation data for the USGS Portland #1 core

Depth (m)	Fe_{ox} (%)	Fe_{mag} (%)	Fe_{carb} (%)	Fe_{py} (%)	Fe_{HR}/Fe_T	Fe_{py}/Fe_{HR}
11.5	0.049	0.035	0.044	1.046	0.628	0.042
17.1	0.051	0.041	0.044	1.061	0.559	0.041
21.2	0.055	0.023	0.038	0.963	0.692	0.040
23.3	0.036	0.035	0.041	1.060	0.641	0.039
26.8	0.038	0.031	0.039	0.928	0.564	0.042
30.9	0.039	0.037	0.053	0.942	0.522	0.056
34.9	0.066	0.012	0.026	0.692	0.599	0.038
37.5	0.064	0.006	0.031	0.733	0.708	0.043
39	0.095	0.010	0.022	1.100	0.632	0.020
41	0.030	0.005	0.016	0.692	0.625	0.023
43	0.019	0.005	0.022	0.435	0.565	0.050
45.1	0.021	0.008	0.019	0.637	0.601	0.029
47.1	0.028	0.004	0.034	0.202	0.595	0.170
51.2	0.017	0.009	0.016	0.533	0.569	0.029
52.7	0.041	0.006	0.042	0.923	0.728	0.046
55.2	0.053	0.021	0.076	0.606	0.640	0.126
57.8	0.031	0.059	0.048	0.515	0.408	0.094
60.8	0.020	0.024	0.099	0.349	0.878	0.285
62.8	0.035	0.071	0.059	0.777	0.641	0.076
64.9	0.027	0.028	0.171	0.032	0.398	5.400
69.4	0.025	0.030	0.096	0.074	0.356	1.305
71	0.021	0.023	0.188	0.036	0.622	5.240
73	0.021	0.015	0.204	0.039	0.593	5.258
75	0.032	0.011	0.191	0.070	0.692	2.729

Table E.4
Bulk elemental geochemistry for the USGS Portland #1 core

Depth (m)	Cd (ppm)	Fe (%)	P (%)	Zn (ppm)
6.1	10.85	1.31	780	252
6.76	8.13	1.24	640	163
7.19	7.29	1.08	510	157
8	8.71	1.5	780	164
8.76	12.3	1.68	750	209
9.65	7.05	1.61	860	170
10.97	4	0.85	470	94
11.05	1.89	8.41	640	64
11.48	5.92	1.87	1040	130
11.96	9.56	2.1	900	202
12.52	6.73	1.89	870	120
13.01	8.12	1.72	840	141
13.56	9.35	2.16	900	236
14.1	7.06	1.99	920	141
14.58	5.2	2.06	880	134
15.14	8.03	1.98	840	162
15.65	7.58	2.23	930	158
16.13	10.1	2.2	930	183
16.61	7.75	2	870	180
17.09	5.88	2.14	920	128
17.65	4.81	1.53	770	126
18.14	5.04	1.96	880	138
18.67	7.24	5.71	870	288
19.18	4.95	1.92	820	124
19.69	4.86	2.53	1040	192
20.19	8.2	1.97	850	165
20.7	11.25	1.94	870	275
21.21	1.54	1.56	760	40
21.72	8.24	1.54	750	225
22.23	4.44	1.6	640	94
22.73	7.01	1.52	680	148
23.27	7.91	1.83	730	166
23.75	9.29	2.11	920	255
24.26	8.73	1.87	790	159
24.77	7.09	2.06	820	178
25.27	10.35	1.85	770	255
25.78	8.63	1.57	610	172
26.29	12.4	1.88	820	229

Depth (m)	Cd (ppm)	Fe (%)	P (%)	Zn (ppm)
27.31	10.35	1.67	660	200
27.84	12.05	1.91	890	429
28.32	3.43	1.96	690	57
28.83	7.57	2.02	790	184
29.34	9.18	1.91	850	167
29.82	9.8	2.03	830	218
30.38	9.92	1.92	810	200
30.86	9.47	2.05	850	198
31.37	7.64	1.94	830	142
31.88	8.48	2.09	930	211
32.36	3.65	1.12	630	133
32.87	2.99	1.16	650	121
33.35	1.2	0.69	490	88
33.91	1.35	0.82	610	84
34.42	4.55	1.36	650	130
34.93	4.85	1.33	640	267
35.46	1.7	0.93	590	94
35.94	3.07	1.38	520	136
36.45	1.39	3.24	210	53
36.96	4.65	1.37	560	198
37.47	6.24	1.18	590	188
37.97	2.09	1.42	550	82
38.48	6.34	1.23	530	215
38.96	7.22	1.94	1060	228
39.52	0.47	0.91	710	58
40.01	9.01	1.65	780	295
40.52	5.67	1.21	550	180
41.02	2.58	1.19	610	149
42.04	4.78	0.95	490	212
42.5	3.42	0.55	350	129
42.55	3.9	1.3	810	177
43.05	0.44	0.85	600	51
43.56	3.96	0.73	370	144
44.09	1.41	1.02	500	90
44.58	0.3	1.04	710	84
45.09	0.51	1.14	680	89
45.59	0.23	0.97	670	51
46.1	0.46	1.18	570	47
46.58	0.12	0.48	470	17
47.12	0.06	0.45	410	8
48.64	0.1	0.58	430	15

Depth (m)	Cd (ppm)	Fe (%)	P (%)	Zn (ppm)
49.15	0.57	0.6	400	45
49.66	0.27	1.46	900	67
50.11	3.63	1.09	440	154
50.62	0.23	0.93	690	47
51.18	0.24	1.01	760	64
51.71	7.19	1.52	680	269
52.2	5.63	1.32	450	144
52.71	6.95	1.39	510	266
53.21	4.76	0.89	470	191
53.7	5.48	1.12	600	205
54.23	2.65	1.42	820	294
54.71	1.97	1.64	1000	147
55.22	2.64	1.18	990	145
55.75	0.12	1.87	490	50
56.26	0.21	1.27	480	105
56.77	0.08	0.63	320	32
57.25	0.12	1.25	550	78
57.81	0.17	1.6	510	88
58.29	0.13	1.79	360	82
58.78	0.06	0.92	450	28
59.28	0.16	1.96	790	89
59.79	0.07	1.15	820	34
60.83	0.05	0.56	360	16
61.34	0.09	1.01	220	31
61.85	0.06	0.8	900	37
62.36	0.08	0.89	350	37
62.84	0.16	1.47	540	76
63.37	0.18	1.27	510	83
63.86	0.06	0.56	330	22
64.39	0.09	0.66	360	26
64.9	0.02	0.65	220	8
65.38	0.08	0.83	310	41
65.89	0.05	0.57	300	19
66.42	0.21	1.26	630	110
67.41	0.03	0.81	1520	16
67.95	0.05	0.7	230	21
68.5	0.04	0.54	310	12
68.86	0.18	2.84	760	74
69.65	0.61	2.1	1290	248
69.93	0.09	0.54	340	22
70.16	0.28	1.5	880	96

Depth (m)	Cd (ppm)	Fe (%)	P (%)	Zn (ppm)
70.97	0.22	0.43	170	91
71.5	0.09	0.5	150	13
72.09	0.5	2.7	750	142
72.47	0.1	0.51	390	27
73.03	0.04	0.47	230	7
73.61	0.44	2.01	980	145
74.12	0.07	0.55	720	28
74.17	0.75	2.21	1610	236
75.03	0.05	0.44	310	10
75.57	0.06	0.45	250	14
76.58	0.04	0.43	250	10
77.04	0.05	0.49	270	11
77.24	0.31	1.56	580	92
77.75	0.06	0.52	370	19
78.18	0.07	0.44	370	21
78.74	0.1	0.54	3780	20
79.76	0.02	0.14	640	3
80.77	0.26	0.23	490	58
86.87	0.04	1.56	870	38

Appendix F.

Data Tables for Chapter 5

Table F.1
Bulk elemental geochemistry for cores 16-4-22-15W4 and 13-20-17-7W4

Sample	Al (%)	Cd (ppm)	Fe (%)	Mo (ppm)	Re (ppm)
16-426	6.05	0.12	2.2	0.65	0.002
16-430	5.05	0.08	2.42	1.82	0.002
16-439	6.9	0.1	3.14	2.5	0.002
16-440	7.69	0.16	2.39	0.43	0.002
16-441	8.06	0.14	2.6	0.4	0.002
16-442	7.08	0.12	2.38	0.59	0.002
16-443	6.42	0.13	2.04	0.56	0.005
16-444	7.33	0.14	2.38	0.38	0.004
16-445	7.53	0.12	3.17	1.8	0.004
16-446	7.26	0.23	3.13	2.89	0.007
16-447	8.22	0.18	3.34	1.9	0.005
16-448	7.4	0.13	3.79	2.01	0.005
16-449	7.43	0.17	3.32	0.93	0.007
16-450	8.3	0.15	3.24	0.97	0.004
16-451	8.25	0.2	3.21	1.19	0.007
16-452	8.02	0.16	2.72	0.63	0.005
16-453	7.9	0.35	3.23	3.13	0.011
16-454	7.3	0.28	2.83	2.01	0.005
16-455	7.66	0.57	3.59	8.21	0.02
16-456	7.8	0.45	3.47	6.72	0.013
16-457	6.54	1.06	3.56	16.2	0.026
16-458	7.73	0.86	3.69	18.6	0.046
16-459	6.76	0.89	3.66	23.2	0.046
16-460	11.1	0.5	2.74	14.35	0.019
16-461	6.46	0.65	3.38	19.4	0.04
16-462	6.06	0.92	3.04	12.8	0.019
16-463	7.14	0.87	3.56	25.5	0.039
16-464	6.49	0.78	3.83	18.55	0.032
16-465	6.53	0.57	3.68	18.3	0.018

Sample	Al (%)	Cd (ppm)	Fe (%)	Mo (ppm)	Re (ppm)
16-466	5.86	0.63	3.46	16.95	0.021
16-467	5.83	0.84	2.98	17.7	0.019
16-468	7.02	0.86	3.64	26.1	0.024
16-469	7.07	1.07	3.83	33.1	0.034
16-470	7	1.47	3.71	27.3	0.028
16-471	6.76	1.32	3.93	29.7	0.052
16-472	7.69	1.19	3.86	22.3	0.054
16-473	7.41	2.05	4.14	20.1	0.043
16-474	7.16	1.57	3.8	27.4	0.049
16-475	7.05	1.22	3.36	10.8	0.021
16-476	8.74	1.22	4.01	12	0.03
16-477	7.95	0.84	3.45	8.21	0.02
16-478	6.29	1.22	3.02	24.7	0.038
16-479	6.92	1.27	3.2	18.3	0.035
16-480	5.7	1.13	3.33	20.6	0.03
16-481	7.59	0.57	3.06	7.53	0.019
16-482	3.08	1.13	1.41	9.52	0.016
16-483	7.93	2.24	3.71	10.35	0.027
16-484	7.9	0.97	3.81	9.96	0.03
16-485	7.37	1.36	3.57	20.2	0.058
16-486	5.91	0.35	2.08	3.27	0.011
16-487	3.8	0.27	1.42	2.43	0.006
16-488	5.06	0.24	1.81	2.6	0.011
16-489	7	0.19	2.93	1.95	0.01
16-490	5.72	0.37	2.37	3.94	0.017
16-491	7.43	0.81	3.76	7.78	0.037
16-492	7.7	1.5	4	21.9	0.043
16-493	7.76	0.23	3.05	1.94	0.012
16-493.5	8.34	0.88	3.48	6.56	0.028
16-494	5.42	0.16	2.82	1.23	0.009
16-495	8.28	0.16	2.84	0.42	0.009
16-496	7.65	0.09	2.83	0.44	0.004
16-497	7.47	0.18	3.16	1.08	0.009
16-498	7.36	0.13	4.12	2.03	0.006
16-499	7.66	0.11	2.98	0.79	0.005
16-500	5.63	0.3	2.5	3.39	0.014
16-501	8.66	0.18	3.15	1.15	0.007
16-502	6.91	0.17	3.04	1.36	0.008
16-503	6.33	0.17	2.37	0.9	0.007
16-504	6.42	0.33	2.85	3.25	0.013
16-505	5.23	0.22	1.9	1.43	0.008
16-505.6	4.89	0.29	5.25	3.76	0.01

Sample	Al (%)	Cd (ppm)	Fe (%)	Mo (ppm)	Re (ppm)
16-506	5.2	0.24	2.04	2.43	0.008
16-508	7.68	0.26	3.08	3.39	0.011
16-509	6.02	0.38	2.56	3.69	0.012
16-510	5.59	0.27	2.27	2.92	0.009
16-511	8.06	0.88	3.26	4.11	0.017
16-512	8.28	0.12	3.57	1.49	0.007
16-513	8.5	0.14	3.29	1.47	0.006
16-514	8.37	0.14	3.64	1.16	0.004
16-515	3.18	0.05	22.9	0.25	0.002
16-516	7.85	0.11	2.7	0.59	0.002
16-517	8.05	0.12	2.79	0.48	0.003
16-518	8.19	0.16	3.52	0.82	0.004
16-519	7.43	0.13	2.97	1.05	0.005
16-521	7.72	0.12	2.86	0.91	0.005
16-522	7.35	0.1	4.14	1.71	0.006
16-523	7.3	0.13	2.79	0.95	0.005
16-524	7.12	0.18	3.13	1.64	0.01
16-525	7.13	0.13	2.68	0.89	0.007
16-526	8.12	0.14	3.15	0.85	0.007
16-527	6.28	0.22	3.36	2.51	0.013
16-528	7.21	0.15	2.77	0.79	0.004
16-529	7.54	0.16	2.88	0.91	0.007
16-531	6.09	0.13	2.51	1.33	0.006
16-533	7.98	0.13	3.61	0.62	0.009
16-534	8.21	0.13	3.16	0.62	0.007
16-535	8.27	0.17	3.03	0.41	0.007
16-536	7.92	0.11	2.9	0.82	0.004
16-537	8.98	0.15	3.74	1.21	0.006
16-538	10.3	0.13	4.03	2.21	0.004
16-539	9.23	0.09	3.7	0.95	0.003
16-540	8.16	0.63	3.99	9.44	0.039
16-541	8.94	0.23	3.57	2.81	0.014
16-542	8.71	0.57	5.57	8.16	0.025
16-543	8.5	0.44	4.34	6.84	0.024
16-544	8.74	0.11	4.25	1.36	0.006
16-545	8.91	0.1	3.94	0.72	0.004
16-546	8.78	0.2	3.69	3.33	0.011
16-547	6.76	0.08	6.26	4.71	0.003
16-548	8.51	0.12	3.71	1.08	0.007
16-549	10.1	0.13	3.7	1.33	0.005
16-550	8.19	0.12	3.35	0.74	0.008
16-551	7.58	0.11	3.31	0.92	0.007

Sample	Al (%)	Cd (ppm)	Fe (%)	Mo (ppm)	Re (ppm)
16-552	8.59	0.15	3.66	1.1	0.011
16-553	6.45	0.11	2.78	1.1	0.008
16-554	7.18	0.15	2.83	0.71	0.007
16-555	8.99	0.22	2.95	1.34	0.014
16-556	8.74	0.09	3.05	0.85	0.005
16-557	8.98	0.21	3.18	0.75	0.011
16-558	8.81	0.16	3.37	1.09	0.012
16-559	8.88	0.18	3.01	0.59	0.009
16-560	8.12	0.11	2.96	0.48	0.006
16-561	8.25	0.21	3.22	0.8	0.011
16-563	8.41	0.24	3.11	1.32	0.01
16-564	8.35	0.14	2.94	0.85	0.007
16-565	8.54	0.16	3.28	0.62	0.01
16-567	8.73	0.13	2.7	0.69	0.004
16-568	8.73	0.14	3.09	1.77	0.006
13-535	9.77	0.11	3.12	1.39	0.014
13-536	9.28	0.48	3.19	2.37	0.029
13-537.5	8.68	0.35	3.42	3.01	0.038
13-538	8.67	0.35	2.85	1.76	0.024
13-539	4.31	0.88	3.92	6.1	0.087
13-539.8	9.73	0.19	2.3	1.43	0.002
13-540	9.13	0.93	3.77	13.05	0.069
13-541	9.42	0.21	3.33	8.33	0.023
13-537	8.67	0.53	2.79	2.86	0.044
13-541.7	9.47	0.33	2.56	7.69	0.009
13-542	8.01	0.36	3.36	6.47	0.008
13-543.8	6.79	0.13	2.5	1.06	0.006
13-545	7.85	0.13	2.98	1.2	0.005
13-546	6.64	0.12	2.61	0.86	0.004
13-547	7.59	0.12	3.07	1.24	0.005
13-548	7.64	0.15	2.9	1.03	0.005
13-549	6.52	0.16	3.43	1.59	0.008
13-550	6.47	0.11	2.61	0.69	0.006
13-551	7.03	0.13	2.44	0.87	0.006
13-552	8.41	0.16	3.01	1.4	0.009
13-553	7.93	0.18	3.1	1.54	0.011
13-554	7.83	0.15	3.16	1.97	0.011

Table F.2
Fe speciation data for cores 16-4-22-15W4 and 13-20-17-7W4

Sample	Fe_{ox} (%)	Fe_{mag} (%)	Fe_{carb} (%)	Fe_{py} (%)	Fe_{HR}/Fe_T	Fe_{py}/Fe_{HR}
16-426	0.206	0.230	0.028	0.131	0.270	0.220
16-430	0.397	0.446	0.159	0.256	0.520	0.204
16-440	0.164	0.153	0.045	0.149	0.214	0.292
16-444	0.137	0.152	0.031	0.212	0.223	0.398
16-448	0.244	0.138	0.026	0.940	0.355	0.698
16-456	0.280	0.085	0.026	1.220	0.464	0.757
16-460	0.223	0.023	0.043	1.498	0.652	0.838
16-468	0.697	0.142	0.047	1.488	0.652	0.627
16-476	0.526	0.152	0.061	1.020	0.439	0.580
16-480	0.877	0.471	0.040	0.624	0.604	0.310
16-484	1.088	0.261	0.043	0.684	0.544	0.329
16-492	1.731	0.329	0.034	0.631	0.681	0.232
16-496	0.332	0.131	0.032	0.297	0.280	0.375
16-500	0.315	0.096	0.047	0.993	0.581	0.684
16-504	0.601	0.119	0.044	0.731	0.525	0.489
16-508	0.418	0.114	0.034	0.617	0.384	0.521
16-512	0.406	0.169	0.067	0.494	0.318	0.435
16-516	0.173	0.167	0.034	0.245	0.229	0.396
16-524	0.545	0.175	0.035	0.252	0.322	0.251
16-528	0.303	0.136	0.022	0.502	0.348	0.522
16-536	0.354	0.161	0.026	0.229	0.266	0.297
16-544	0.211	0.096	0.031	1.242	0.372	0.786
16-548	0.512	0.315	0.021	0.445	0.349	0.344
16-556	0.136	0.087	0.026	0.816	0.349	0.766
16-560	0.089	0.066	0.016	0.714	0.299	0.807
16-564	0.081	0.066	0.010	0.699	0.291	0.816
16-568	0.049	0.059	0.020	0.766	0.289	0.857
13-535	0.040	0.044	0.015	1.181	0.410	0.923
13-540	0.060	0.030	0.109	2.179	0.631	0.916
13-547	0.100	0.058	0.020	1.558	0.565	0.897
13-551	0.046	0.048	0.016	0.971	0.443	0.898